

FROM MOLECULAR TINKERTOYS TO INORGANIC-ORGANIC HYBRID
COMPOSITES - FUNCTIONAL MATERIALS FEATURING METAL
CHALCOGENIDE CLUSTERS

by

Bryan Kruger Roland

A Dissertation Submitted to the Faculty of the

DEPARTMENT OF CHEMISTRY

In Partial Fulfillment of the Requirements

For the Degree of

DOCTOR OF PHILOSOPHY

In the Graduate College

THE UNIVERSITY OF ARIZONA

2003

UMI Number: 3107034

UMI[®]

UMI Microform 3107034

Copyright 2004 by ProQuest Information and Learning Company.

All rights reserved. This microform edition is protected against
unauthorized copying under Title 17, United States Code.

ProQuest Information and Learning Company
300 North Zeeb Road
P.O. Box 1346
Ann Arbor, MI 48106-1346

THE UNIVERSITY OF ARIZONA @
GRADUATE COLLEGE

As members of the Final Examination Committee, we certify that we have
read the dissertation prepared by Bryan Kruger Roland

entitled FROM MOLECULAR TINKERTOYS TO INORGANIC-ORGANIC HYBRID

COMPOSITES - FUNCTIONAL MATERIALS FEATURING METAL

CHALCOGENIDE CLUSTERS

and recommend that it be accepted as fulfilling the dissertation
requirement for the Degree of Doctor of Philosophy

John H. Enemark
Dr. John Enemark

8-8-03
Date

Eugene Mash
Dr. Eugene Mash

8-8-03
Date

Dominic McGrath
Dr. Dominic McGrath

8/8/03
Date

Ann Walker
Dr. Ann Walker

8/8/03
Date

Zhiping Zheng
Dr. Zhiping Zheng

8/8/03
Date

Final approval and acceptance of this dissertation is contingent upon
the candidate's submission of the final copy of the dissertation to the
Graduate College.

I hereby certify that I have read this dissertation prepared under my
direction and recommend that it be accepted as fulfilling the dissertation
requirement.

Dissertation Director

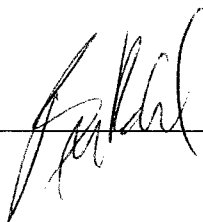
8/8/03
Date

STATEMENT BY AUTHOR

This dissertation has been submitted in partial fulfillment of requirements for an advanced degree at The University of Arizona and is deposited in the University Library to be made available to borrowers under rules of the Library.

Brief quotations from this dissertation are allowable without special permission, provided that accurate acknowledgment of source is made. Requests for permission for extended quotation from or reproduction of this manuscript in whole or in part may be granted by the head of the major department or the Dean of the Graduate College when in his or her judgment the proposed use of the material is in the interests of scholarship. In all other instances, however, permission must be obtained from the author.

SIGNED: _____

A handwritten signature in black ink, written over a horizontal line. The signature is stylized and appears to be the author's name.

Acknowledgments

Several people have contributed to this body of work and are in need of acknowledgment. Dr. Mike Carducci, Hugh Selby, and Jenine Cole of the Molecular Structures Laboratory provided outstanding X-ray crystallographic services. Dr. Neil Jacobsen, director of the Nuclear Magnetic Resonance Facility, assisted in the ^{77}Se NMR experiments reported in Chapter 4. Ware Flora under the direction of Dr. Armstrong, contributed significantly to the electrochemical studies. Mike Szalai helped with molecular weight determination of the hybrid materials reported in Chapter 5 by Gel Permeation Chromatography.

I need to acknowledge Dr. Ann Walker, Dr. John Enemark, Dr. Dominic McGrath, and the late Dr. O'Brien for believing in me enough to allow me the chance to prove my worth as a scientist even though the choice may not have been clear, as well as Dr. Eugene Mash for agreeing to be on my committee at such a late date. Finally, the person in need of the highest acclaim is my research advisor, Dr. Zhiping Zheng. Dr. Zheng has been a constant support and guide through my graduate career, both in and out of the laboratory.

Dedication

This work is dedicated to my mother and father for their constant and unconditional support in whatever I choose to do. Also, to my wife, who has always been there when I need somebody the most.

Table of Contents

LIST OF FIGURES.....	9
LIST OF TABLES.....	13
CHAPTER 1. METAL CLUSTER-SUPPORTED SUPRAMOLECULAR DESIGN AND DISCOVERY.....	14
CHAPTER 2. STAR-SHAPED SUPRAMOLECULAR ARRAYS FEATURING THE $[\text{Re}_6(\mu_3\text{-Se})_8]^{2+}$ CORE-CONTAINING CLUSTERS.....	28
2.1. INTRODUCTION	29
2.2. EXPERIMENTAL	36
2.3. SYNTHESIS AND CHARACTERIZATION	42
2.3.1. Synthesis of a Star-Shaped Tricluster.....	42
2.3.2. X-ray Structural Determination of 13.....	46
2.3.3. Synthesis of the Tetrapyrrolylporphyrin-Supported Tetracluster Array.....	52
2.4. ELECTRONIC SPECTROSCOPIC STUDIES OF TRI- AND TETRACLUSTER ARRAYS.....	56
2.5. ELECTROCHEMICAL STUDIES.....	59
2.5.1. Cyclic Voltammetry.....	59
2.5.2. Coulometry.....	60
2.6. ATTEMPTS TO CONSTRUCT MORE EXTENDED SUPRAMOLECULAR ARRAYS OF CLUSTERS.....	62
2.7. SUMMARY AND PERSPECTIVES.....	67

Table of Contents - continued

CHAPTER 3. CLUSTER-STUDED METALLOPORPHYRINS: SPECTROSCOPIC AND ELECTROCHEMICAL STUDIES.....	68
3.1. INTRODUCTION.....	69
3.2. EXPERIMENTAL.....	76
3.3. SYNTHESIS AND CHARACTERIZATION.....	78
3.4. ELECTRONIC SPECTROSCOPIC STUDIES.....	84
3.5. ELECTROCHEMICAL STUDIES.....	89
3.6. SUMMARY AND PERSPECTIVES.....	91
CHAPTER 4. METALLODENDRIMERS SUPPORTED BY THE $[\text{Re}_6(\mu_3\text{-Se})_8]^{2+}$ CLUSTERS.....	92
4.1. INTRODUCTION.....	94
4.2. EXPERIMENTAL.....	103
4.3. SYNTHESIS AND CHARACTERIZATION.....	107
4.3.1. Synthesis of Cluster Dendrons.....	107
4.3.2. X-ray Structural Determination of 28.....	110
4.3.3. Synthesis of Cluster-Based Metallodendrimers.....	113
4.4. ELECTRONIC SPECTROSCOPIC STUDIES.....	119
4.5. ELECTROCHEMICAL STUDIES.....	121
4.6. SUMMARY AND PERSPECTIVES.....	124

Table of Contents - continued

CHAPTER 5. ISOSTERIC $[\text{Re}_6(\mu_3\text{-Se})_8]^{2+}$ CLUSTERS AS PRECURSORS TO CLUSTER-POLYMER HYBRID MATERIALS.....	125
5.1. INTRODUCTION.....	126
5.2. EXPERIMENTAL.....	135
5.3. SYNTHESIS AND CHARACTERIZATION.....	141
5.3.1. Synthesis of Polymerizable Cluster Complexes	141
5.3.2. X-ray Structural Determination of 34 and 35.....	145
5.3.3. Synthesis of Cluster-Polystyrene Hybrids.....	150
5.4. ELECTROCHEMICAL STUDIES.....	154
5.5. SUMMARY AND PERSPECTIVES.....	156

List of Figures

Figure 1.1. The structure of the $[\text{Re}_6(\mu_3\text{-Q})_8]^{2+}$ cluster core shown with terminal ligands (T).....	19
Figure 2.1. Examples of (a) rods and (b) connectors.....	30
Figure 2.2. Pyridyl-based star-shaped connectors.....	32
Figure 2.3. Structural rendering of a prismatic cage prepared by Lu and coworkers.....	32
Figure 2.4. A Mandala-type pattern of porphyrins.....	33
Figure 2.5. An example of a tetrapyrrolylporphyrin and a phthalocyanine peripherally modified by metal complexes.....	34
Figure 2.6. A sketch of the thin layer electrode.....	40
Figure 2.7. (a) ^1H NMR spectra of 11 (bottom) and 13 (top). Only the aromatic resonances are shown. (b) ^{31}P NMR spectra of 8 (bottom) and 13 (top).....	44
Figure 2.8. MALDI-TOF Mass spectrum of 13	45
Figure 2.9. An ORTEP view (50% probability) showing two units of the cationic cluster core of 13 , in a staggered disposition with a separation of 11.27 Å between the central aromatic rings. Ethyl groups are omitted for clarity. Color schemes: C (gray), N (blue), P (purple), Re (green), Se (brown).....	49
Figure 2.10. Crystal packing of 13	50
Figure 2.11. Edge-on view of crystal packing of 13	51
Figure 2.12. (a) ^1H NMR spectra of 11 (bottom) and 14 (top). Only the aromatic resonances are shown. (b) ^{31}P NMR spectra of 8 (bottom) and 14 (top).....	53
Figure 2.13. MALDI-TOF mass spectrum of 14	54
Figure 2.14. An ORTEP view of a preliminary structure of 14	55

List of Figures - continued

Figure 2.15. Electronic spectra of 8 (—), 11 (—), and 13 (—).....	57
Figure 2.16. Electronic spectra of 12 (—) and 14 (—).....	58
Figure 2.17. The Gouterman four-orbital model and energy level representation of electronic excitation of porphyrins.....	58
Figure 2.18. The overlay of cyclic voltammograms of 8 and three "clusters of clusters" (9 , 13 , and 14) showing qualitatively the correlation of the number of cluster units and the number of electrons involved in the redox event....	60
Figure 2.19. ¹ H NMR of 15 (bottom), 16 (middle), and 17 (top).....	66
Figure 3.1. Representative porphyrin complexes studied by Toma and Anson.....	70
Figure 3.2. Structural representation of M(TCP), where M = 2H, Co ³⁺ , Mn ³⁺ , Zn ²⁺	73
Figure 3.3. The structure of [Mn(TPP)] ₄ [Re ₆ (μ ₃ -Se) ₈ (CN) ₆]. All hydrogen atoms are omitted for clarity.....	75
Figure 3.4. (a) ¹ H NMR spectra of 14 (bottom) and 19 (top). Only the aromatic resonances are shown. (b) ³¹ P NMR spectrum of 19	82
Figure 3.5. Electronic spectra of 19 (—), 20 (—), and 21 (—).....	85
Figure 3.6. Electronic spectra of non-cluster modified zinc porphyrin complex (—) and 22 (—).....	86
Figure 3.7. Cyclic voltammogram of 19	90
Figure 3.8. Cyclic voltammogram of 20	90
Figure 4.1. A generic dendrimer structure highlighting specific structural regions.....	94
Figure 4.2. Structural depiction of Gorman's first-generation dendrimer featuring a Fe ₄ S ₄ cluster at the core.....	96
Figure 4.3. Electronic spectra of 5 (—), 23 (—), and 24 (—).....	99

List of Figures - continued

Figure 4.4.	Representative dendrimers featuring surface-bound metal clusters.....	100
Figure 4.5.	Molecular structure of dendrimer supported by a cobalt carbonyl cluster....	101
Figure 4.6.	(a) ^1H NMR spectra of 25 (bottom) and 28 (top). Only the aromatic resonances are shown. (b) ^{31}P NMR spectrum of 28	109
Figure 4.7.	An ORTEP view (50% probability) showing the cationic cluster of 28 Color schemes: C (gray), N (blue), P (purple), Re (green), Se (brown).....	112
Figure 4.8.	(a) ^1H NMR spectra of 28 (bottom) and 31 (top). Only the aromatic resonances are shown. (b) ^{31}P NMR spectra of 28 (bottom) and 31 (top).....	116
Figure 4.9.	^{77}Se NMR spectra of 8 (bottom), 28 (middle), and 31 (top).....	117
Figure 4.10.	Electronic spectra of 28 (—), 29 (—), and 30 (—).....	120
Figure 4.11.	Electronic spectra of 31 (—), 32 (—), and 33 (—).....	120
Figure 4.12.	Cyclic voltammograms of 32 (bottom), 31 (middle), and 33 (top).....	123
Figure 4.13.	Cyclic voltammogram of 32	123
Figure 5.1.	Structures of representative polyhedral oligomeric silsesquioxanes.....	127
Figure 5.2.	Molecular structure of $\text{Zr}_6(\text{OH})_4\text{O}_4(\text{methacrylate})_{12}$	130
Figure 5.3.	Structural representation of the Mo_6Cl_8 cluster core.....	130
Figure 5.4.	Partial showing of the ^1H NMR spectra of 4-vinylpyridine (bottom) and 34 (top).....	144
Figure 5.5.	^{31}P NMR spectra of 35 (top), 34 (middle), and 36 (bottom).....	144
Figure 5.6.	An ORTEP view (50% probability) showing the cationic cluster core of 34 and 35 . Color schemes: C (gray), N (blue), P (purple), Re (green), Se (brown).....	149

List of Figures - continued

- Figure 5.7.** (a) Partial showing of the ^1H NMR spectra of **34** (bottom) and **37** (top). (b) ^{31}P NMR spectra of **34** (bottom) and **37** (top).....151
- Figure 5.8.** GPC trace of **37**.....152
- Figure 5.9.** Cyclic voltammograms of **34** and **37** in CH_3CN solutions. The current scale for the hybrid (**37**) has been normalized such that the voltammograms can be compared at the same effective molar concentration of clusters.....155

List of Tables

Table 2.1. Crystallographic Data and Structural Refinement of 13	47
Table 2.2. Selected bond lengths (Å) and angles (°) of 13	48
Table 2.3. Electronic Absorption Data of 13 and 14	56
Table 2.4. Electrochemical Data of 13 and 14	61
Table 3.1. Electronic Absorption Data of 19-22	85
Table 3.2. Electronic Absorption Data of 22 in Various Solvents.....	88
Table 3.3. Cluster-based Electrochemical Data of 19-22	89
Table 4.1. Crystallographic Data and Structural Refinement of 28	111
Table 4.2. Selected bond lengths (Å) and angles (°) of 28	112
Table 4.3. Electrochemical Data of 28-33	121
Table 5.1. Crystallographic Data and Structural Refinement of 34	146
Table 5.2. Crystallographic Data and Structural Refinement of 35	147
Table 5.3. Selected bond lengths (Å) of 34 and 35	148
Table 5.4. Selected bond angles (°) of 34 and 35	148

CHAPTER 1

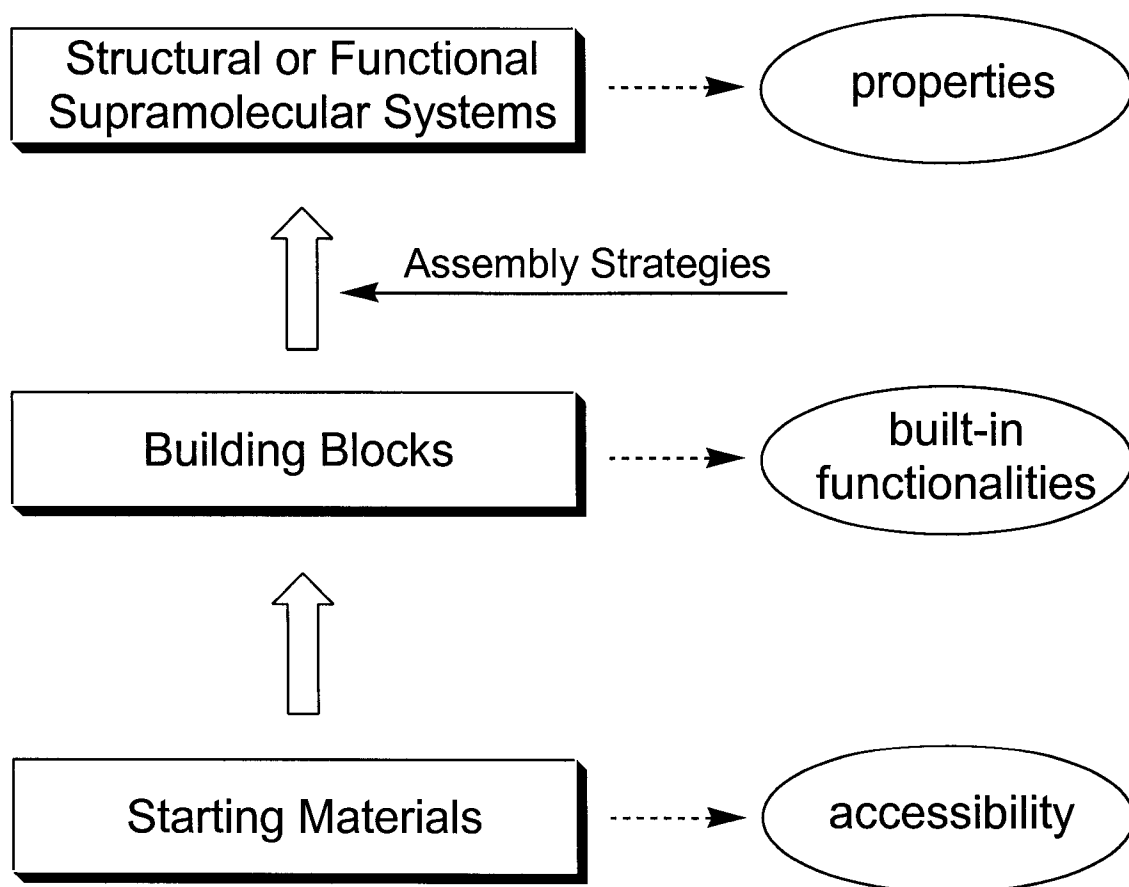
Metal Cluster-Supported Supramolecular Design and Discovery

Supramolecular chemistry, the "chemistry beyond the molecule", is based on the notion of creating novel structural and functional extended systems by linking prefabricated molecular or ionic building blocks via intermolecular interactions such as hydrogen bonding and metal-ligand coordination, among others.¹ Distinct aims and goals of this relatively nascent yet highly futuristic endeavor include (1) strategic and methodological concerns; (2) aesthetically motivated supramolecular synthesis based upon symmetry, topology, and network properties; and (3) efforts directed toward functional materials of practical importance.

The practice of supramolecular chemistry can be divided into three steps (Scheme 1.1). From the top down, the first step concerns the conception of a specific synthetic target. The primary impetus is the potential application of the supramolecular system to be realized. Such applications can be fundamental, practical, or simply derived from intellectual curiosity. The second step is to identify an appropriate building block or blocks for the targeted supramolecule. This is more or less in line with the strategy of retro-synthesis extensively employed in synthetic organic chemistry. The principal consideration involved in the design of these building blocks is whether these preformed components are capable of engaging in noncovalent interactions, as alluded to above, which will eventually lead to the formation of the supramolecular systems. Generally speaking, suitably functionalized building blocks are not commercially available, and therefore, need to be synthesized from

easily accessible starting materials. This constitutes the third step in this top-down scheme of rational supramolecular design. However, one should realize that, in principle, the creation of any supramolecules takes a "bottom-up" approach. By judiciously designing the building blocks and making use of various intermolecular forces to assemble these individual construction pieces, one has enormous control over the structure, property, and ultimately, function of the eventual supramolecular systems.

Scheme 1.1



Extensive research in the past few decades has produced numerous supramolecular constructs, many of which are not only of consummate structural beauty, but also have interesting and potentially useful properties.²⁻¹⁰ In the course of such studies, chemists have learned a great deal of the principles of supramolecular design, namely the intermolecular forces that glue the building blocks together.¹¹ Although there are certainly underlying principles and design rules yet to be discovered, further development in the immediate future of this highly interdisciplinary research field appears to hinge upon our creativeness to design and synthesize building blocks in order to manipulate and utilize the known intermolecular forces.

In light of this observation, over the past few years, the Zheng group has been focusing on the development of metal cluster-based building blocks and their applications for supramolecular construction. The term "cluster" takes on many meanings within the field of chemistry. To inorganic chemists, the definition most generally recognized is the one provided by Cotton, namely, "compounds containing a finite group of metal atoms which are held together entirely, mainly, or at least to a significant extent, by bonds directly between the metal atoms, even though some nonmetal atoms may be associated intimately with the cluster".¹² Sometimes for the sake of convenience, dinuclear complexes with metal-metal bonds are included as the starting point of the group clusters. The community has become increasingly forgiving, however, and under many circumstances, accepts the inclusion of polynuclear complexes such as polyoxometallates and oligomeric species of main group elements, $[\text{Al}(\text{OPr}^t)_3]_4$ for example, as clusters; the metal atoms are merely brought together through the agency of bridging ligands in these compounds.

The unique structural and functional properties of a metal cluster, both propitious to supramolecular design, are easily appreciated. First and foremost, the availability of multiple metal sites in a cluster allows for site-differentiation, that is, selective binding of purpose-specific ligands. A range of building blocks with systematically varied and rigidly fixed stereochemistry may be realized. The fixed stereochemistry imparts the shape and directionality critical to supramolecular synthesis. In contrast, supramolecular construction relying on the coordination of single metal ions is frequently complicated by flexible coordination. Fixing the stereochemistry of monocluster complexes usually constitutes the first, although nontrivial, step in the design of the building blocks. The expanded size of a cluster constitutes a second attractive feature of this unique class of building blocks, as dimensionally enlarged molecular or polymeric assemblies are expected. This aspect is particularly attractive for the preparation of porous solids with extra large pores - a class of materials that are being vigorously pursued for potential separation, storage, and sensing applications.¹³ Further, in terms of making functional supramolecular systems, metal clusters are unique and attractive because, in addition to the anticipated magnetic, electronic, optical, or catalytic properties associated with mononuclear metal complexes, clusters frequently exhibit interesting and potentially useful traits that are inherent to metal-metal bonded species.¹⁴ Thus, the efforts to build cluster-supported supramolecular structures are expected to offer many fascinating research problems with potentially significant ramifications. A number of groups have investigated the supramolecular chemistry of certain metal cluster systems. In some cases interesting properties and potentially important applications of the supramolecular materials have been identified. For example, Yaghi and coworkers

synthesized porous metal-organic frameworks supported by zinc carboxylate clusters showing capacity of methane and hydrogen storage.^{15,16} Using a trinuclear zinc cluster complex with an enantio-pure carboxylate ligand, homo-chiral metal-organic porous materials have been realized by Kim and coworkers for enantio-selective separation and catalysis.¹⁷ More recently, Cotton and coworkers have elaborated supramolecular constructions using metal-metal bonded dimeric clusters as building blocks.¹⁸ In a similar capacity, Shriver and coworkers have applied hexanuclear clusters containing the $[\text{Mo}_6(\mu_3\text{-Cl})_8]^{4+}$ core and bridging 4,4'-bipyridine ligands for the preparation of microporous xerogels that are capable of size-selective ion exchange.¹⁹ They have also created network structures of the hexamolybdenum clusters mediated by hydrogen bonding interactions.²⁰ Utilizing the structurally related octahedral tungsten cluster anion $[\text{W}_6(\mu_3\text{-S})_8(\text{CN})_6]^{6-}$ as a cluster complex-based ligand, three-dimensional extended coordination networks with a number of transition metal ions have recently been obtained.²¹

Stimulated by these previous efforts and also by the potential applications of metal chalcogenide clusters for heterogeneous catalysis, photovoltaics, and semiconductor fabrication,²² this dissertation work focuses on supramolecular construction by employing as building blocks the hexarhenium chalcogenide clusters containing the $[\text{Re}_6(\mu_3\text{-Q})_8]^{2+}$ (Q = S, Se, Te) core;^{23,24} these clusters structurally resemble the well-known superconducting Chevrel phases.²⁵

The 24-electron, face-capped cluster core can be viewed as an octahedron of rhenium atoms enclosed in a cube formed by substitutionally inert chalcogenide ligands

(Figure 1.1). Using the dimensional reduction protocol,²⁶ halide-terminated clusters of the general formula $[\text{Re}_6(\mu_3\text{-Q})_8\text{X}_6]^{4-}$ ($\text{X} = \text{Cl}, \text{Br}, \text{I}; \text{Q} = \text{S}, \text{Se}$) are obtained from high-temperature solid-state synthesis.^{27,28}

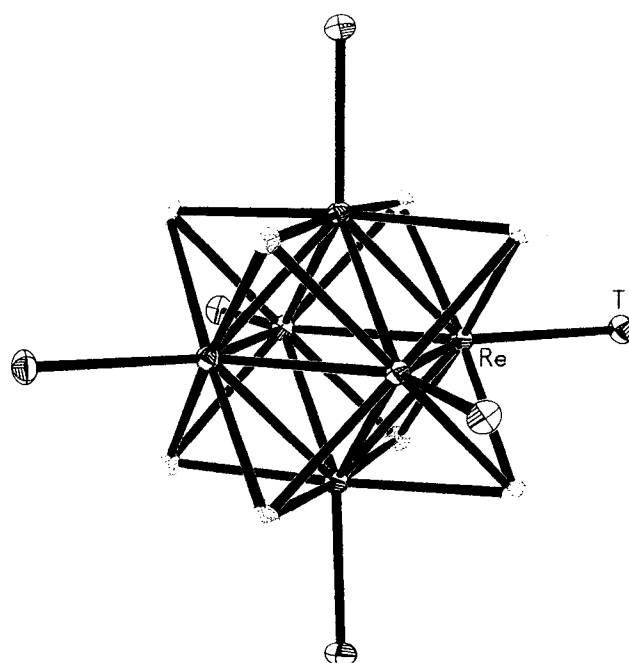


Figure 1.1. The structure of the $[\text{Re}_6(\mu_3\text{-Q})_8]^{2+}$ cluster core shown with terminal ligands (T).

The foundation of this cluster system's application in supramolecular synthesis is its favorable synthetic chemistry. Unlike their well-known isomorphs of the earlier transition metal halides or chalcogenides,^{29,30} these clusters are stable to aerobic handling and vigorous

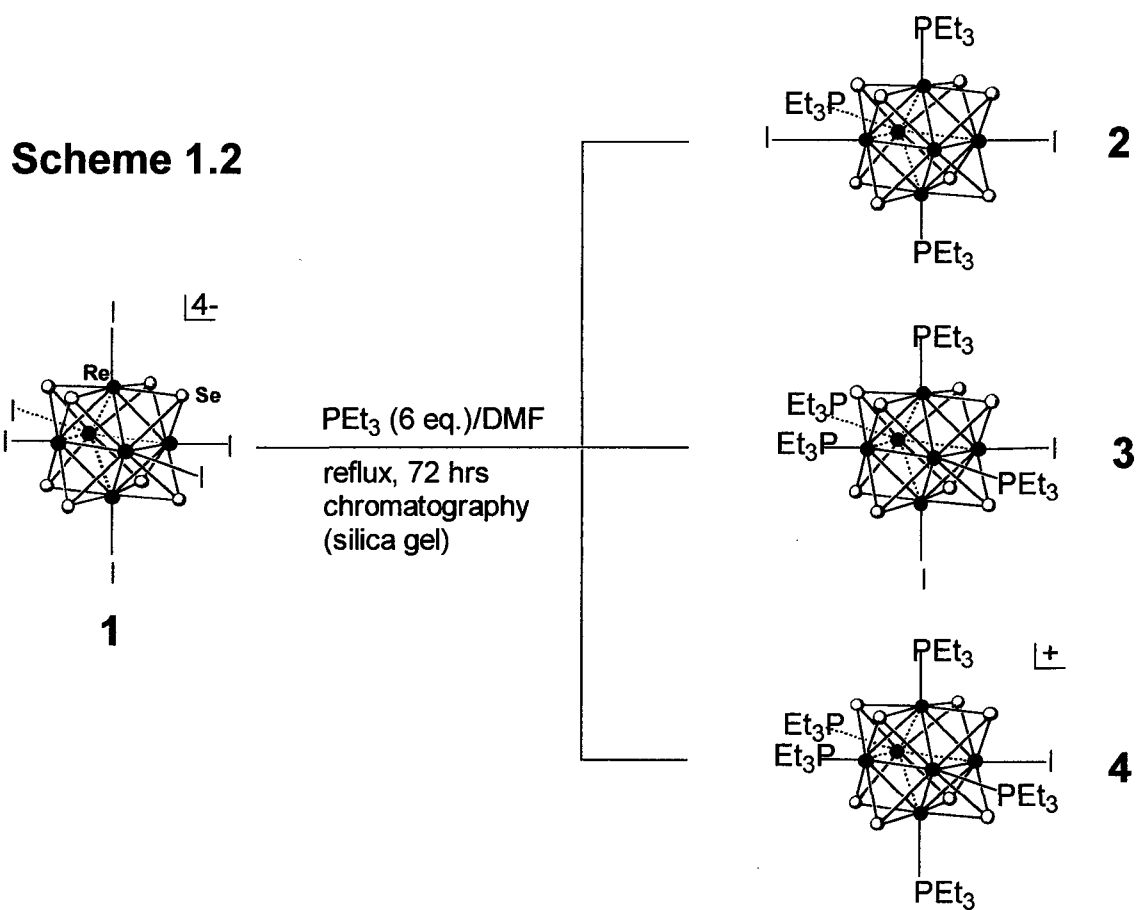
synthetic conditions, yet labile enough that multiple-step, solution-phase transformations are easily accomplished.³¹⁻³⁶ It has been found that the terminal halides of the starting cluster undergo facile ligand substitution reactions with triethylphosphine to yield site-differentiated complexes of the general formula $[\text{Re}_6(\mu_3\text{-Q})_8(\text{PEt}_3)_n\text{X}_{6-n}]^{(n-4)+}$ (Q = S: $n = 2-6$, X = Br⁻; Q = Se: $n = 4-6$, X = I⁻) (Scheme 1.2).^{31,34} Subsequent de-halogenation in coordinating media L, often a coordinating solvent, leads to corresponding derivatives of the general formula $[\text{Re}_6(\mu_3\text{-Q})_8(\text{PEt}_3)_n\text{L}_{6-n}]^{2+}$ with unperturbed stereochemistries (L = acetonitrile, Scheme 1.3).³¹⁻³⁴ The weakly coordinated solvent molecules offer increased reactivity for further chemical transformations. In the context of supramolecular design, the halide clusters can be viewed as the starting materials while the cluster solvates serve as the immediate precursors to the final supramolecular constructs via an appropriate assembly strategy. Of course, the cluster solvates can be further converted into other derivatives; with the desired functions for the final step of synthesis, these new derivatives, rather than the solvates, are now the building blocks.

More attractive from the perspective of creating novel functional materials are the interesting electrochemical and photophysical properties of these clusters. A reversible, one-electron oxidation event is typically observed.^{32,33} The parent and oxidized clusters exhibit markedly different absorption characteristics, and more intriguingly, both are luminescent and the luminescence is dependent on both the oxidation state and coordination environment of the cluster.³⁶⁻⁴⁰ These interesting traits, though not yet fully understood due largely to the complicated electronic structures of the cluster system, suggest the possibility of tuning the

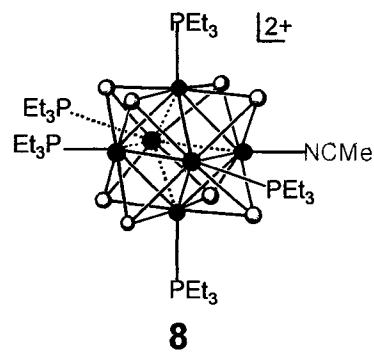
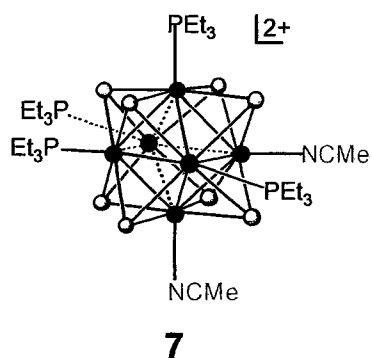
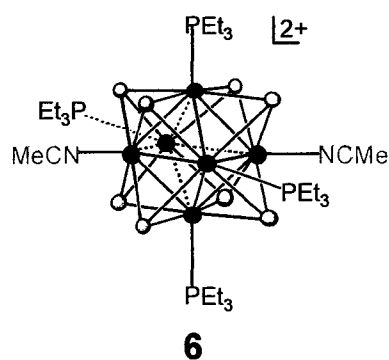
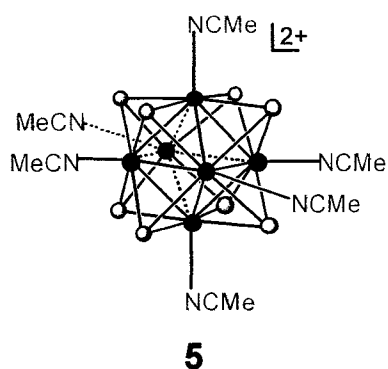
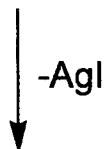
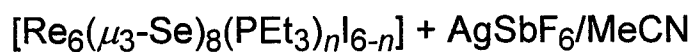
absorption and emission characteristics of the cluster by altering electrochemical conditions.

For example, electrochromic and electroluminescent materials featuring these clusters may

be envisaged.^{41,42}



Scheme 1.3



Indeed, the well-behaved chemistry and interesting electrochemical and photophysical properties have made these clusters the subject of recent intensive research. Recent literature has seen some impressive demonstrations of cluster-expanded networks with remarkable properties. For example, Long⁴³⁻⁴⁵ and Fedorov⁴⁶ have independently

prepared cyano ligand-bridged $[\text{Re}_6(\mu_3\text{-Q})_8]^{2+}$ cluster-metal framework solids, including cluster-expanded Prussian blue analogues by Long and coworkers.⁴³ Some of these materials display rather interesting host-guest chemistry that may be useful for sensory applications.^{44,45} Using the cluster core as a scaffold, Sasaki and coworkers attached six porphyrin units as ligands to the central cluster.⁴⁷ Kim and coworkers have prepared framework structures of manganese complexes utilizing the cyano complexes of the hexarhenium clusters as ligands,⁴⁸⁻⁵⁰ and have shown the potential of these arrays of metalloporphyrins to catalyze the oxidation of alkenes to epoxides.⁵⁰

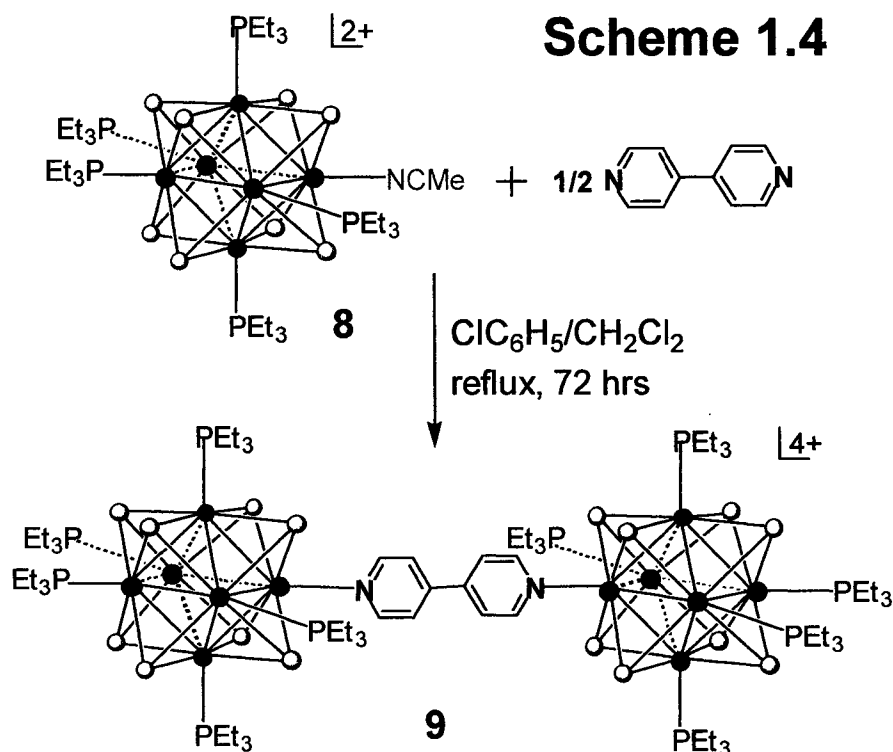
Rather than relying on a single highly symmetric building block such as $[\text{Re}_6(\mu_3\text{-Q})_8(\text{CN})_6]^{4+}$, more extensive and versatile supramolecular chemistry may be anticipated with the use of stereospecific cluster complexes featuring two different types of terminal ligands, one of which serves to protect certain metal sites, while the other provides the reactive sites necessary for subsequent supramolecular construction.⁵¹ The cluster core's relative inertness prohibits stereochemical scrambling, ensuring a fixed geometry for a given isomer. In effect, the site-differentiated clusters form a set of rigid building blocks with defined geometry that limit the structural possibilities of a multicluster array upon assembly and effectively eliminates the flexibility that frequently complicates supramolecular synthesis based on mononuclear and even dinuclear complexes.⁵²

The relevant stereospecific precursors for the supramolecular chemistry currently undertaken in the Zheng group are the acetonitrile solvates of the general formula $[\text{Re}_6(\mu_3\text{-Se})_8(\text{PEt}_3)_n(\text{MeCN})_{6-n}]^{2+}$ $\{n = 0$ (**5**), 4 [*trans*- (**6**) and *cis*- (**7**)], 5 (**8**) $\}$, readily prepared by deiodination of the corresponding $[\text{Re}_6(\mu_3\text{-Se})_8(\text{PEt}_3)_n\text{I}_{6-n}]^{(n-4)+}$ complexes with AgSbF_6 in the

presence of MeCN (Scheme 1.3).³¹⁻³³ In our investigation, these conveniently prepared solvates have acted as the geometric basis.

Their applications in actual supramolecular construction fall into two distinct methodologies. In one approach, the solvates react with specific multitopic ligands to create arrays, wherein a number of clusters are "condensed" by the bridging ligands with concomitant expulsion of the acetonitrile molecule(s) from the cluster solvates.^{33,53-56} The second method, representing something of a paradigm shift, entails solvent displacement by ligands that bear additional functional groups capable of secondary (with respect to primary cluster ligation) non-covalent interactions, such as hydrogen bonding and metal-ligand coordination.⁵⁷⁻⁶⁰ In this way, multicluster arrays mediated by the secondary interactions can be fabricated.

Some previous efforts have provided stimulation for the present work. Zheng and Holm have conceived and realized several dumbbell-shaped diclusters featuring two units of $[\text{Re}_6(\mu_3\text{-Se})_8(\text{PEt}_3)_5]^{2+}$ bridged by dipyridyl-based ditopic ligands (Scheme 1.4).³³ In addition, the first examples of molecular squares composed of four corner-occupying clusters and four bridging ligands have recently been prepared by Selby and coworkers (Scheme 1.5).⁵³ In addition to the appealing structures, these soluble, highly charged entities with nanosized pores invite examination of their potential of guest binding and activation, with an eye to possibilities in separation technology and homogeneous catalysis.

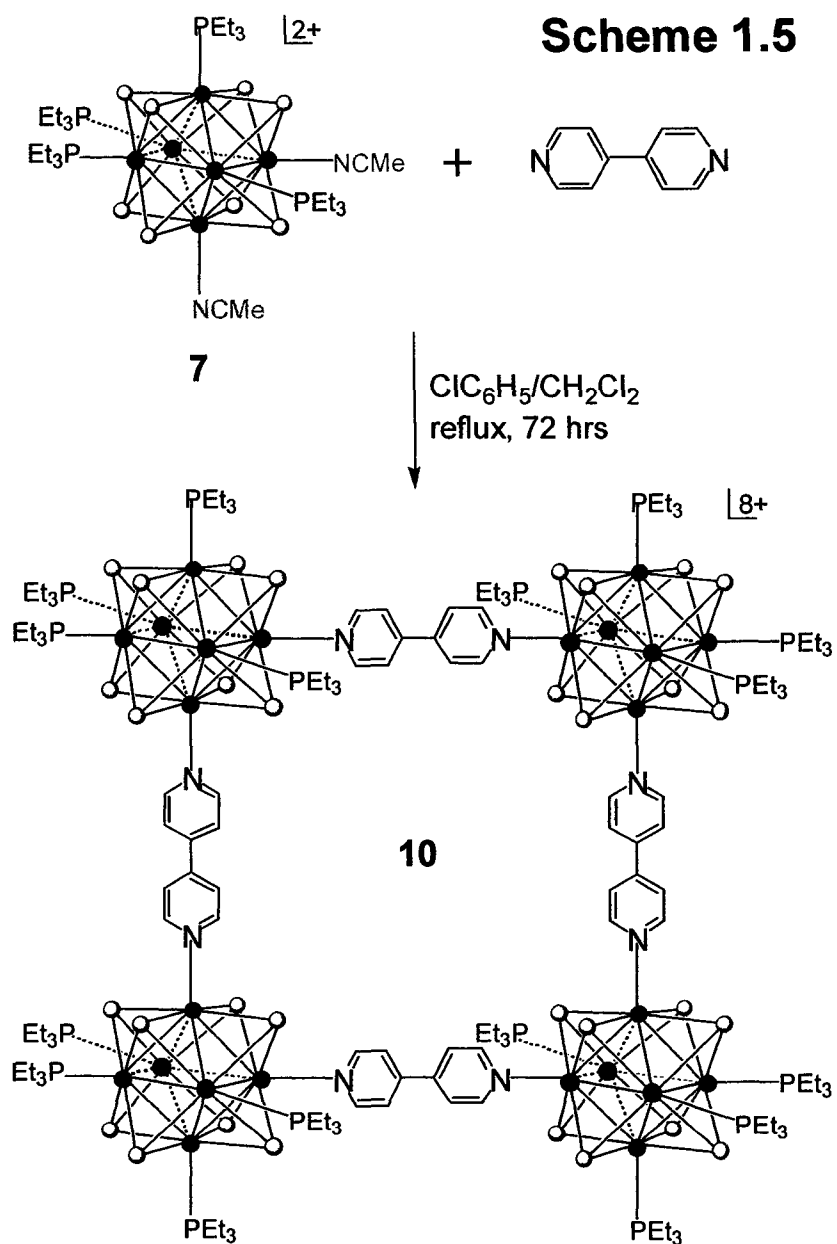


Detailed in this dissertation are the design, synthesis, characterization, and property investigation of a number of discrete and preprogrammed supramolecular architectures utilizing structurally well-defined hexanuclear octahedral rhenium chalcogenide clusters as the fundamental building blocks. Distinctly different from the aforementioned cluster dumbbells or cluster squares, the cluster arrays discussed herein are *geometrically divergent*, expanding into two and three dimensions. In **Chapter 2**, the construction of a molecular Tinkertoy set consisting of site-differentiated cluster solvates and two pyridyl-based star-shaped multitopic ligands is described.⁵⁴ The design, synthesis, and characterization of two-dimensional tri- and tetraclusters stationed at these planar platforms will be presented. Metallation of one of these novel cluster arrays, the tetrapyridylporphyrin-supported

tetracluster, is detailed in **Chapter 3**. Electronic spectroscopy and electrochemical studies of these cluster-studded metalloporphyrins are presented and discussed in the spirit of possibly designing new metalloporphyrin catalysts. The efforts to extend the molecular Tinkertoy approach to constructing even more sophisticated supramolecular systems, namely, cluster-supported dendritic architectures are detailed in **Chapter 4**. The very first examples of *bona fide* metallodendrimers of clusters featuring cluster building blocks at the core, within the branch, and on the periphery of a dendritic framework are presented.⁵⁶ Also provided is the successful application of ⁷⁷Se NMR techniques for the structural determination of these unique multicluster arrays, whose characterization is otherwise difficult.⁶¹ The work presented in Chapters 2-4 aims at creating novel supramolecular systems with the hope of identifying interesting and potentially useful properties; the research is therefore exploratory in nature. Representing a somewhat unconventional supramolecular design, cluster-polymer hybrid materials have been prepared by copolymerization of judiciously designed cluster-based monomers and styrene, and the demonstration-of-feasibility synthesis is detailed in **Chapter 5**. The characterization and electrochemical studies of these novel inorganic-organic hybrid materials is also discussed.⁶² This particular research project puts our synthetic efforts into an even broader context of supramolecular design and discovery, and offers a glimpse of what may be achieved in this exciting and rapidly growing research area.

Although we have explored a range of structural types and their synthetic methods, often with interesting and unexpected results, we are only at the beginning of a very exciting journey. With continuing efforts from our group and others, we anticipate many new

discoveries and rapid advancement of the chemistry of the $[\text{Re}_6(\mu_3\text{-Q})_8]^{2+}$ cluster chemistry and supramolecular chemistry in general.



CHAPTER 2

Star-Shaped Supramolecular Arrays of the $[\text{Re}_6(\mu_3\text{-Se})_8]^{2+}$ Core-Containing Clusters

Abstract

The reaction between the tritopic ligand 2,4,6-tri(4-pyridyl)-1,3,5-triazine (**11**) and $[\text{Re}_6(\mu_3\text{-Se})_8(\text{PEt}_3)_5(\text{MeCN})](\text{SbF}_6)_2$ (**8**), a hexarhenium(III) selenide cluster complex site-differentiated with five inert PEt_3 and one substitutionally labile MeCN ligands, produced a star-shaped tricluster array (**13**). An analogous reaction involving the same cluster solvate and 5, 10, 15, 20-tetra(4-pyridyl)-21*H*, 23*H*-porphine (**12**) led to the formation of a tetracluster array (**14**), where the component cluster units are supported by the tetratopic ligand. These novel "clusters of clusters" were characterized by microanalysis (CHN), NMR (^1H and ^{31}P), and MALDI-TOF mass spectrometry. Their molecular and solid-state structures were determined crystallographically. Cyclic voltammetry revealed one chemically reversible oxidation step corresponding to simultaneous removal of one electron from each of the cluster units. Attempts to create other extended arrays utilizing preformed multiclusters similar to **13** and **14** were made, and the preliminary results will be presented.

2.1 Introduction

One of the ultimate goals of supramolecular chemistry is to construct electronic, photonic, or mechanical devices using well-defined molecular.^{63,64} Although the applications of such molecular machinery remain in the realm of speculation, the challenges it presents have inspired the development of various synthetic strategies. One of these techniques is the creation of molecular "Tinkertoy" kits (analogous to the children's toy sets) which permits the assembly of complicated objects from a limited number of connectors and rods. In recent years, much attention has been devoted to the research of supramolecular arrays whose construction kit contains well-defined geometrical and functional connectors and rods that allow for precise control over the geometry and incorporation of specific properties within the resulting structure.^{6,15}

Present in the literature are numerous choices for both the connectors and rods. A rod can be a linear molecule that contains moieties at either end to permit coupling with connectors (a, Figure 2.1).⁶⁵⁻⁶⁸ Connectors can be divided into two broad categories, "points" and "stars"(b, Figure 2.1).^{7,69-74} Point connectors are bare central units with multitopic reactive sites capable of linking rod molecules at regular angles in a plane. Connectors of this type are typically transition metals ions or complexes. Although a large number of such connectors exist, most have limited synthetic use due largely to the lack of geometrical control about the central unit. In contrast, applications of star-shaped connectors have been very successful. Such a connector features a center carrying three or more rigid arms with terminal functionalities capable of coupling to a rod or to other star connectors. Planar star-

shaped connectors featuring a number of metal-coordinating sites arranged at fixed angles, **11** and **12** (Figure 2.2), for example, can introduce structural sophistication, such as branches, angles, or loops which are necessary for constructing geometrically complex supramolecules.

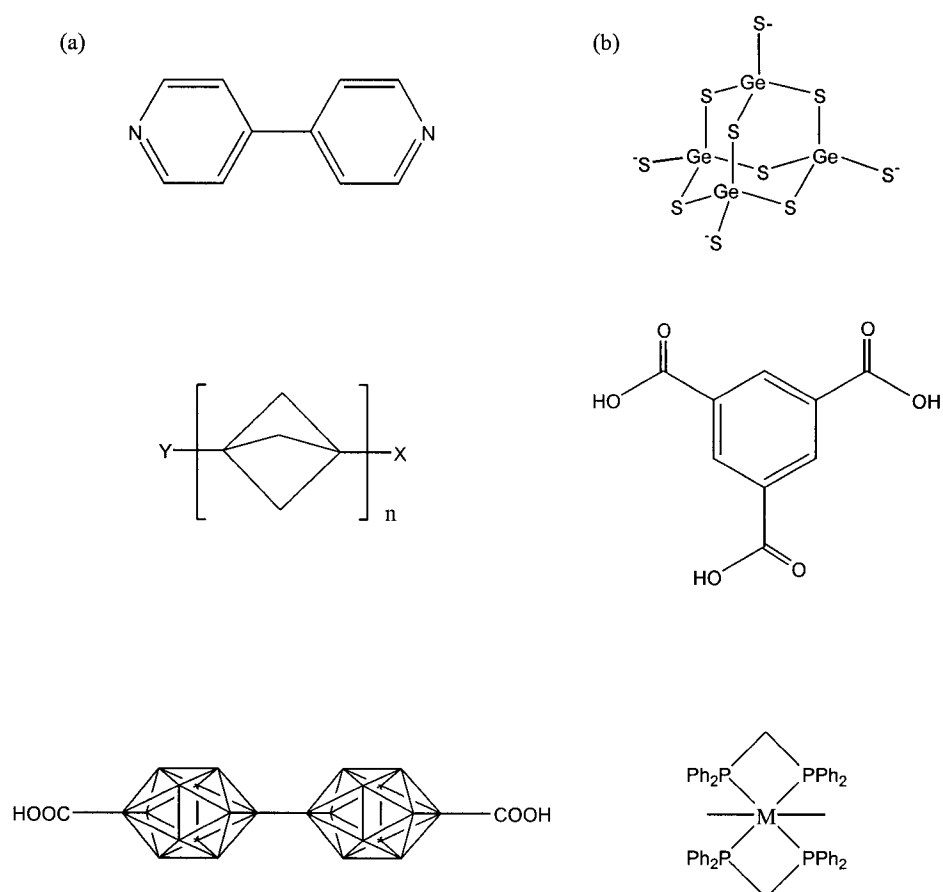


Figure 2.1. Examples of (a) rods and (b) connectors.

Two- and three-dimensional coordination polymers have been prepared using pyridyl-based star connectors.^{8,9,75-77} However, there are problems associated with assemblies of this kind. First, the geometry of the resulting structure can be difficult to predict. Second, there is little ability to manipulate the structure once the array is formed. Finally, such large assemblies can be prone to solubility problems. As a solution, the preparation of discrete assemblies containing star connectors is becoming increasingly popular. For example, Lu and coworkers have prepared a neutral prismatic cage by connecting two star ligands to six alkoxo-bridged rhenium centers (Figure 2.3).⁷⁸ Solvatochromic properties of the cage have been demonstrated. Lindsey, Sanders, and others⁷⁹⁻⁹² have utilized the molecular Tinkertoy methodology to create porphyrin and mixed porphyrin-phthalocyanine assemblies. The first of these arrays contains one central metalloporphyrin connector linked through alkynyl benzene rods to four other metalloporphyrins to form a large tetra-pointed star-shaped structure. Continued research in this area has culminated in the preparation of a supramolecular array composed of twenty-one linked porphyrins with a Mandala-type pattern (Figure 2.4).⁹³ In efforts to incorporate other potentially useful properties into such supramolecular arrays, metal complexes have been attached to the periphery of porphyrins and phthalocyanines. These additional functional groups include ruthenium⁹⁴⁻⁹⁶ and osmium complexes⁹⁷ and ferrocene⁹⁸⁻¹⁰¹ (Figure 2.5).

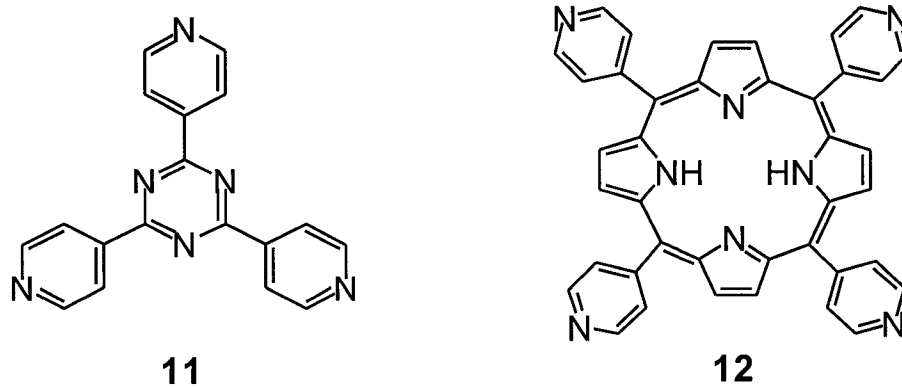


Figure 2.2. Pyridyl-based star-shaped connectors.

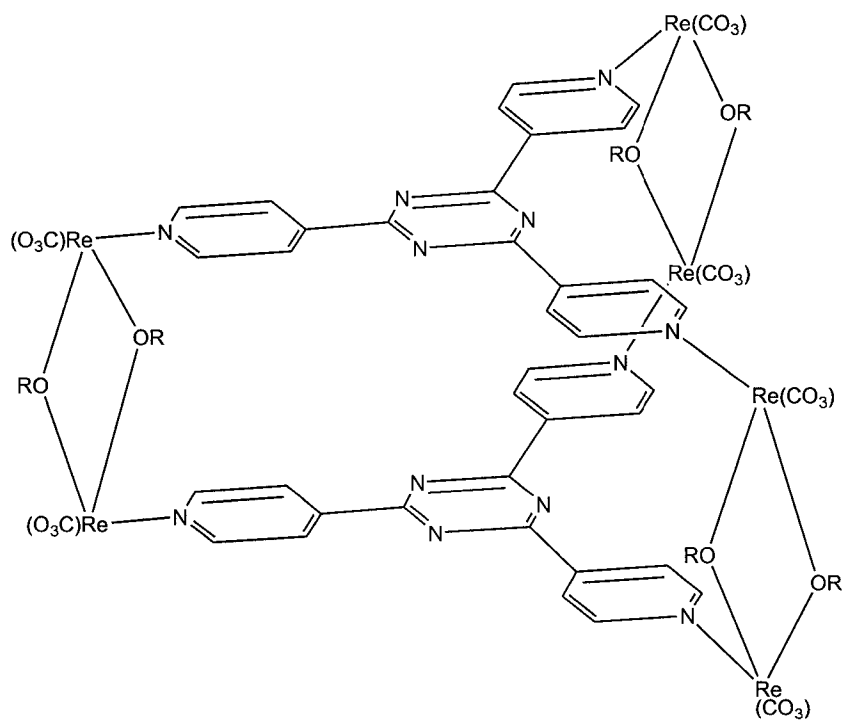


Figure 2.3. Structural rendering of a prismatic cage prepared by Lu and coworkers.

Metal clusters owing to their well-defined geometry and intrinsically interesting electronic, photophysical, magnetic, and catalytic properties are excellent choices for building functional supramolecular structures. Surprisingly, they have only recently been recognized in this capacity.

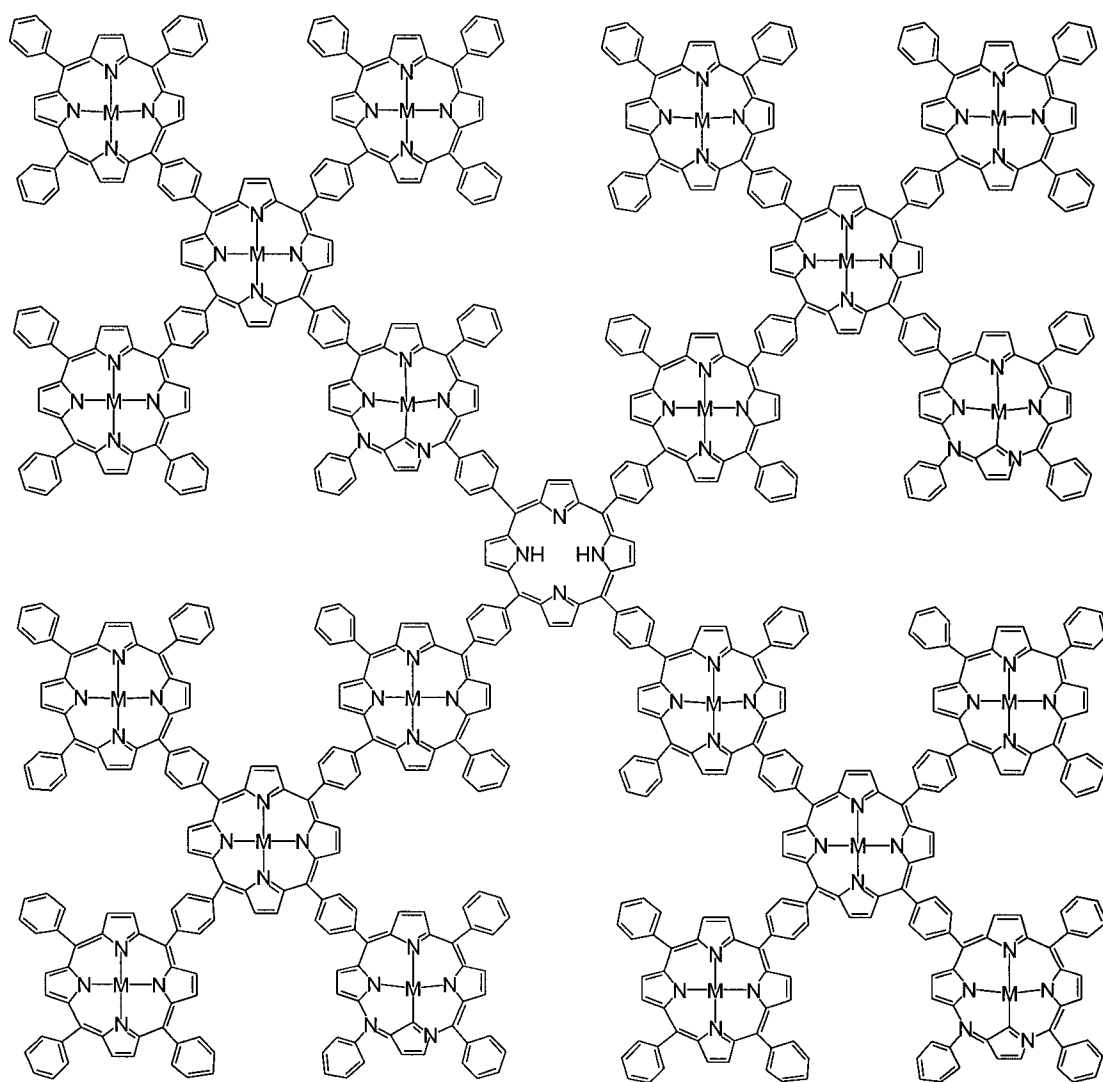


Figure 2.4. A Mandala-type array of porphyrins.

For example, Toma and coworkers have prepared μ_3 -oxo-triruthenium clusters supported by a central tetrapyrridylporphyrin.¹⁰²⁻¹⁰⁶ They have also studied extensively the interesting electrochemical properties of these novel materials. Applications of other potentially interesting clusters in a similar role may be envisioned. One candidate is the structurally well-defined hexanuclear clusters. Albeit a recent development in transition metal cluster chemistry, the $[\text{Re}_6(\mu_3\text{-Se})_8]^{2+}$ core-containing clusters have received much attention due largely to their well-behaved chemistry and interesting electrochemical and photophysical properties.

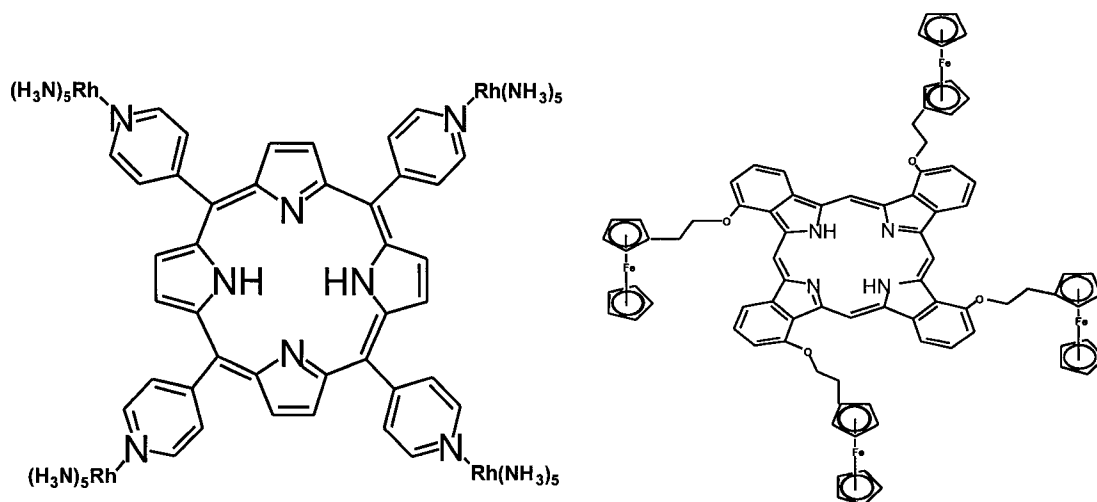


Figure 2.5. An example of a tetrapyrridylporphyrin and a phthalocyanine peripherally modified by metal complexes.

This chapter describes the creation of a new molecular Tinkertoy set composed of solvates of the $[\text{Re}_6(\mu_3\text{-Se})_8]^{2+}$ core-containing clusters and two star-shaped connectors. The assemblies of supramolecular arrays featuring multiple clusters stationed on the planar divergent connectors are also detailed here. The potentially interesting electronic structures of these cluster arrays add interest to these novel supramolecules. Furthermore, with appropriate modification to the cluster building blocks, formation of even more extended arrays of the clusters with new interesting properties may be possible.

2.2. Experimental

General Considerations.

5, 10, 15, 20-Tetra(4-pyridyl)-21*H*, 23*H*-porphine (**12**), (*n*-Bu₄N)PF₆, and AgSbF₆ were purchased from Aldrich and used as received. 2,4,6-tri(4-pyridyl)-1, 3, 5-triazine (**11**) and cluster complexes **4** and **8** were prepared according to published procedures.³¹⁻³³ The silica gel (mesh size 200-400) used for column chromatography was purchased from Natland International Corporation, Research Triangle Park, North Carolina. ¹H and ³¹P NMR spectra were recorded on a Varian Unity-300 spectrometer in CD₂Cl₂. Chemical shifts of ³¹P spectra were referenced to 85% H₃PO₄ (δ = 0 ppm, with negative values meaning upfield). NMR resonance multiplicities are designated: s (singlet), d (doublet), t (triplet), q (quartet), and m (multiplet). Elemental analyses (CHN) were performed by Desert Analytics Laboratory, Tucson, Arizona.

Complex 13. A mixture of **8** (274 mg, 0.0962 mmol) and **11** (10.0 mg, 0.0323 mmol) in 30 mL of chlorobenzene was stirred under reflux for 72 hours. The orange-red residue obtained upon removal of solvent was dissolved in 5 mL of dichloromethane, and the solution was triturated with ether to give an orange-colored powder. Recrystallization (ether/dichloromethane) produced light-brown crystals. Yield: 200 mg (72.2%). ¹H NMR: 1.00-1.20(m), 2.10-2.30(m), 8.45(d), 9.56(s). ³¹P NMR: -25.05(s), -28.59(s). MS: m/z 2679.4 [M-3SbF₆]³⁺, 1951.0 [M-4SbF₆]⁴⁺. Anal. Calcd. Re₁₈Se₂₄P₁₅N₆C₁₀₈H₂₃₈Sb₆F₃₆: C,

14.8; H, 2.72; N, 0.96. Found: C, 15.95; H, 2.82; N, 0.98.

Complex 14 was obtained as a purple-red powder in a manner similar to complex **13** except that **12** was used in place of **11**. Upon recrystallization using ether and dichloromethane, dark red crystals were obtained Yield: 157 mg (82.0%). ^1H NMR: -3.00 (s), 1.05-1.30(m), 2.10-2.40(m), 8.18(d), 9.04(s), 9.72(d). ^{31}P NMR: -23.64(s), -27.59(s). MS: m/z 2729.4 $[\text{M}-4\text{SbF}_6^-]^{4+}$, 2137.9 $[\text{M}-5\text{SbF}_6^-]^{5+}$, 1742.5 $[\text{M}-6\text{SbF}_6^-]^{6+}$, 1459.2 $[\text{M}-7\text{SbF}_6^-]^{7+}$. Anal. Calcd. for $\text{Re}_{24}\text{Se}_{32}\text{P}_{20}\text{N}_8\text{C}_{160}\text{H}_{324}\text{Sb}_8\text{F}_{48}$: C, 16.19; H, 2.73; N, 0.94. Found: C, 16.50; H, 2.75; N, 0.98.

Trans-[Re₆(μ₃-Se)₈(PEt₃)₄(MeCN)(I)](SbF₆) (15). To a solution of **2** (479 mg, 0.193 mmol) in 300 mL of dichloromethane was added a solution of AgSbF₆ (66.0 mg, 0.193 mmol) in 10 mL of acetonitrile over 10 hours in a dark room maintained at 5 °C. The red residue obtained after removal of solvent was treated with 20 mL of dichloromethane. The resulting mixture was filtered through a plug of Celite, and the filtrate was collected. The red residue obtained upon removal of the solvent was subjected to flash column chromatography using silica gel and an eluting solvent of dichloromethane and acetonitrile (v/v 20:1; R_f = 0.50). Yield: 329 g (65.4%). ^1H NMR: 1.05-1.24(m), 2.10-2.30(m), 2.82(s). ^{31}P NMR: -21.44(s). MS: m/z 2625.4 $[\text{M}^+]$.

Trans-[Re₆(μ₃-Se)₈(PEt₃)₄(isonicotinamide)(I)](SbF₆) (16). A mixture of **15** (150 mg, 0.0578 mmol) and isonicotinamide (240 mg, 1.96 mmol) in 50 mL of chlorobenzene/nitromethane (v/v 5:1) was stirred under reflux for 12 hours. The orange-red residue obtained upon removal of the solvent was extracted using dichloromethane and

water (4 x 50 mL). The organic phase was dried over anhydrous MgSO_4 . The red residue obtained upon removal of the solvent was subjected to flash column chromatography using silica gel and an eluting solvent of dichloromethane and acetonitrile (v/v 5:1; $R_f = 0.75$). Yield: 142 mg (92.5%). ^1H NMR: 1.05-1.24(m), 2.10-2.35(m), 6.42(s), 6.96(s), 7.58(d), 9.39(d). ^{31}P NMR: -21.39(s).

***Trans*-[$\text{Re}_6(\mu_3\text{-Se})_8(\text{PEt}_3)_4(\text{isonicotinamide})(\text{MeCN})](\text{SbF}_6)_2$ (17).** To a solution of **16** (80 mg, 0.029 mmol) in 30 mL of dichloromethane/acetonitrile (v/v 1:1) was added AgSbF_6 (66 mg, 0.085 mmol). The mixture was stirred in a dark room maintained at 5°C for 30 minutes, exposed to light for 2 hours, and then filtered to afford a light orange solution. The red-orange residue obtained upon removal of the solvent was treated with 10 mL of dichloromethane. The resulting mixture was filtered through a plug of Celite, and the filtrate was collected. Upon recrystallization from ether and dichloromethane, orange-red crystals were obtained. Yield: 787 mg (93.1%). ^1H NMR: 1.08-1.20(m), 2.24-2.35(m), 2.69(s), 6.42(s), 6.98(s), 7.58(d), 9.36(d). ^{31}P NMR: -16.65(s).

Other Physical Measurements.

Electronic absorption spectra in dichloromethane solutions were recorded on a Perkin Elmer Lambda 10 spectrophotometer. Mass spectrometry data were collected on a Bruker Reflex III MALDI-TOF instrument. Dithranol (DTH) was used as the matrix. The samples were mixed with saturated DTH solutions in a 1:10 ratio so that the estimated sample/matrix ratio was about 1:100 on the MALDI plate. An N_2 laser (337 nm) was used to ionize the samples. The reflectron was used to achieve a good enough resolution (> 5000) to separate

the isotopes. The acquisition file was optimized for the range of m/z 1000-3500 by using a peptide mixture. Cyclic voltammograms were acquired with an EG&G Instruments 283 potentiostat, using 500- μm diameter Pt working electrode, a Pt counter electrode, and an Ag/AgCl pseudo-reference electrode freshly prepared by plating a thin layer of AgCl onto a Ag wire from a saturated KCl solution at 100 mV/s. $(n\text{-Bu}_4\text{N})\text{PF}_6$ (0.1 M acetonitrile solution) was used as the supporting electrolyte. The working electrode was cleaned between each experiment by polishing with 0.3- μm alumina paste for 1 minute, followed by copious solvent rinses. After each voltammetric experiment, ferrocene was added (ca. 1 mM). An additional voltammogram was then recorded, and the potential axis was calibrated against the formal potential of the ferrocenium/ferrocene (Fc^+/Fc) redox couple.

An electrode was designed such that coulometry measurements could be made using the above setup for standard cyclic voltammetry, where the working electrode is simply replaced with a thin layer electrode (TLE) (Figure 2.6). A 0.25-mm diameter Pt wire was threaded through a 0.7-mm inner diameter (ID) glass capillary tube and the distal end was fused, such that 6-mm of Pt wire extended beyond the distal end of the capillary. A 0.4-mm glass capillary tube was cut to 7 mm and was used to sheath the exposed Pt wire. A small kink in the wire near the distal end of the larger capillary was sufficient to hold the sheath in place, producing a thin open layer surrounding the wire with a theoretical gap of 75 μm and a volume of approximately 0.5 μL . The TLE was stabilized by threading the entire assembly through a fritted glass holder with an NMR septum cap. This entire assembly is placed in the solution cell, and the distal end is submerged (2-5 mm) into the analyte

solution, causing the solution to reproducibly fill the entire cavity created between the Pt wire and the small capillary as a result of capillary action. Thin-layer cyclic voltammograms were collected at 1 mV/s, and the cell volume was first calibrated using a 1 mM solution of ferrocene.

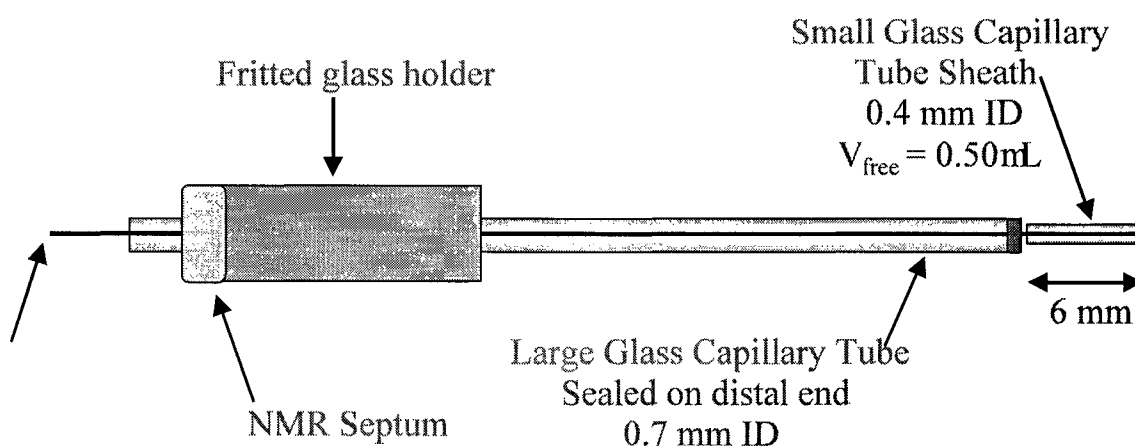


Figure 2.6. A sketch of the thin layer electrode.

X-ray Structure Determinations.

Single crystals suitable for X-ray diffraction were grown from a dichloromethane solution by ether vapor diffusion. A red rod of **13** having approximate dimensions of 0.15 x 0.15 x 0.30 mm was mounted on a glass fiber in a random orientation. Data were collected on the SMART1000 system using graphite monochromated Mo K α radiation ($\lambda=0.71073\text{\AA}$).

Cell constants and an orientation matrix for integration were determined from reflections obtained in three orthogonal 5° wedges of reciprocal space. A total of 3736 frames at 1 detector setting covering $0^\circ < 2\theta < 60^\circ$ were collected, having an omega scan

width of 0.2° and an exposure time of 30 seconds. The frames were integrated using the Bruker SAINT software package's narrow frame algorithm. A total of 91310 reflections were integrated and retained, of which 4640 were unique. Of the unique reflections, 2674 (57.6%) were observed $I > 2\sigma(I)$. Empirical absorption and decay corrections were applied using the program SADABS.

The structure was solved using SHELXS in the Bruker SHELXTL (Version 5.0) software package. Refinements were performed using SHELXL, and illustrations were made using XP and XShell. Solution was achieved utilizing direct methods followed by Fourier synthesis. Hydrogen atoms were added at idealized positions, constrained to ride on the atom to which they are bonded and given thermal parameters equal to 1.2 or 1.5 times U_{iso} of that bonded atom. Due to the low data to parameter ratio, only the best defined atoms were refined anisotropically. The final anisotropic full-matrix least squares refinement based on F^2 of all reflections converged (maximum shift/esd = 0.011) at $R1 = 0.1865$, $wR2 = 0.2792$, and goodness-of-fit = 1.115. "Conventional" refinement indices using the 2674 reflections with $F > 4 \sigma(F)$ are $R1 = 0.0910$, $wR2 = 0.1962$. The model consisted of 543 variable parameters, 0 constraints, and 207 restraints. There were 24 correlation coefficients greater than 0.858. The highest and lowest peaks on the final difference map were 1.529 and -1.235 $e/\text{\AA}^3$, respectively. Scattering Factors and anomalous dispersion were taken from International Tables Vol C Tables 4.2.6.8 and 6.1.1.4.

2.3. Synthesis and Characterization

Utilizing the pentaphosphine-substituted nitrile solvate **8** and the star-shaped connectors **11** and **12**, two-dimensional cluster-based supramolecules were obtained, wherein three or four cluster units are attached to the planar scaffold (**13** and **14**, Scheme 2.1). Spectroscopic and structural characterizations of these assemblies are discussed below.

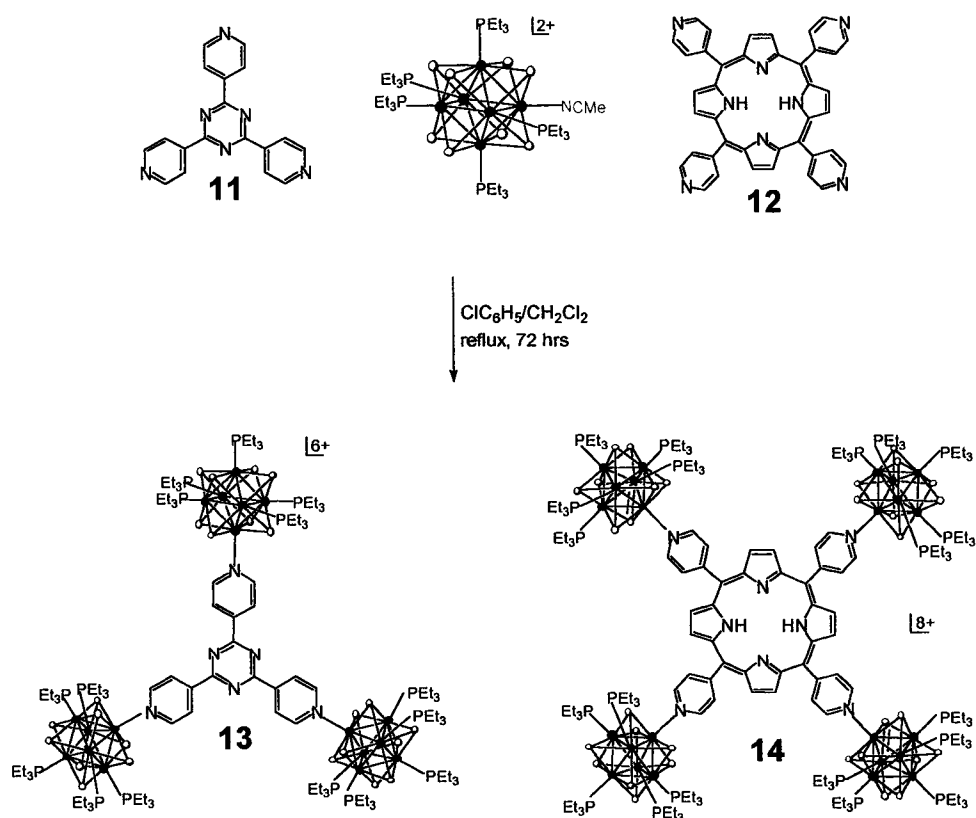
2.3.1. Synthesis of a Star-Shaped Tricluster

This supramolecular complex features three units of $[\text{Re}_6(\mu_3\text{-Se})_8(\text{PEt}_3)_5]^{2+}$ attached to a central tritopic pyridyl-based ligand via N-Re coordination. The synthesis takes advantage of the substitutional lability of the coordinated nitrile molecule of **8** when reacted with pyridyl-based ligands (Scheme 1.4). Thus, reacting stoichiometric amounts of **8** and **11** in chlorobenzene under reflux led to the displacement of the solvent ligand and the concomitant formation of the tricluster **13**. This cluster array is soluble in dichloromethane, acetonitrile, and other common polar organic solvents to yield brown-red solutions.

Several lines of spectroscopic evidence supported the successful production of **13**. Upon formation of **13**, the ^1H signal of the coordinated nitrile of **8** disappears, indicating the displacement of the previously attached solvent molecule. This is accompanied by a new signal corresponding to the $\alpha\text{-H}$ of the coordinated pyridyl moieties at 9.56 ppm (top, a, Figure 2.7) which is shifted by 0.62 ppm downfield from that of the free ligand (bottom, a,

Figure 2.7). There is also a small but noticeable upfield shift of the β -H of the pyridyl moiety from 8.62 to 8.45 ppm. The simplicity of the ^1H NMR spectrum is consistent with the anticipated symmetric structure. The unsophisticated ^{31}P NMR spectrum of **13** (b, top, Figure 2.7), showing two resonances at -25.05 and -28.59 ppm in a 4:1 relative ratio consistent with the stereochemistry of a pentaphosphine-substituted isomer, serves as further evidence supporting the highly symmetrical construction.

Scheme 2.1



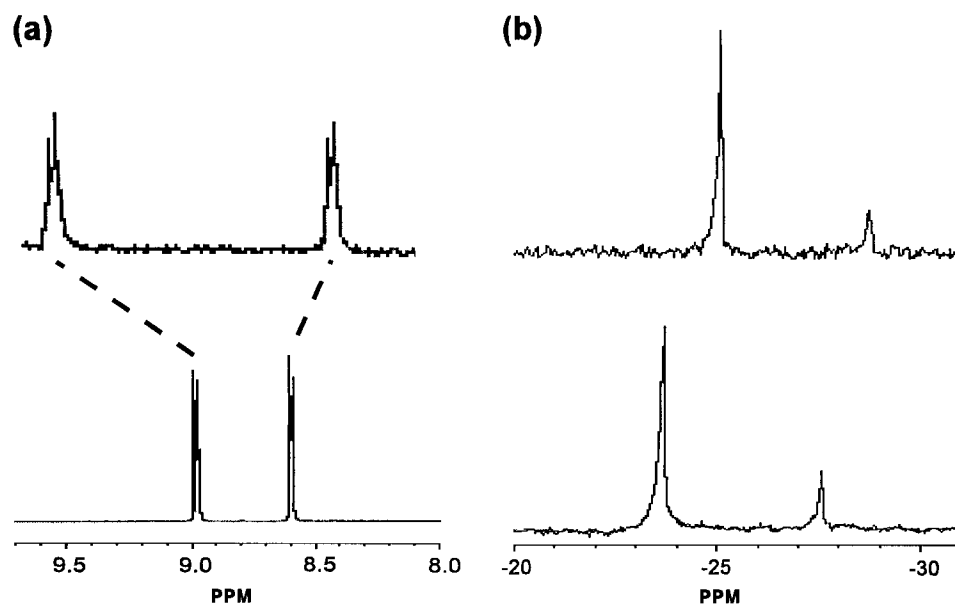


Figure 2.7. (a) ^1H NMR spectra of **11** (bottom) and **13** (top). Only the aromatic resonances are shown. (b) ^{31}P NMR spectra of **8** (bottom) and **13** (top).

MALDI-TOF mass spectrometry revealed two major envelopes centering at 2679.4 and 1951.0 a.m.u, corresponding to the molecular ion less 3 and 4 counter ions, respectively (Figure 2.8). The existence of the tricluster **13** is clearly suggested. The composition of **13** is further confirmed by satisfactory elemental analyses (CHN).

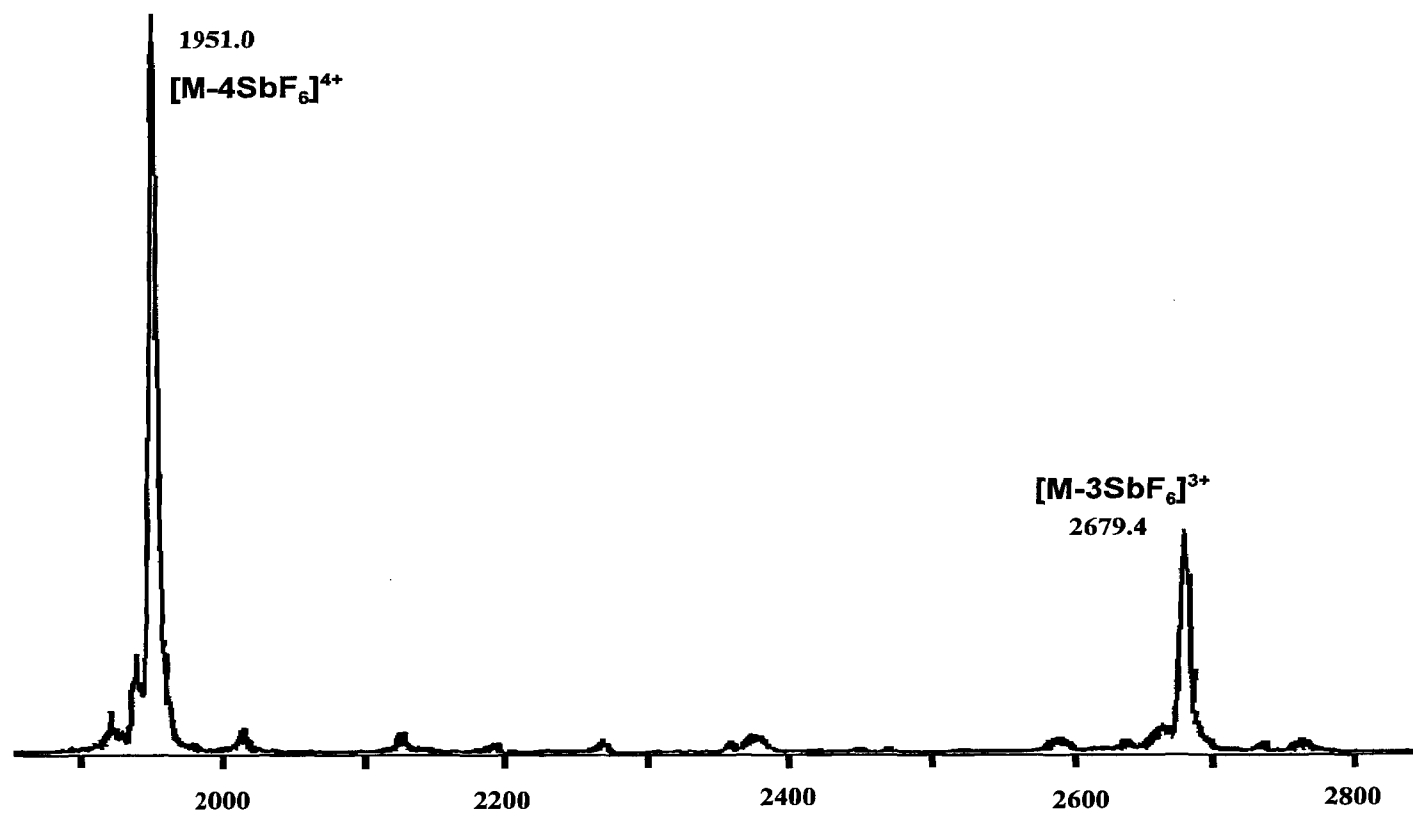


Figure 2.8. MALDI-TOF mass spectrum of 13.

2.3.2. X-ray Structural Determination of 13

Reported in Table 2.1 are the crystallographic data and structural refinement parameters. The metrical parameters describing the cluster core and its terminal bonding are summarized in Table 2.2. As shown in Figure 2.9, the $[\text{Re}_6(\mu_3\text{-Se})_8]^{2+}$ cluster core consists of a regular Re_6 octahedron which closely approaches O_h symmetry and is concentric with an Se_8 cube. However, this symmetry is somewhat disrupted by the terminal ligands, which lie slightly and irregularly displaced from their ideal positions along the four-fold axes. The mean Re-Re bond distance of 2.623(5) Å, is comparable to that observed in other $[\text{Re}_6(\mu_3\text{-Se})_8]^{2+}$ core-containing complexes and corresponds to a Re-Re single bond. The trigonal symmetry of the complex cation contributes to the trigonal symmetry of the space group. The packing is dominated by the formation of pseudo-dimers in which two cations interlock to form a unit. The two central rings in a pseudo-dimer unit are separated by 11.26 Å. The distance between the mean planes of two closest rings in different pseudo-dimer units is 7.51 Å (Figures 2.10 and 2.11). Within a unit cell there are four layers, each of which contains one complex cation and three anions. The remaining cations and solvent fit in between layers and between pseudo-dimers in the same stack.

Table 2.1. Crystallographic Data and Structural Refinement of **13**.

Empirical formula	$C_{108}H_{237}F_{36}N_6O_{9.05}P_{15}Re_{18}Sb_6Se_{24}$
Formula weight	8897.73
Crystal size	0.30 x 0.15 x 0.15 mm
Crystal system	Trigonal
Space group	<i>P</i> -31c
Unit cell dimensions	$a = 16.960(2) \text{ \AA}$ $b = 20.695(2) \text{ \AA}$ $c = 20.184(6) \text{ \AA}$
Volume, <i>Z</i>	22822(4) \AA^3 , 4
Density, calcd. Mg/m ³	2.590
Abs. coeff., mm ⁻¹	14.196
<i>F</i> (000)	16096
Theta range for data collection	1.85 to 17.25°
Limiting indices	$-22 \leq h \leq 22, -22 \leq k \leq 22, -31 \leq l \leq 31$
Reflections utilized	91310
Independent reflections	4640 [R(int) = 0.2629]
Data/restraint/parameter	4640/207/543
<i>GOF</i> on <i>F</i> ²	1.115
R indices [<i>I</i> > 2σ(<i>I</i>)]	R1 = 0.0910, wR2 = 0.1962
R indices (all data) ^a	R1 = 0.1865, wR2 = 0.2792

$$^a R1 = \frac{\sum ||F_o| - |F_c||}{\sum |F_o|}, wR2 = \left\{ \frac{\sum [w(F_o^2 - F_c^2)^2]}{\sum [w(F_o^2)^2]} \right\}^{1/2}.$$

Table 2.2. Selected bond lengths (Å) and angles (°) of **13**.

Bond lengths	
Re-Re	2.605(5)-2.642(5); mean 2.623
Re-Se	2.466(10)-2.518(10); mean 2.498
Re-P	2.45(15)-2.49(14); mean 2.47
Re-N	2.17(3)
Bond angles	
Re-N-C	120(2) and 120(2)

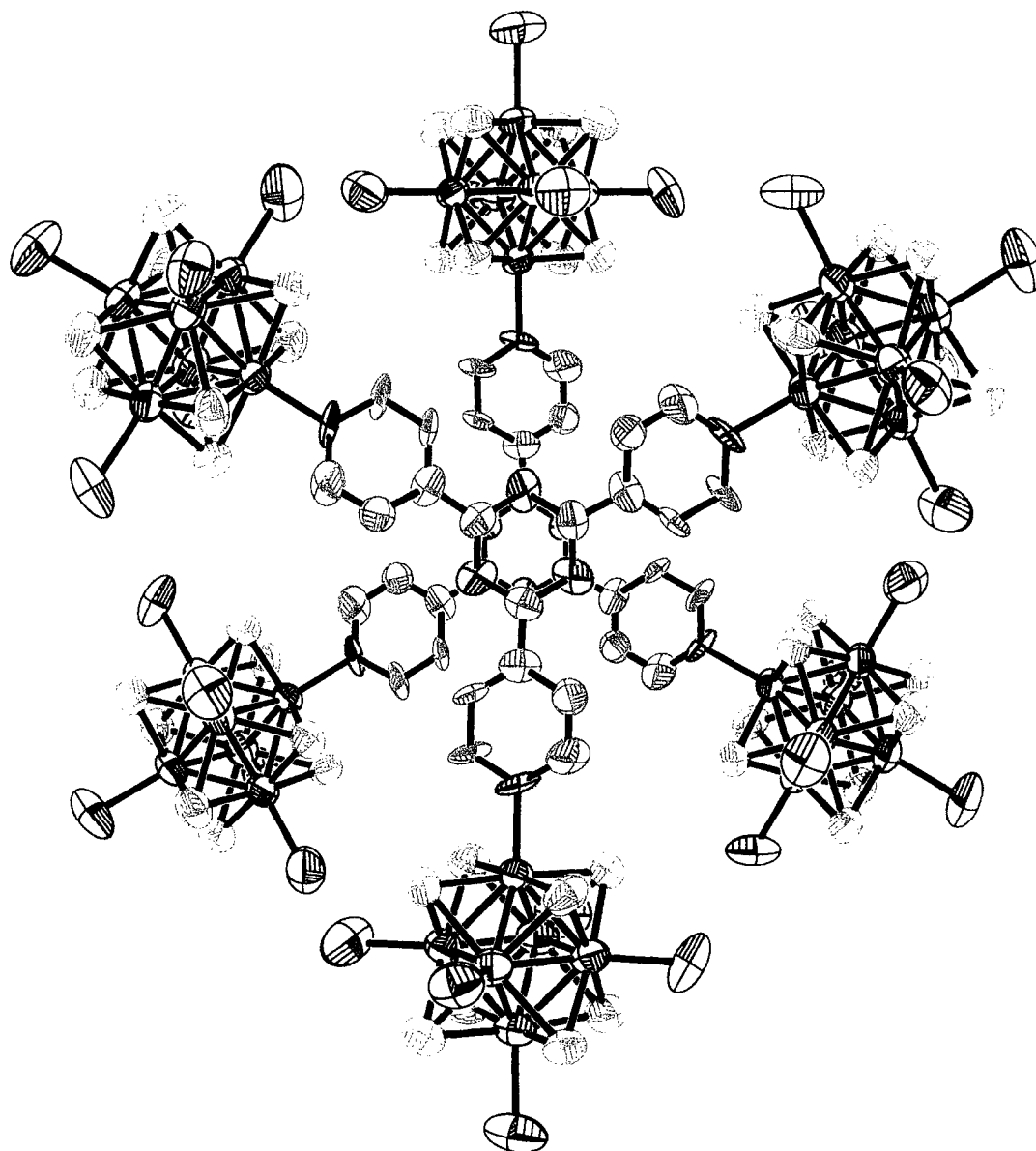


Figure 2.9. An ORTEP view (50% probability) showing two units of the cationic cluster core of **13**, in a staggered disposition with a separation of 11.27 Å between the central aromatic rings. Ethyl groups are omitted for clarity. Color schemes: C (gray), N (blue), P (purple), Re (green), Se (brown).

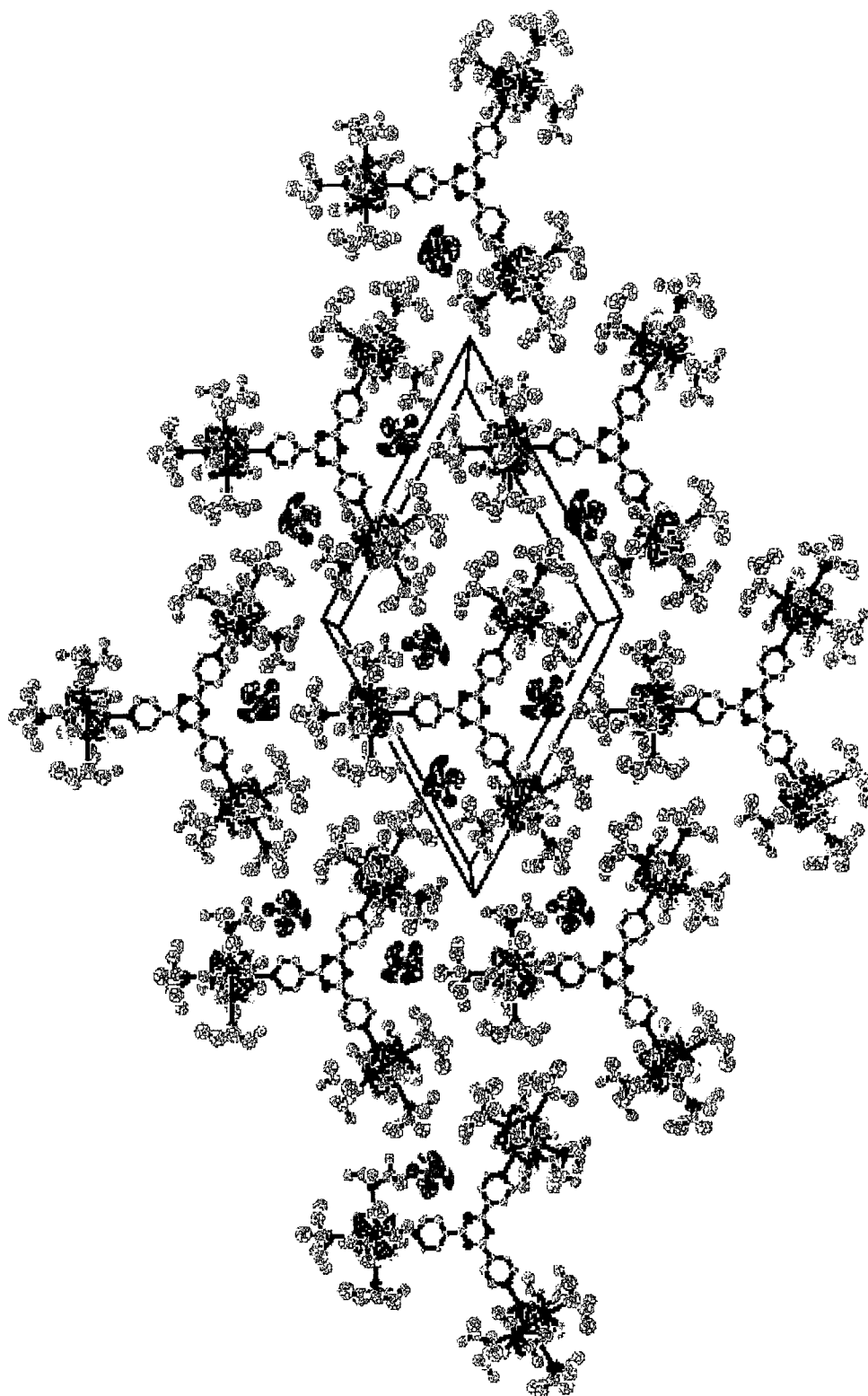


Figure 2.10. Crystal packing of 13.

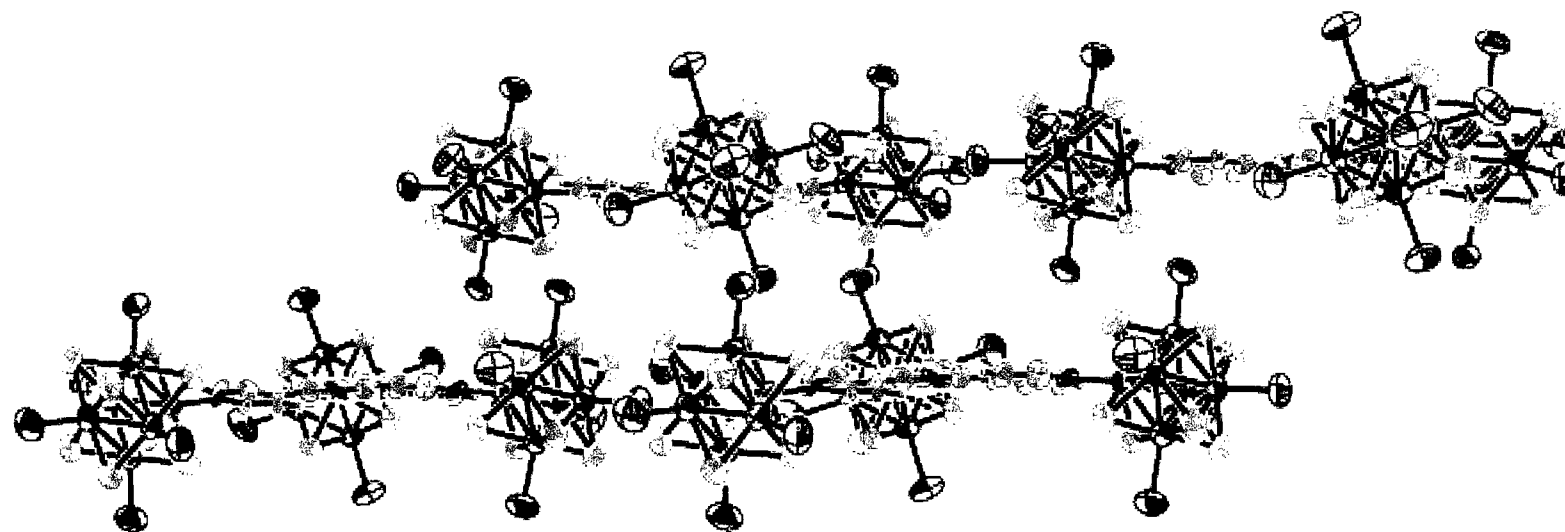


Figure 2.11. Edge-on view of the crystal packing of 13.

2.3.3. Synthesis of the Tetrapyrrolylporphyrin-Supported Tetracluster Array

The tetrapyrrolylporphyrin-supported cluster array **14** was prepared in an analogous manner to **13** with the substitution of the tritopic ligand for the tetratopic one. The formation of **14** is clearly established by comparative ^1H and ^{31}P NMR studies of **14** and **8**. Specifically, the proposed structure was confirmed by several spectroscopic methods. The ^1H NMR spectrum, of **14** displays resonances due to the coordinated tetrapyrrolyl moiety. The α -H of the pyridyl portion of the porphyrin shifts from 9.05 for the free ligand to 9.72 ppm for **14** (a, Figure 2.12). The β -H also shifts downfield from 8.13 to 8.18 ppm, though it is less noticeable. The pyrrole protons are slightly shifted from 8.86 to 9.04 ppm. There is a peak at -3.00 ppm that is diagnostic of unmetallated porphyrins due to the two protons associated with the interior nitrogens. Corroborating is the disappearance of the resonance observed for **8**. The simplicity of the ^1H NMR spectrum is consistent with the symmetry of the cluster array. Additional supporting evidence comes from the simple ^{31}P NMR spectrum (top, b, Figure 2.12) of **14**, which shows two resonances in a 4:1 ratio at -23.64 and -27.59 ppm, respectively. Tetracluster **14** has further been characterized by MALDI-TOF mass spectroscopy (Figure 2.13). A series of peaks corresponding to the loss of 4, 5, 6, and 7 counter ions are observed at 2729.4, 2137.9, 1742.5, and 1459.2 a.m.u, respectively.

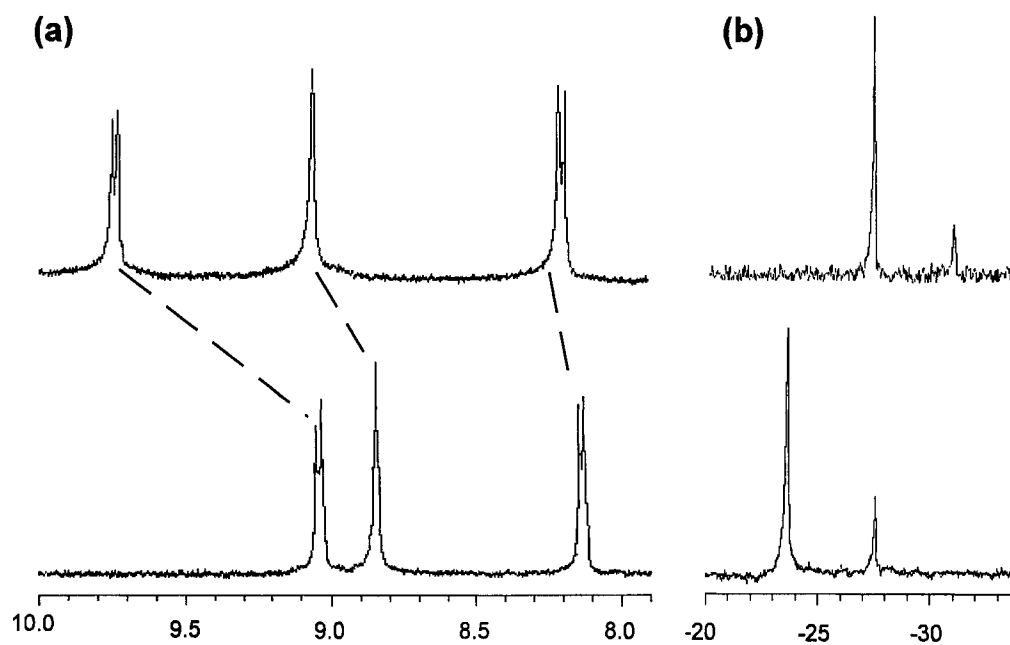


Figure 2.12. (a) ^1H NMR spectra of **11** (bottom) and **14** (top). Only the aromatic resonances are shown. (b) ^{31}P NMR spectra of **8** (bottom) and **14** (top).

Low-quality single crystals of **14** were obtained by slow evaporation of a concentrated nitromethane solution. Albeit a preliminary crystal structure, (Figure 2.14), it clearly shows four cluster units peripherally organized by the central tetrapyrrolylporphyrin platform to give a star-shaped structure.

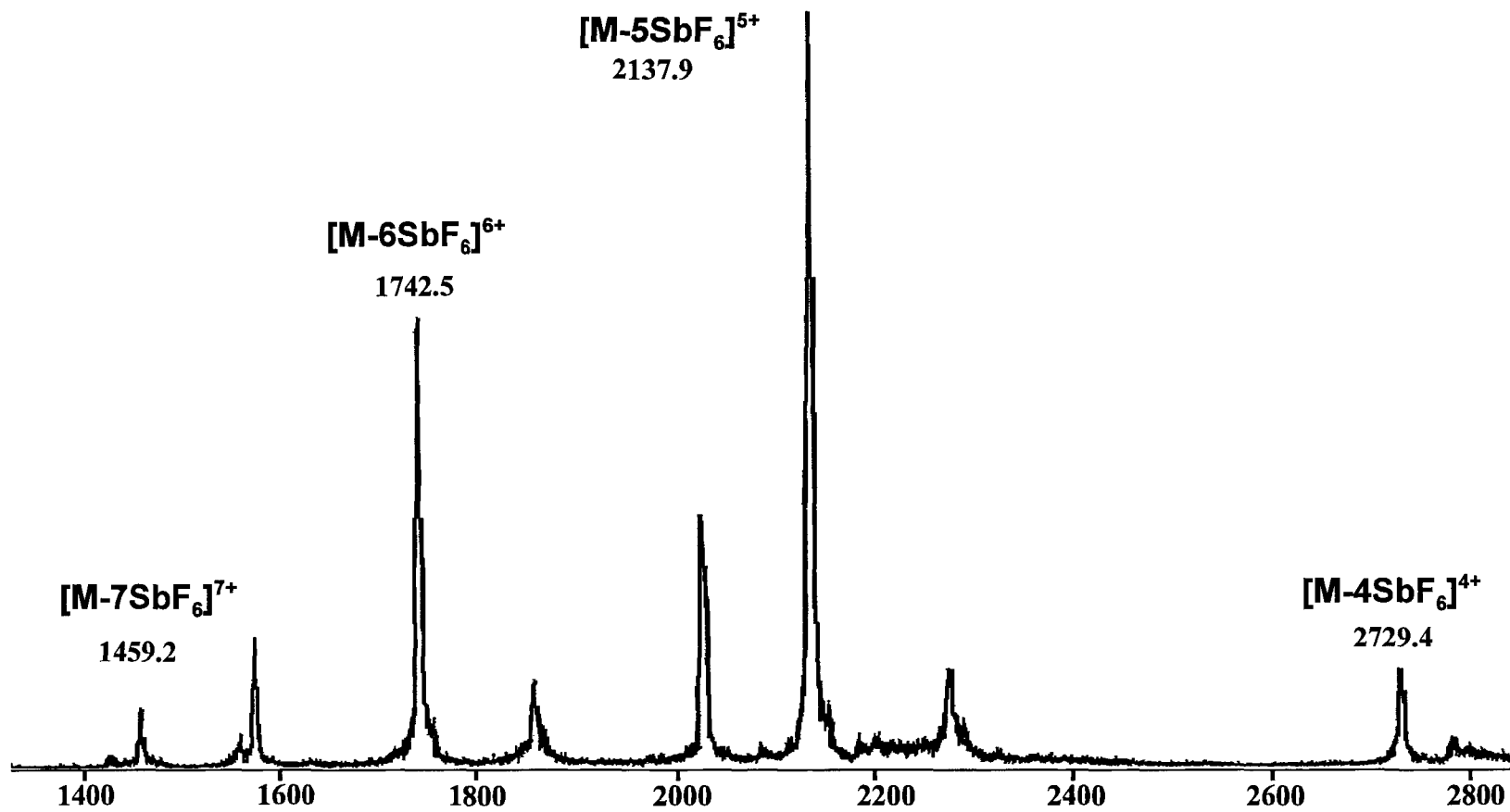


Figure 2.13. MALDI-TOF mass spectrum of 14.

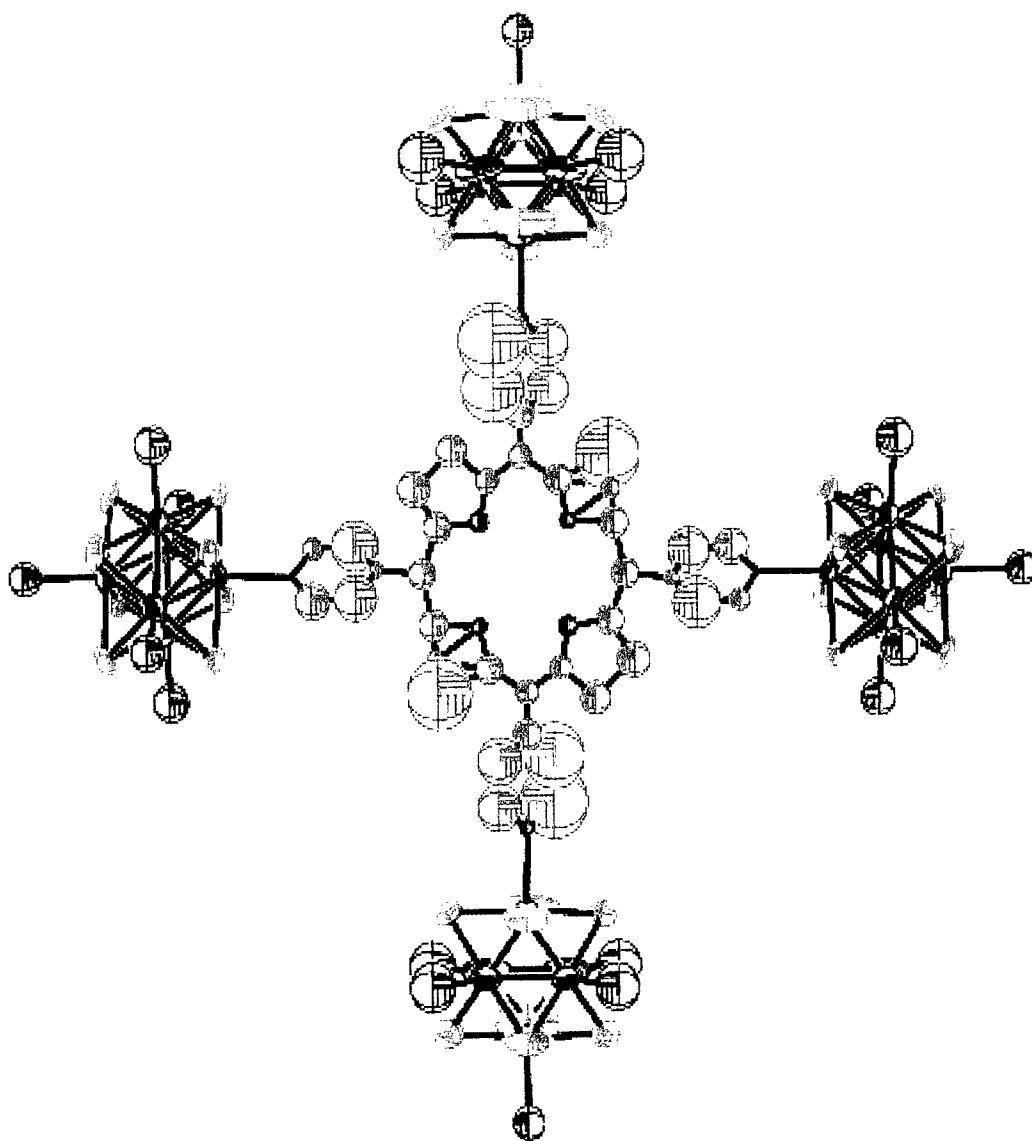


Figure 2.14. An ORTEP view of a preliminary structure of 14.

2.4. Electronic Spectroscopic Studies of Tri- and Tetraclusters

The electronic absorption data for **13** and **14** at 295 K are collected in Table 2.3. UV-visible spectra of **8**, **11**, and **13** are shown in Figure 2.15. The poorly defined broad absorption between 250 and 500 nm is due to the ligand-to-cluster charge transfer.³¹ The absorption due to the organic moiety is obscured by the cluster absorption, reflecting the dominance of the charge-transfer transitions.

Table 2.3. Electronic Absorption Data of **13** and **14**.

Complex	Wavelength (nm)	Absorbance	Concentration (mol/L)	ϵ (L mol ⁻¹ cm ⁻¹)
13	245	0.87790	3.32 x 10 ⁻⁶	266030.3
14	644	0.00968	1.85 x 10 ⁻⁶	5128.2
	589	0.01917		10333.9
	553	0.03000		16172.1
	517	0.05381		29007.3
	426	0.85280		459718.1

The absorption spectra of **12** and **14** are shown in Figure 2.16, and are typical of this class of molecules. A strong transition to the second excited state ($S_0 \rightarrow S_2$) at 426 nm (the Soret or B band) and weak transitions to the first excited state ($S_0 \rightarrow S_1$) at 517, 553, 539, and 664 nm (the Q bands) were observed. The B and Q bands both arise from $\pi\text{-}\pi^*$ transitions

and can be explained by considering the Gouterman four-orbital model¹⁰⁷ (Figure 2.17): two π orbitals (a_{1u} and a_{2u}) and a degenerate pair of π^* orbitals (e_{gx} and e_{gy}). The two highest occupied π orbitals happen to have about the same energy. Instead of almost coincident absorption bands due to $a_{1u} \rightarrow e_g$ and $a_{2u} \rightarrow e_g$, these two transitions mix together by a process called configuration interaction, which results in two bands with very different intensities and wavelengths: Constructive interference leads to the intense short-wavelength B band, while destructive combinations lead to the weak long-wavelength Q band. The tetracluster array absorption spectrum shows a combination of **8** and the porphyrin Soret and Q-band, though upon coordination of the clusters, the absorption peaks are red shifted. This clearly shows that the fundamental properties of both components remain intact upon formation of the supramolecular array, but interactions between these building blocks are significant.

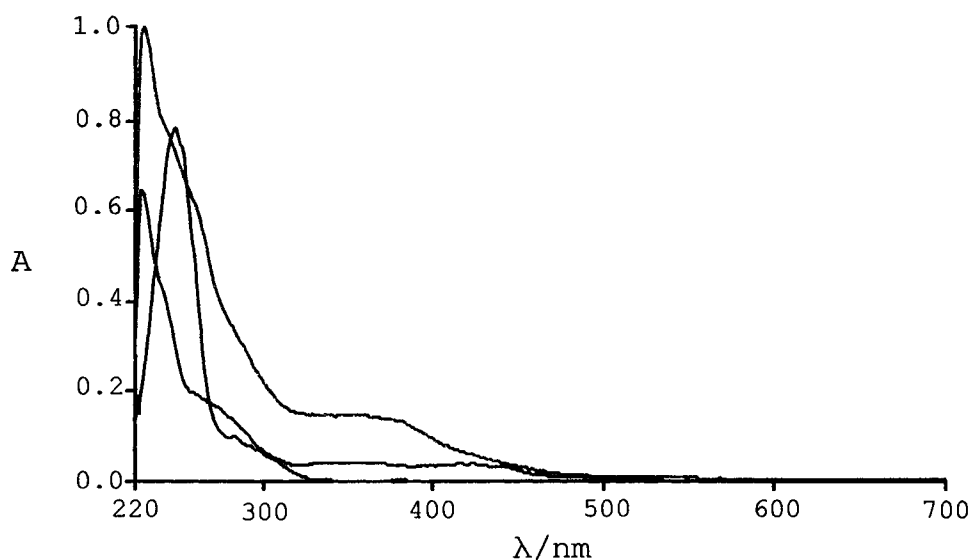


Figure 2.15. Electronic absorption of **8** (—), **11** (---), and **13** (····).

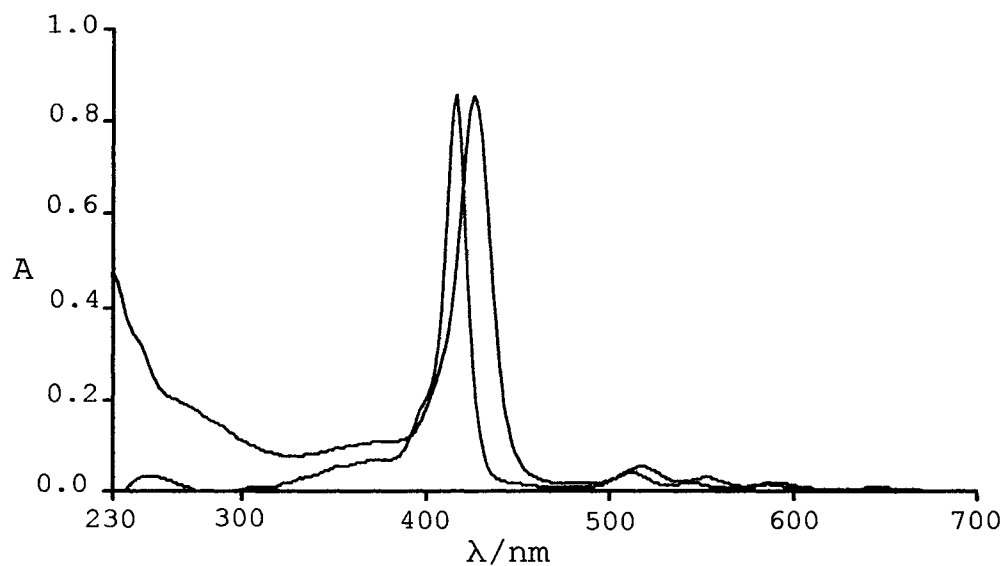


Figure 2.16. Electronic absorption of **12** (—) and **14** (---).

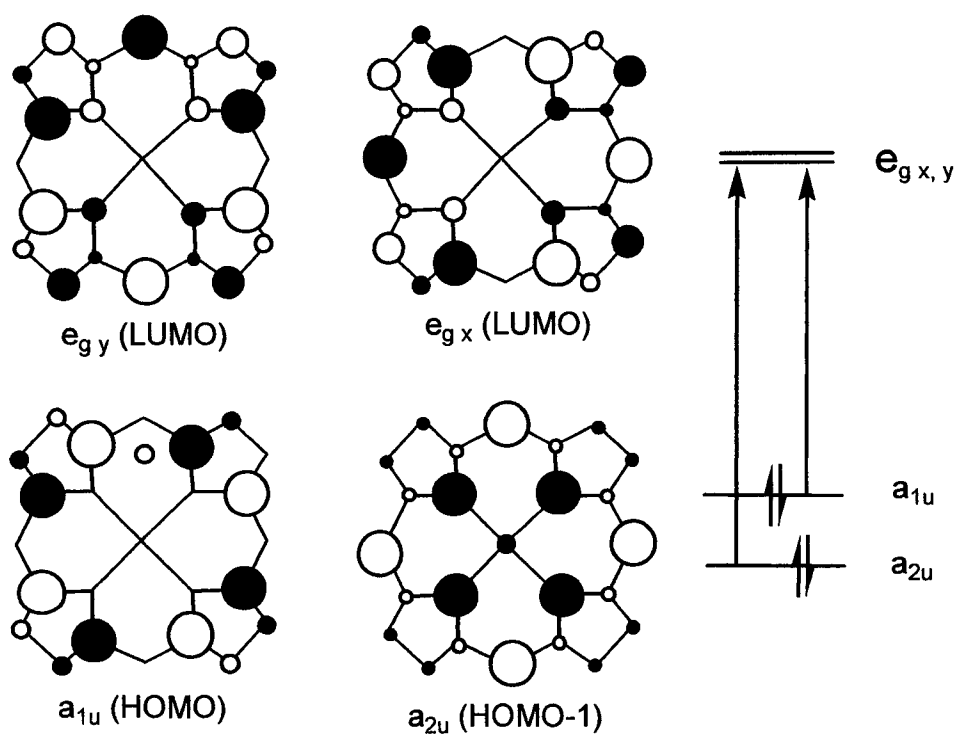


Figure 2.17. The Gouterman four-orbital model and energy level representation of the electronic excitation of porphyrins.

2.5. Electrochemical Studies

The ability of the $[\text{Re}_6(\mu_3\text{-Se})_8]^{2+}$ cluster core to undergo a one-electron oxidation is a well-known phenomenon. Zheng and coworkers^{33,32} have investigated the electrochemistry of mono- and dicluster derivatives. It has been concluded that there is very little difference in the oxidation potentials for derivatives with ligands of similar molecular structure. They also performed oxidative coulometry and discovered that in the 4,4'-dipyridyl bridged dicluster, two electrons, one from each cluster unit, are removed simultaneously. It has been postulated that this behavior arises as a consequence of the extended bridge which places the cluster cores too far apart from each other to interact. In an effort to explore the potential intercluster electronic coupling of the two supramolecular arrays, cyclic voltammetry and oxidative coulometry were performed.

2.5.1. Cyclic Voltammetry

Cyclic voltammetry results of four relevant cluster derivatives are presented in Figure 2.18. The potential axis is referenced to the Fc^+/Fc redox couple ($E^\circ = 0.46 \text{ V vs. SCE}$; 0.70 V vs. NHE). A reversible oxidation process is clearly visible for each of the cluster complexes. These derivatives, regardless of the number of cluster units, are oxidized at essentially the same potential that is also close to those reported for similar compounds containing the $[\text{Re}_6(\mu_3\text{-Se})_8]^{2+}$ cluster core.

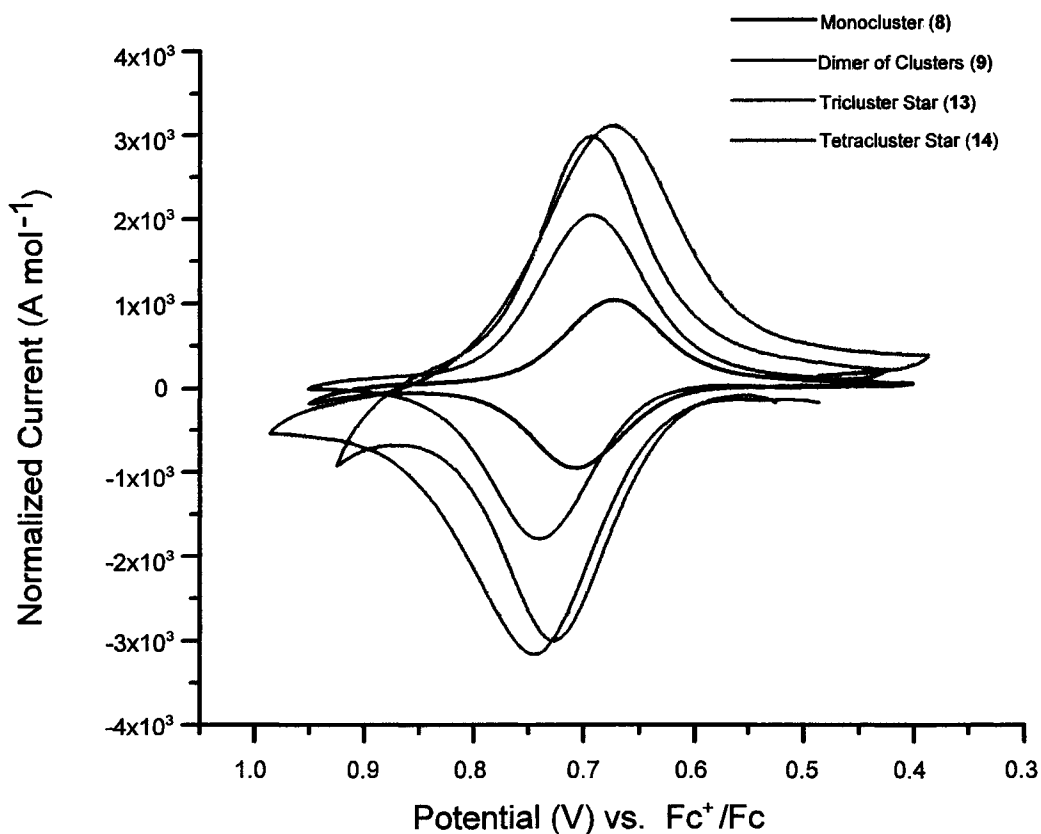


Figure 2.18. The overlay of cyclic voltammograms of **8** and three "clusters of clusters" (**9**, **13**, and **14**) showing qualitatively the correlation of the number of cluster units and the number of electrons involved in the redox event.

2.5.2. Coulometry

With coulometry the quantity of electricity required to carry out an exhaustive electrolysis is determined.¹⁰⁸ The amount of materials or the number of electrons involved in the electrolysis can then be determined. The method used to acquire the results reported here were obtained by thin-layer electrolysis using controlled potential methodology. To enable a successful experiment, three conditions must be satisfied: (1) It must be of known stoichiometry; (2) it must be a single reaction or at least without a side reaction of

different stoichiometry; and (3) it must occur with close to 100% efficiency. The following relationship (Equation 2.1) relates the total amount of charge passed (Q) to the number of electrons per redox event (n), where F is Faraday's constant, C is the bulk analyte concentration, and V is the cell volume. Table 2.4 summarizes the important values in determining the number of electrons transferred. It is clear from the value of n , there is no electronic communication existing between the cluster units of the tri- or tetracluster arrays, as simultaneous removal of three and four electrons, one from each of the clusters, have been determined.

$$Q = n F C V \quad (\text{Eq. 2.1})$$

Table 2.4. Electrochemical Data.

Complex	E_{ox} vs. Fc^+/Fc (V)	Electrode Volume (μL)	Q/C ($\mu\text{C}/\text{mM}$)	n
1	0.69	0.466	40	0.9
9	0.72	0.373	79	2.2
13	0.71	0.415	119	3.0
14	0.68	0.373	153	3.8

2.6. Attempts to Construct More Extended Supramolecular Arrays of Clusters

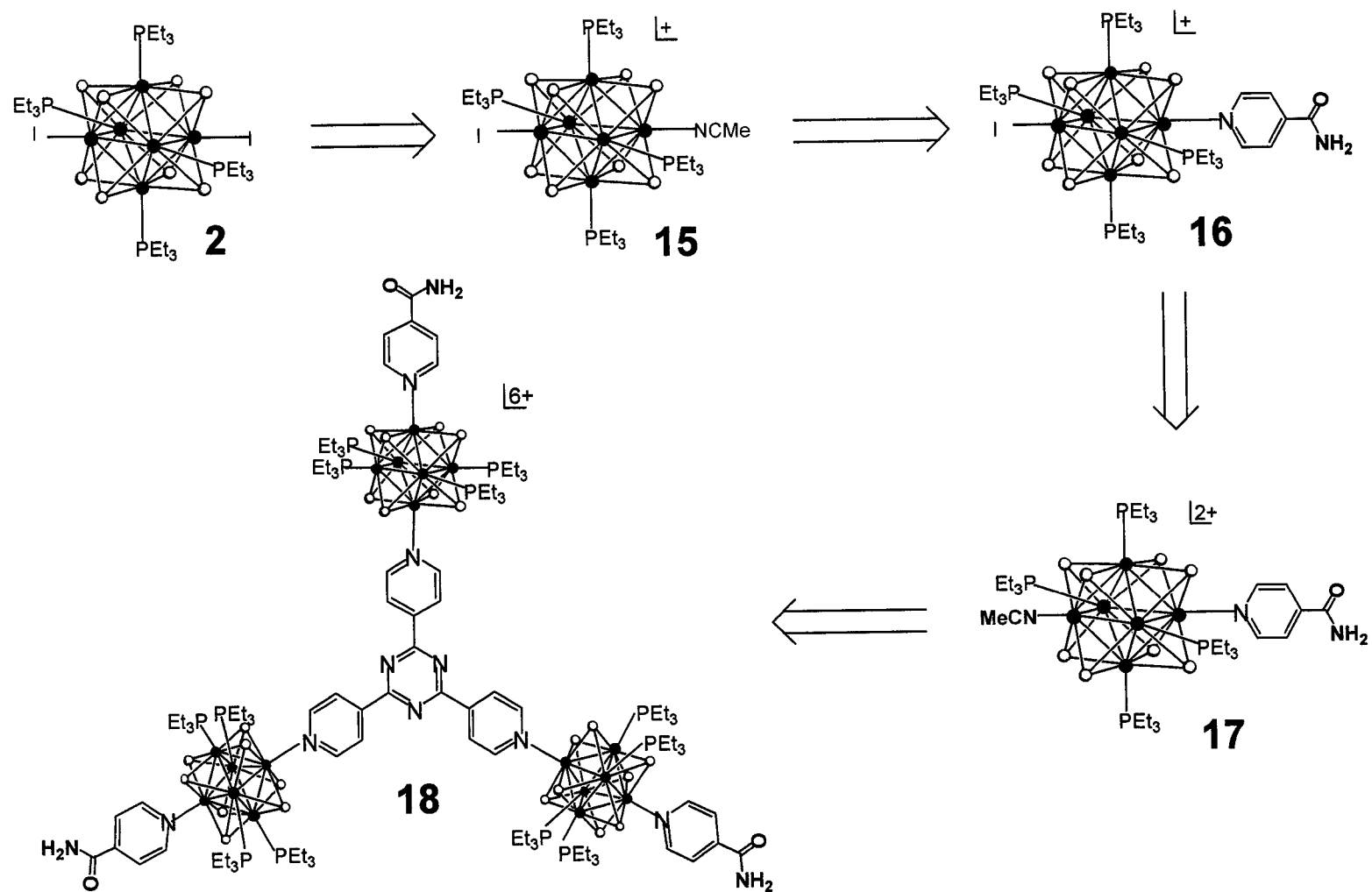
By utilizing and manipulating hydrogen-bonding interactions between prefabricated cluster arrays similar to **13** and **14**, the construction of new and more sophisticated supramolecular species is anticipated. The recent surge of research activities aiming at the creation of inorganic-organic materials by assembling metal complexes through hydrogen bonds provides some inspiration. Below the efforts to create hydrogen-bonded extended structures utilizing prefabricated cluster arrays are discussed.

The idea is to equip a prefabricated cluster Tinkertoy with functional groups that are capable of hydrogen-bonding interactions. The retrosynthesis of one such target is depicted in Scheme 2.2. The targeted tricluster **18** is different from **13** in that each of the three clusters possesses one isonicotinamide ligand that is known to engage in strong hydrogen-bonding interactions. The first step is to differentiate the two reactive sites of **2**. This was accomplished by carefully controlling the reaction temperature, the amount of AgSbF_6 added, and the addition rate. The reaction mixture contained, not surprisingly, unreacted **2**, the known disolvate **6**, the desired complex **15**, and AgI byproduct. The product was separated by column chromatography and its structure can be easily be established by a combination of ^1H and ^{31}P NMR. Specifically, the ^1H NMR shows (Figure 2.19), in addition to the resonances of the ethyl groups of the phosphine ligand, a signal at 2.82 ppm. This peak is due to the coordinated acetonitrile molecule. The ratio of these three resonances of 12:8:1 (phosphine CH_3 : phosphine CH_2 : acetonitrile CH_3) is in agreement with the structure

of **15**. ^{31}P NMR spectrum, showing only one signal at -21.44 ppm, indicates retention of the *trans* stereochemistry of the cluster.

The next step is the introduction of isonicotinamide to replace the nitrile ligand. Upon formation of complex **16**, the resonance corresponding to the coordinated solvent molecule disappears, and a number of downfield signals appear. These signals arise from the coordinated isonicotinamide ligand. The coupling scheme shown by these resonances is one expected for isonicotinamide. Nevertheless, the coordination to a cationic cluster causes some distinct downfield shifts of these signals. The α -pyridyl proton appears at 9.36 ppm with respect to its counterpart at 8.70 ppm in the free ligand. The β -H signals are less significantly shifted, upfield from 7.67 to 7.56 ppm. The two broad singlets due to the amide protons do not shift noticeably when compared to those of the free ligand. The integration of the signals agrees with the coordination of only one isonicotinamide ligand.

Scheme 2.2



With **16** in hand, the remaining iodide can be displaced for a solvent molecule to achieve the reactivity necessary for its conversion into the tricluster. The synthesis of **17** was first attempted under the conventional de-iodination conditions (excess AgSbF_6 , 12 hours). However, the desired product could not be isolated. A mixture of inseparable products was formed instead. It has been found, however, by using only two equivalents of AgSbF_6 and a much shorter reaction time (30 minutes), **17** can be prepared in excellent yields. The ^1H NMR spectrum of **17** is shown in Figure 2.19. As compared with **16**, there is little change in the downfield region except that a new peak at 2.69 ppm due to a coordinated acetonitrile molecule now appears. The integration of the peaks provides additional confirmation of the stoichiometry.

The final step is to transform **17** into a hydrogen-bonding-capable cluster array. The reaction between **17** and the tritopic star-shaped connector was thus carried out, using a procedure similar to the one used for the synthesis of **13**. Unfortunately, despite the formation of **17**, its isolation from the rather complicated product mixture, was unsuccessful. Several other solvent systems were used to vary the reaction temperature from 80°C to 105°C . It was found that at 80°C or below, no reaction took place, but as the temperature became high enough to remove the coordinated acetonitrile, the isonicotinamide ligand also began to be exchanged. It was decided at this point that with the current knowledge of the reactivity of these clusters, it was not possible to create the desired molecules without also forming the undesired ligand-exchange products. Furthermore, the mixture could not be separated due to the similar properties of its components.

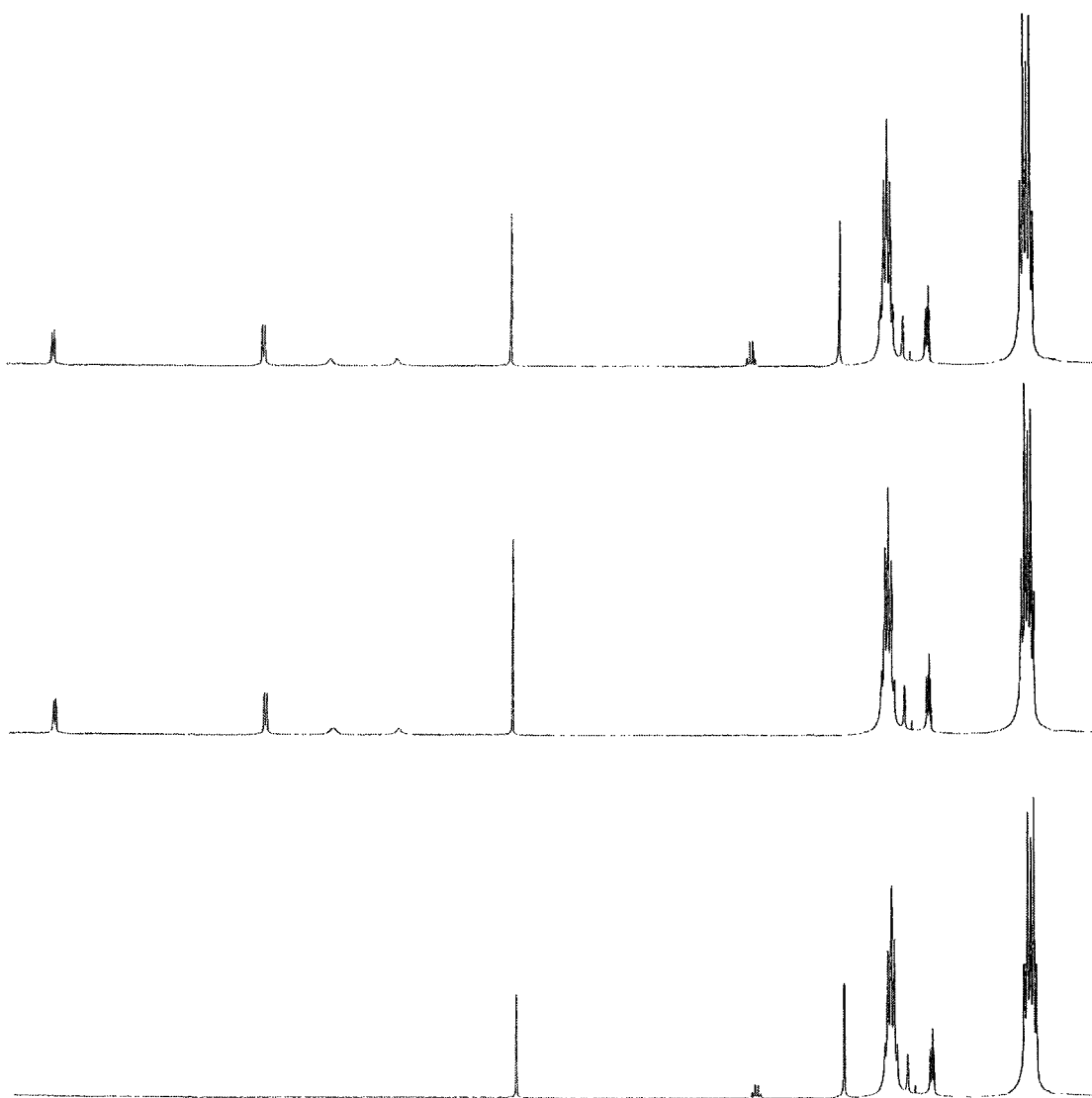


Figure 2.19. ^1H NMR of **15** (bottom), **16** (middle), and **17** (top).

2.7. Summary and Perspectives

In summary, two star-shaped cluster arrays have been successfully prepared. One features three $[\text{Re}_6(\mu_3\text{-Se})_8]^{2+}$ cluster units organized by the tritopic ligand 2,4,6-tri(4-pyridyl)-1,3,5-triazine, while the second contains four cluster units supported by 5,10,15,20-tetra(4-pyridyl)-21*H*,23*H*-porphine, a tetratopic scaffold. The synthetic approach, based upon step-wise build-up of metal clusters with organic linking groups, offers the potential for exquisite control over the structure of the final assembly. It has been found by cyclic voltammetric and coulometric studies that intercluster electronic couplings are negligible, if present at all, in these novel cluster arrays. Attempts to expand the discrete multiclusters into more extended and sophisticated supramolecular assemblies have also been made, but were not successful. Nevertheless, a number of potentially useful cluster precursors have been prepared, and other structurally unique cluster arrays may be possible by making use of these intermediates. Further investigation is needed to explore the potential application of the tritopic star assembly as octapolar non-linear optical materials.¹⁰⁹

CHAPTER 3

Cluster-Studded Metalloporphyrins: Spectroscopic and Electrochemical Studies

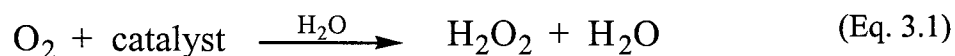
Abstract

Metallation of **14** with metal (Co^{2+} , Ni^{2+} , Cu^{2+} , Zn^{2+}) salts successfully produced the corresponding cluster arrays supported by the metallated porphyrins (**19-22**). These novel cluster complexes were characterized by microanalysis (CHN) and NMR spectroscopy (^1H and ^{31}P). Detailed electrochemical studies revealed one chemically reversible oxidation event attributable to the simultaneous removal of four electrons, one from each of the four cluster units. In addition, the cyclic voltammetry of the Ni^{2+} complex revealed a second oxidation event corresponding to two electrons, which can be ascribed to metal-based oxidation. For the Cu^{2+} complex two additional oxidation events, each attributable to the loss of one electron, were observed. These cluster arrays have also been studied by UV-visible spectroscopy. The electronic spectra of Co^{2+} , Ni^{2+} , and Cu^{2+} complexes each show the absorptions due to the metalloporphyrins and the cluster complex. For the Zn^{2+} complex, solvatochromism was observed and its electronic absorption in a variety of solvents of different dielectric constants were studied.

3.1. Introduction

Metalloporphyrins occupy a special position in catalysis. Over the years, metal complexes of specifically designed porphyrins have been synthesized, and their properties have been investigated including those related to catalysis. Specifically modified porphyrin systems have found use in diverse applications such as living polymerization initiators¹¹⁰⁻¹²⁴ and efficient modeling of certain proteins and enzymes.¹²⁵⁻¹³²

Of specific interest is the rich chemistry associated with the tetrapyridylporphyrin (TPyP). The ability of this porphyrin to coordinate metal ions through the peripheral pyridyl nitrogens, combined with the photophysical and redox properties inherent to porphyrins, has made TPyP a popular choice for creating supramolecular arrays. One of the most interesting subareas within this field is the modification of TPyP with metal complexes, chosen for their propensity to serve as electron donors. The idea is to attach one, two, three, or four metal complexes to the periphery of the porphyrin. Upon oxidation of the metal centers, a total of four electrons could be donated to assist in the reduction of O₂ to H₂O (Equation 3.1). To this end, Anson, Toma, and their respective coworkers independently studied TPyPs modified by ruthenium complexes on the periphery.



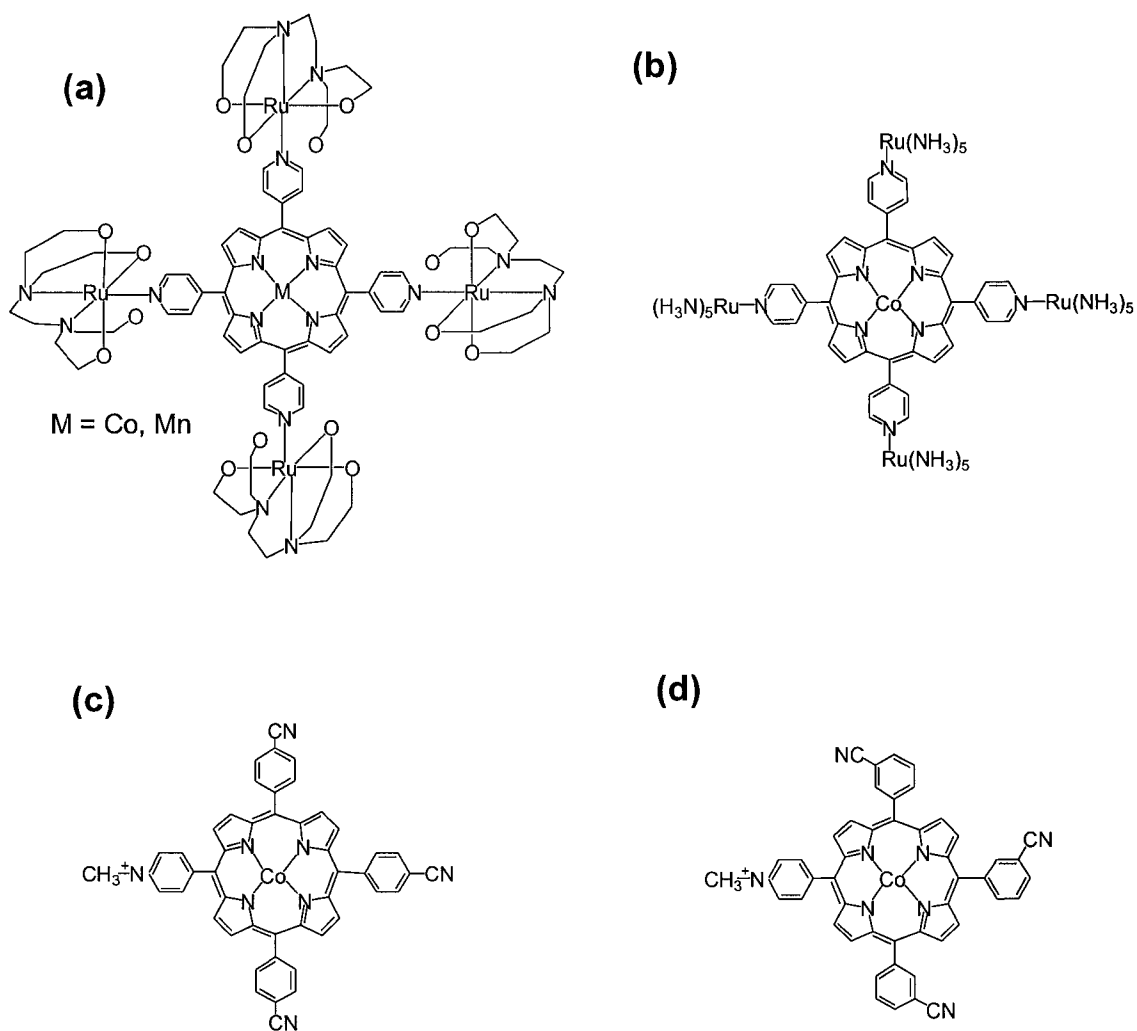


Figure 3.1. Representative ruthenium porphyrin complexes studied by Toma and Anson.

Toma and coworkers^{133,134} investigated systems that contain peripheral $[\text{Ru}^{\text{III}}(\text{edta})]^{2-}$ groups attached to cobalt or manganese TPyP complexes (a, Figure 3.1, carbonyl oxygens removed for clarity). They demonstrated enhanced catalytic activity of the modified metalloporphyrin over the unsubstituted analog towards the four-electron reduction of

molecular oxygen. The first series of catalysts that Anson and coworkers studied were based on cobalt TPyP with four $\text{Ru}(\text{NH}_3)_5^{2+}$ moieties covalently bound through the pyridyl nitrogen (b, Figure 3.1).¹³⁵⁻¹³⁷ Prior to ruthenation, the porphyrin complex catalyzes only the two-electron reduction of O_2 to H_2O_2 . In comparison, three-quarters of the O_2 present was reduced to H_2O and only one-quarter to H_2O_2 when the ruthenated analog was utilized. This result was consistent with the notion that rapid intramolecular electron-transfer within the metal complex-modified metalloporphyrins converted the reduction of O_2 from a two-electron to a four-electron process.

Anson and coworkers also synthesized cobalt porphyrins containing three or fewer ruthenium complexes to further explore the catalytic mechanism.^{138,139} Experiments showed that only porphyrins with three or four ruthenium complexes gave the four-electron reduction product. This result was in conflict with their expectation because if intramolecular electron-transfer was indeed the correct mechanism, only one ruthenium group would be necessary to supply all of the electrons needed to produce the four-electron reduction product. They continued the investigation into this problem by preparing metalloporphyrins that contain four $[\text{Ru}(\text{edta})]^{2-}$ groups.¹³⁸ Since $[\text{Ru}(\text{edta})]^{2-}$ is a significantly stronger reductant than $[\text{Ru}(\text{NH}_3)_5]^{2+}$, $[\text{Ru}(\text{edta})]^{2-}$ should engage in electron-transfer even more readily, but only H_2O_2 is formed under otherwise identical conditions. Knowing that intramolecular electron-transfer was unlikely to be the correct catalytic mechanism, other sources for the enhanced catalytic activity of the porphyrins were explored.

The back-bonding argument seemed to provide a reasonable understanding of the above observations because $[\text{Ru}(\text{NH}_3)_5]^{2+}$ is a stronger back-bonder than $[\text{Ru}(\text{edta})]^{2-}$. To

explore this possibility, Anson and coworkers synthesized ruthenated cobalt porphyrins with the more strongly π accepting 4-cyanophenyl ligands (c, Figure 3.1) instead of pyridyls, and discovered that these molecules are indeed potent catalysts for the reduction of O_2 to H_2O .¹⁴⁰⁻¹⁴² Since the amount of electron density transferred through back-bonding is dependant on the position of the cyano group on the phenyl ring, Anson and co-worker further prepared 3-cyanophenyl porphyrin derivatives (d, Figure 3.1), which should have little electron density transferred via back-bonding. Indeed, these molecules did not catalyze the four-electron reduction of molecular oxygen. It has since been concluded that back-bonding rather than intramolecular electron-transfer is responsible for enhanced catalytic activity of the cobalt complex of the porphyrins.

The recent work by Toma and coworkers focused on an extremely interesting area of research involving the synthesis and catalytic studies of supramolecular porphyrin species containing four μ_3 -oxo-ruthenium acetate clusters (Figure 3.2).^{104,105} The first complex they reported was the manganese complex of the tetracenter porphyrin (MnTCP).^{102,106} They found that this compound efficiently catalyzed the selective epoxidation of cyclooctene (Equation 3.2), but its capacity is no better than the unsubstituted manganese porphyrin (MnTPyP). When MnTPyP was used as the catalyst for oxidation of cyclohexane (Equation 3.3), a less reactive substrate, cyclohexanone and cyclohexanol resulted. However, the use of the Mn(TCP) catalyst led to the formation of cyclohexanol alone. It has been found that CoTCP, the Co^{2+} analog of MNTCP, was also capable of efficiently reducing O_2 to H_2O .

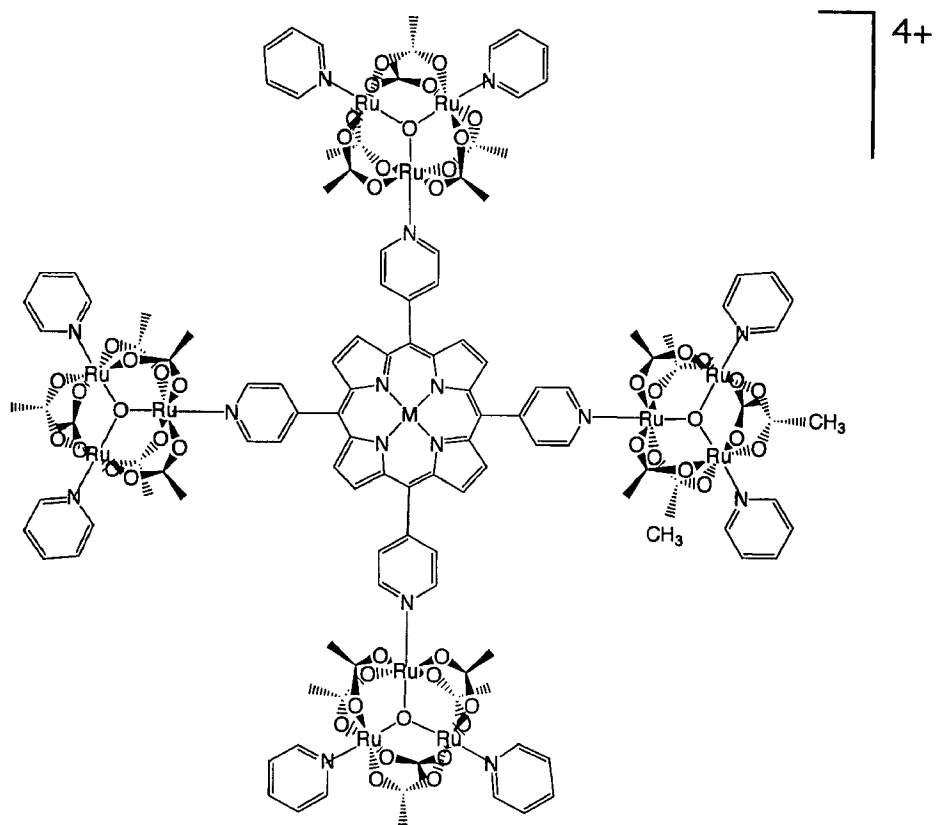
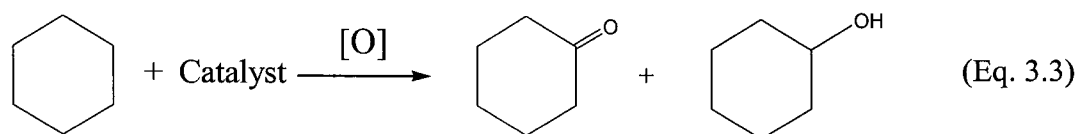
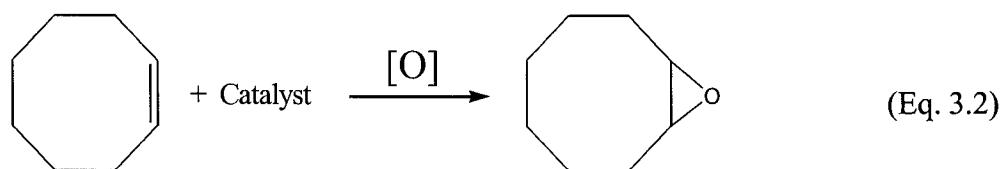


Figure 3.2. Structural representation of $M(\text{TCP})$, where $M = 2\text{H}, \text{Co}^{3+}, \text{Mn}^{3+}, \text{Zn}^{2+}$.



Only one research group to date has used octahedral hexanuclear chalcogenide clusters in catalytic studies. Kim and coworkers⁵⁰ reported the synthesis of a new rhenium cluster-containing Mn(TPP) (TPP = tetraphenylporphyrin dianion) complex where manganese(III)porphyrin units are linked through the axial position to the cluster via cyanide bridges to form discrete supramolecular assemblies shown in Figure 3.3. They evaluated the potential of this cluster-modified porphyrin array as a heterogeneous catalyst for the epoxidation of olefins with iodosylbenzene. It was found that cyclooctene was completely converted to cyclooctene oxide, in a much higher conversion ratio than the unsubstituted Mn(TPP) complex. Also, while only a trace amount of *trans*-stilbene was converted to the epoxide when Mn(TPP) was used, the epoxide was obtained in high yields when the cluster derivative was the catalyst.

The results described above clearly demonstrate the propensity of porphyrin cluster supramolecular arrays to catalyze the epoxidation of olefins or the four-electron reduction of O₂ to H₂O. However, there is still much room for improvement in the selectivity, conversion rate, and overall stability of these catalytic systems. [Re₆(μ₃-Se)₈]²⁺ cluster-containing metalloporphyrins might have potential in this role and could further expand this research field. The focus of the research described in this chapter is to prepare new metalloporphyrins with the [Re₆(μ₃-Se)₈]²⁺ core-containing cluster attached to their periphery and to examine their photophysical and electrochemical properties.

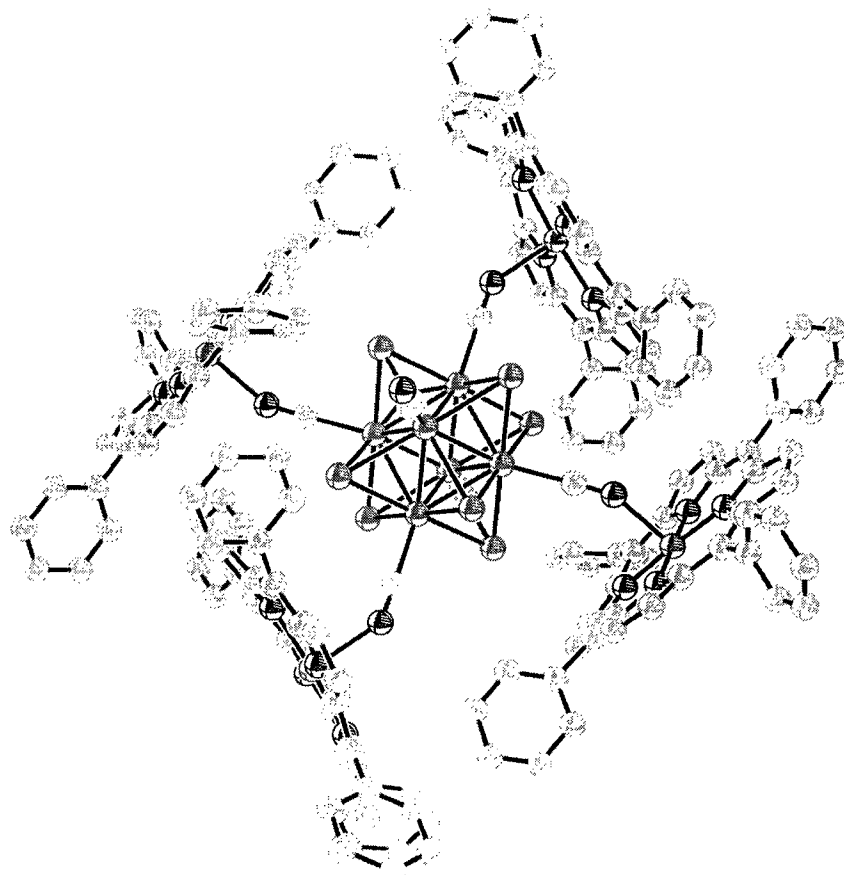


Figure 3.3. The structure of $[\text{Mn}(\text{TPP})_4][\text{Re}_6(\mu_3\text{-Se})_8(\text{CN})_6]$.⁵⁰ Hydrogen atoms are omitted for clarity.

3.2. Experimental Section

General Considerations.

5, 10, 15, 20-Tetra(4-pyridyl)-21*H*, 23*H*-porphine (**12**), (*n*-Bu₄N)PF₆, and AgSbF₆ were obtained from Aldrich and used as received. Cluster complexes **4** and **8** were prepared according to published procedures.³¹⁻³³ The silica gel (mesh size 200-400) used for flash column chromatography was purchased from Natland International Corporation, Research Triangle Park, North Carolina. ¹H and ³¹P NMR spectra were recorded on a Varian AM-300 spectrometer in CD₂Cl₂. Chemical shifts of ³¹P spectra were referenced to 85% H₃PO₄ (δ = 0 ppm, with negative values meaning upfield). Elemental analyses (CHN) were performed by Desert Analytics Laboratory, Tucson, Arizona.

Complex 19. A mixture of **14** (50.0 mg, 0.004 mmol) and Ni(C₂H₃O₂)₂•4H₂O (60.0 mg, 0.241 mmol) in 30 mL of chloroform was stirred under reflux for 48 hours. The red residue obtained upon removal of the solvent was extracted using dichloromethane and water. The combined organic phase was dried over MgSO₄. A purple-red residue was obtained upon removal of the solvent. Upon recrystallization from ether and dichloromethane purple-red crystals were obtained. Yield: 45.0 mg (90.3%). ¹H NMR: δ 1.00-1.30 (m), 2.00-2.40 (m), 7.91 (d), 8.85 (s), 9.62 (d). ³¹P NMR: δ -19.50 (s), -22.79 (s). Anal. Calcd for Re₂₄Se₃₂P₂₀N₈C₁₆₀H₃₂₄NiSb₈F₄₈: C, 16.13; H, 2.72; N, 0.94. Found: C, 16.48; H, 2.89; N, 1.10.

Complex 20 was obtained as a purple powder in a similar manner to complex **19** except that $\text{Cu}(\text{C}_2\text{H}_3\text{O}_2)_2 \cdot \text{H}_2\text{O}$ was used in place of $\text{Ni}(\text{C}_2\text{H}_3\text{O}_2)_2 \cdot 4\text{H}_2\text{O}$. Yield: 0.046 g (92%). ^1H NMR: δ 0.80-1.10 (m), 1.85-2.25 (m), 9.30 (bs). ^{31}P NMR: δ -24.85 (s), -28.30 (s). Anal. Calcd for $\text{Re}_{24}\text{Se}_{32}\text{P}_{20}\text{N}_8\text{C}_{160}\text{H}_{324}\text{CuSb}_8\text{F}_{48}$: C, 16.12; H, 2.72; N, 0.94. Found: C, 16.42; H, 2.90; N, 1.07.

Complex 21 was obtained as a purple powder in a similar manner to complex **19** except that $\text{Co}(\text{C}_2\text{H}_3\text{O}_2)_2 \cdot 4\text{H}_2\text{O}$ was used in place of $\text{Ni}(\text{C}_2\text{H}_3\text{O}_2)_2 \cdot 4\text{H}_2\text{O}$. Yield: 0.046 g (92%). ^1H NMR: δ 0.55-1.33 (m, 180), 1.85-2.50 (m, 120), 9.03 (bs), 10.32 (bs), 12.49 (bs). ^{31}P NMR: δ -25.36 (4), -28.65 (1). Anal. Calcd for $\text{Re}_{24}\text{Se}_{32}\text{P}_{20}\text{N}_8\text{C}_{160}\text{H}_{324}\text{CoSb}_8\text{F}_{48}$: C, 16.13; H, 2.72; N, 0.94. Found: C, 16.18; H, 2.91; N, 1.07.

Complex 22 was obtained as a green powder in a similar manner to complex **19** except that $\text{Zn}(\text{C}_2\text{H}_3\text{O}_2)_2 \cdot 2\text{H}_2\text{O}$ was used in place of $\text{Ni}(\text{C}_2\text{H}_3\text{O}_2)_2 \cdot 2\text{H}_2\text{O}$. Yield: 0.047 g (94%). ^1H NMR: δ 1.00-1.30 (m), 2.04-2.40 (m), 8.09 (d), 8.95 (s), 9.67 (d). ^{31}P NMR: δ -19.32 (s), -22.62 (s). Anal. Calcd for $\text{Re}_{24}\text{Se}_{32}\text{P}_{20}\text{N}_8\text{C}_{160}\text{H}_{324}\text{ZnSb}_8\text{F}_{48}$: C, 16.12; H, 2.72; N, 0.94. Found: C, 16.47; H, 2.69; N, 1.11.

Other Physical Measurements.

Electronic absorption spectra in dichloromethane solutions were recorded on a Perkin Elmer Lambda 10 spectrophotometer. Electrochemical experiments were carried out using a thin layer electrode whose design has been described in Chapter 2.

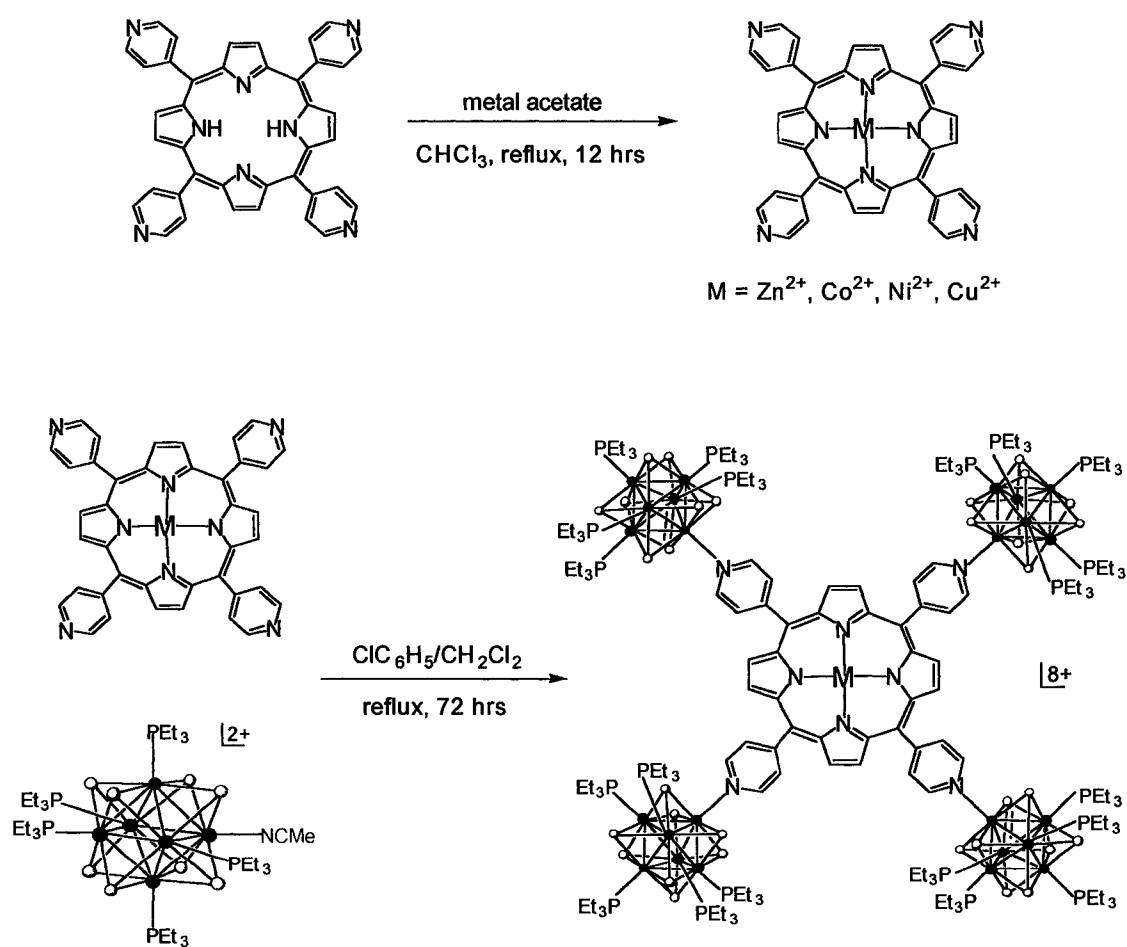
3.3. Synthesis and Characterization

In this study, we sought the synthesis of metal complexes of tetrapyrrolylporphyrin modified at the peripheral pyridyl with $[\text{Re}_6(\mu_3\text{-Se})_8]^{2+}$ clusters. Two synthetic routes may be used to prepare the tetracluster-studded metalloporphyrins. One way is to metallate the porphyrin first and then to attach the four clusters, as shown in Scheme 3.1. Alternatively, the supramolecular array **14** is prepared first, followed by the introduction of the metal ion (Scheme 3.2). Both methods have their respective advantages and disadvantages. The former allows for large quantities of the metalloporphyrins to be prepared and purified prior to cluster attachment, but de-metallation in the following reaction is of potential concern, as the coupling with clusters is carried out under rather forcing conditions. By adopting the latter strategy, porphyrin-supported cluster arrays can be prepared and purified, but cluster dissociation may occur because of the acetic acid byproduct generated in the subsequent metallation step. The former route was tested first because of the difficult purification anticipation of the latter route.

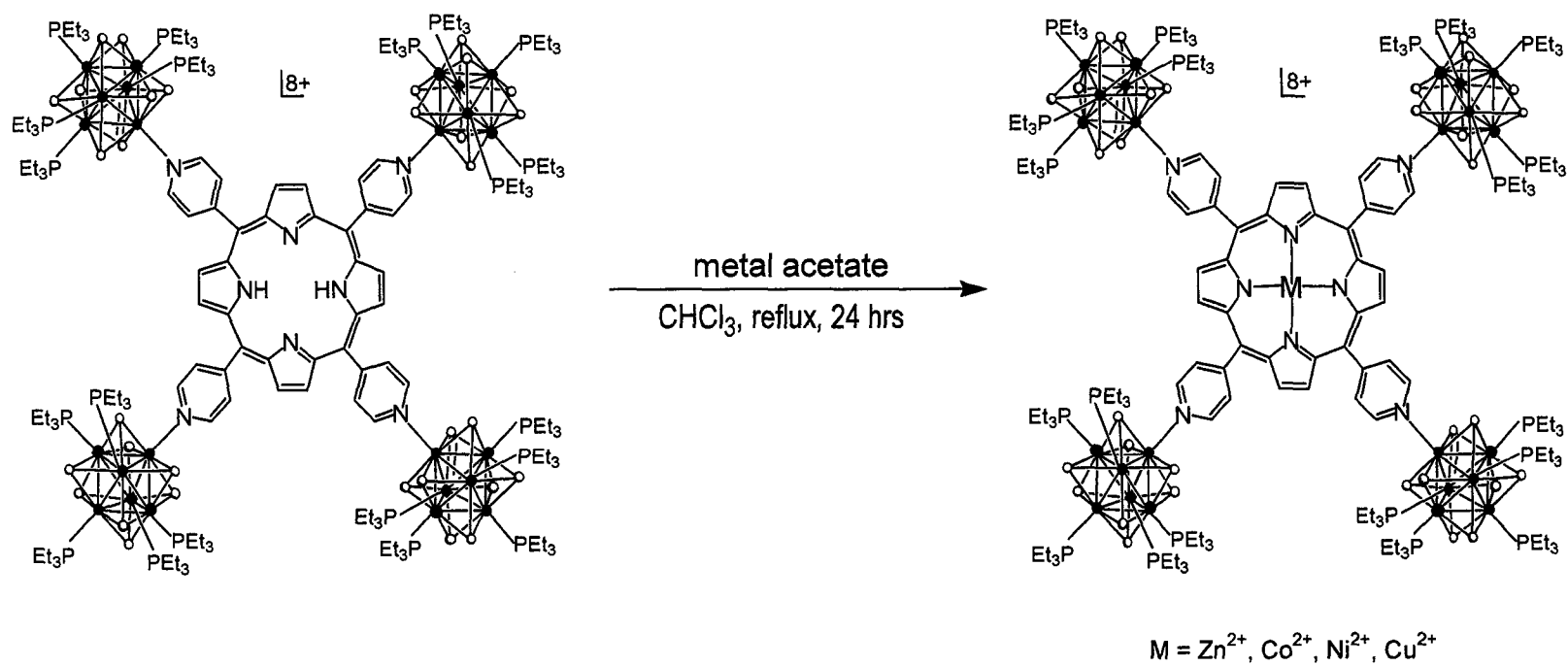
As an example, **12** and a large excess of nickel acetate were dissolved in chloroform and stirred under reflux overnight. The solvent was then removed, and the remaining solid was extracted with methanol for 12 hours using a Soxhlet apparatus. The product was shown to be pure by electronic absorption and ^1H NMR spectroscopy. The purified metallated porphyrin was then combined with **8**, in chlorobenzene, and the mixture was stirred under reflux overnight. Unfortunately, the potential problem of de-metallation did occur during

the cluster-coupling experiment. The reaction mixture contained both the metallated and unmetallated tetracluster porphyrins. Purification by recrystallization or extraction was unsuccessful.

Scheme 3.1



Scheme 3.2



Undaunted by the first unsuccessful attempt to synthesize the metallated tetracluster arrays, we resorted to the second synthetic route. In a representative synthesis, **14** and an excess of nickel acetate was dissolved in dichloromethane and stirred under reflux. The resulting mixture contained only the desired metallated product as well as unreacted nickel acetate. The solvent was removed, and the product was extracted into dichloromethane. The excess metal salt was removed by repeated washing with water. The complex is soluble in dichloromethane, acetonitrile, and other common polar organic solvents to yield red and purple solutions, depending on the solvent used. ^1H and ^{31}P NMR and electronic absorption spectroscopy are in agreement with the proposed structure. The ^1H and ^{31}P NMR of the unmetallated tetracluster porphyrin array (**14**) was described in detail in Chapter 2. The following discussions will only focus on the changes to the spectra of **14** upon metallation of the porphyrin. The ^1H NMR of **19** is shown in Figure 3.4. The effect of metallation upon the spectrum is small. The α -H of the pyridyl moiety shifts the least from 9.72 to 9.62 ppm. The pyrrole protons and the β -H of the pyridyl have more noticeable shifts of 0.19 and 0.27 ppm, respectively. The most convincing evidence of successful metallation is the disappearance of the resonance at -3.00 ppm, which corresponds to the protons bound to the interior nitrogens in **14**. The ^{31}P NMR (b, Figure 3.4) has two resonances at -24.3 and -27.6 ppm in a 4:1 ratio, indicating that the pentasubstituted cluster motif is present and remains intact. UV-visible spectroscopic studies of porphyrins are diagnostic of both the porphyrin type and the nature of the metal ions, and can be used reliably as evidence for metallation. Details of such studies will be discussed in a separate section below.

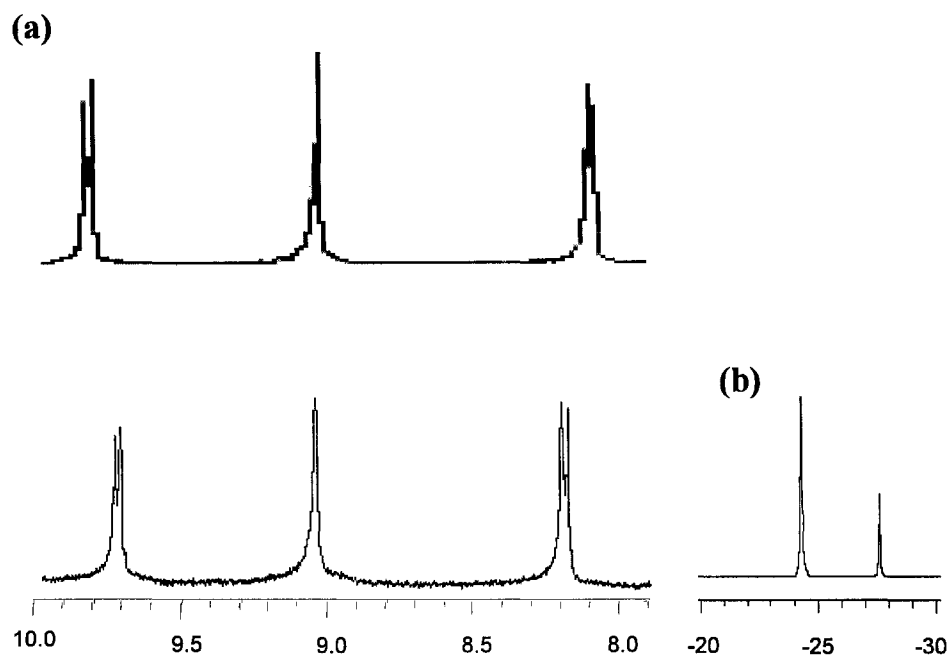


Figure 3.4. (a) ^1H NMR spectra of **14** (bottom) and **19** (top). Only the aromatic resonances are shown. (b) ^{31}P NMR spectrum of **19**.

Insertion of Cu^{2+} was achieved in an analogous manner to that of **19**. Upon metallation of the tetracluster porphyrin, dramatic changes to the ^1H NMR spectrum occurred. There are three important observations: (1) The peak at -3.00 ppm is no longer present, suggesting the copper ion has replaced the two protons; (2) the upfield resonances are noticeably broader and less well-defined; and (3) the original resonances in the aromatic region are not visible and only a broad resonance at 9.30 ppm is present. The last two observations are probably due to the influence of the paramagnetic species Cu^{2+} . Little change to the ^{31}P NMR spectra was observed upon metallation, however. There are two

slightly broadened resonances at -24.9 and -28.8 ppm in a 4:1 ratio, consistent with the stereochemistry of a of pentaphosphine-substituted cluster.

The tetracluster cobalt porphyrin complex can be synthesized if cobalt acetate and **14** are refluxed in dichloromethane. As with the copper complex, the ^1H NMR of **21** is dramatically different than that of its unmetallated parent. Again, this can be ascribed to the influence caused by the paramagnetic Co^{2+} ion. Disappearance of the original upfield proton signals corroborates the insertion of a metal and the complete displacement of the interior protons. The signals due to the triethylphosphine ligands are broadened, but most interesting are again the signals in the aromatic region. The well-defined resonances associated with the pyridyl and pyrrole protons are replaced by three new resonances, but only one of them is clearly visible at 10.32 ppm. The other two resonances, at 9.03 and 12.49 ppm, are too broad to be detected. The ^{31}P NMR shows two characteristic signals at -25.36 and -28.65 ppm in a 4:1 ratio.

The Zn^{2+} ion was incorporated into the tetracluster array analogously. However, the complex is red-green in color when dissolved in dichloromethane, distinctly different from the purple-red solutions of its Cu^{2+} , Co^{2+} , and Ni^{2+} . The ^1H NMR spectrum clearly indicates the insertion of Zn^{2+} because the resonance of the protons bound to the interior nitrogen at -3.00 ppm disappears. The downfield resonances are still clearly visible, but slightly shifted upfield when compared with the unmetallated **14**. The ^{31}P NMR has two resonances at -19.32 and -22.62 ppm in a 4:1 ratio, in agreement with the penta-substituted stereochemistry.

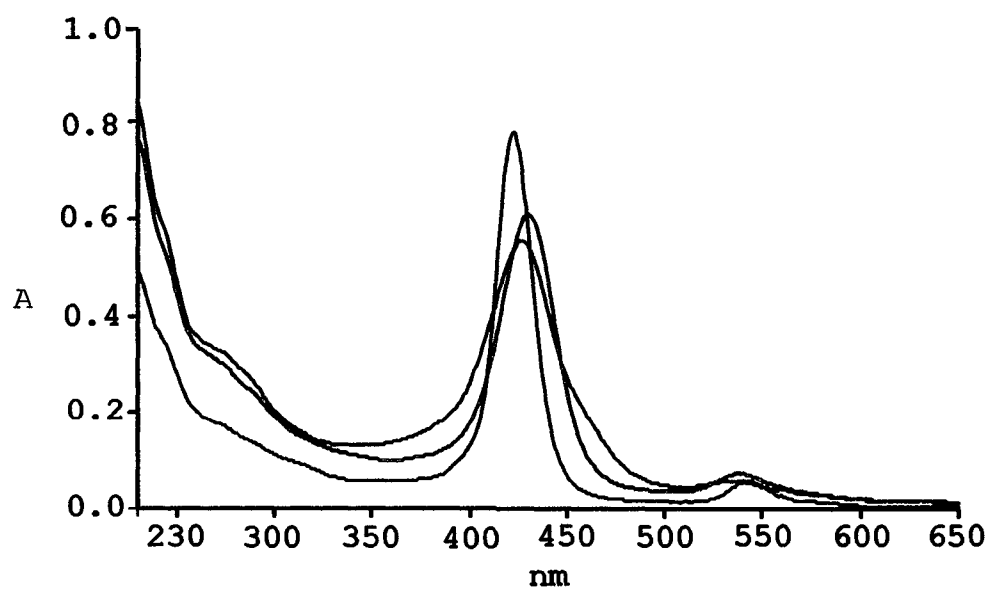
3.4. Electronic Spectroscopic Studies

The basic theory behind the electronic absorption of porphyrin complexes is outlined briefly in Chapter 2. The effect of porphyrin metallation will be discussed here. Upon introduction of a metal ion, bonds are formed with the nitrogen atoms, causing changes to the symmetry of the molecule, and therefore, the π - π^* transition. This leads to a change in the mixing of the $a_{1u} \rightarrow e_g$ and $a_{2u} \rightarrow e_g$ transitions, the effects of which can be seen in the alteration of the Q band absorbance pattern, and therefore, can be used for identification of specific metallated porphyrin species. As discussed in Chapter 2, the addition of four metal clusters to the porphyrin periphery only changes the wavelength of the electronic absorptions, but not the configurational interactions. It is therefore reasonable to expect similar electronic spectra of the cluster-modified metalloporphyrins and their unmodified parent.

The electronic spectra of **19-21** are shown in Figure 3.5, and the data are summarized in Table 3.1. Upon insertion of a metal ion into the tetracluster porphyrin, the absorption of the Q band changes significantly. The unmetallated porphyrin has four Q band peaks. In contrast, only one absorption is visible for its nickel, copper, and cobalt complexes. Complete metallation of the porphyrin is thus inferred.

Table 3.1. Electronic Absorption Data of 19-22.

Complex	Wavelength (nm)	Absorbance	Concentration (mol/L)	ϵ ($\text{L mol}^{-1}\text{cm}^{-1}$)
19	530	0.0654	2.51×10^{-6}	25977.3
	422	0.7478		297031.4
20	544	0.0567	2.51×10^{-6}	30159.5
	422	0.7770		413776.5
21	535	0.0588	2.51×10^{-6}	23426.3
	426	0.5530		220318.7
22	617	0.0335	2.51×10^{-6}	13313.9
	568	0.0529		21024.0
	443	0.7205		286348.5

**Figure 3.5.** Electronic spectra of 19 (—), 20 (---), and 21 (····).

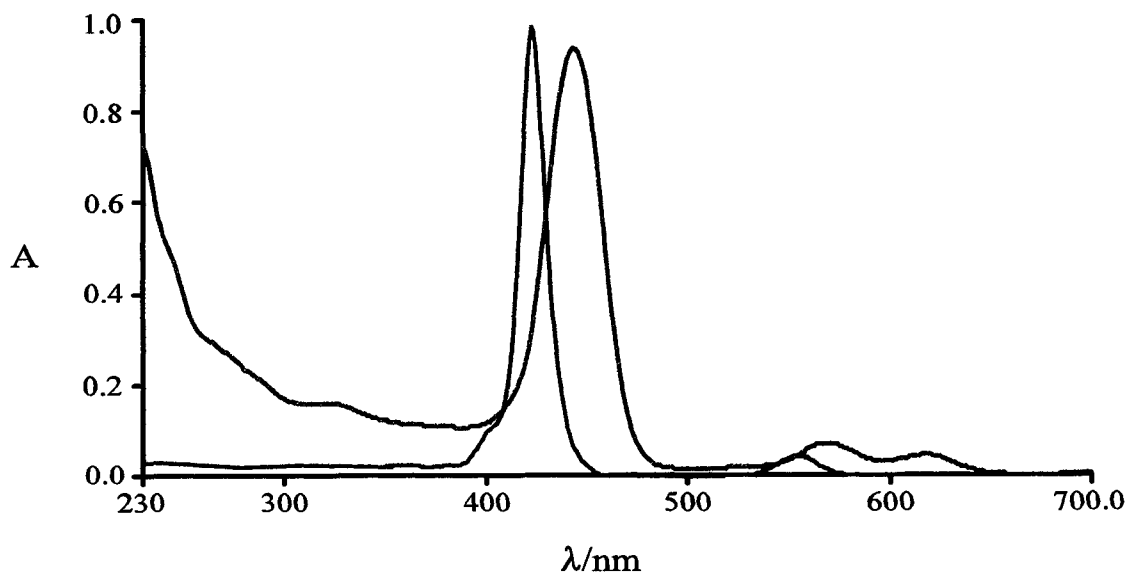
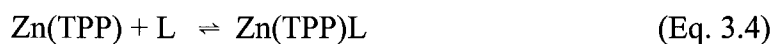


Figure 3.6. Electronic spectra of the non-cluster modified zinc porphyrin (---) and **22** (—).

The electronic spectrum of the non-cluster modified zinc porphyrin (Figure 3.6) has only one Q-band at 559 nm. However, in the spectrum of **22**, not only is there a band at 569 nm, but a new absorption at 617 nm is observed. Since fluorescence is only detectable from the $S_1 \rightarrow S_0$ (Q band) transition because internal conversion from S_2 to S_1 is rapid, the appearance of a new Q band at 617 nm greatly affects the color observed. Furthermore, upon dissolution in solvents of different polarity, the color of the resulting solution varies significantly. To explore such solvatochromic properties of this supramolecular system, the differences in the electronic absorptions of **22** were observed in organic solvents of varying polarity (Table 3.2). As seen in the cases of other zinc metalloporphyrins, the band positions of the zinc tetracluster porphyrin exhibits a pronounced solvent dependence. The spectral shift of the intense Soret absorption is the easiest to follow. This band can shift up to 14 nm,

depending on the solvent used. The accepted description of the Lewis acid-base interaction is the equilibrium (Equation 3.4) in which zinc(II) has fourfold coordination with the porphyrin ring and can accept only a single additional ligand L.



Many attempts have been made to correlate various experimental parameters with the Soret shifts. For example, free energy changes for the reaction relate linearly to the $\text{p}K_{\text{a}}$ of the donor, but only if the ligands are closely related structurally.¹⁴³ There is no general correlation between the red shift and dielectric constant,¹⁴⁴ Drago's parameters,¹⁴⁵ or Gutmann's Donor numbers.¹⁴⁶ The behavior of the present porphyrin system is similar to the results reported in the literature; when a limited number of solvents were used, a correlation with the parameters previously mentioned could be obtained. However, when a larger number of solvents are incorporated, there is no general correlation observed. It was postulated that the limited data set reflects a minor trend of a much more complex phenomenon. Other analyses based upon combinations of parameters fit better with the observed shifts.^{147,148} However, if the parameters include contributions from many effects, the significance of such a correlation is diminished. Clearly, more data is required before any specific contribution to the spectral shifts can be understood.

Table 3.2. Electronic Absorption Data of **22** in Various Solvents

Solvent	Soret λ (nm)	Q Band 1 λ (nm)	Q Band 2 λ (nm)
Acetone	451.89	563.98	609.57
Acetonitrile	441.81	562.72	606.55
Chloroform	451.39	570.28	611.08
Dichloroethane	440.50	562.72	605.04
Dichloromethane	440.30	558.19	598.99
Dimethylformamide	453.90	574.81	623.17
Dimehtyl sulfoxide	444.84	565.74	608.06
Nitromethane	440.83	562.72	605.04
Tetrahydrofuran	447.86	567.25	609.57

3.5. Electrochemical Studies

Metalloporphyrins have their own unique electrochemistry. Upon addition of metal clusters to the periphery of a metalloporphyrin, a combination of cluster and metalloporphyrin properties is anticipated. New electrochemical processes may even be possible due to the change of electronic state upon cluster attachment. Similar to the unmetallated cluster porphyrin array, the zinc and cobalt metalloporphyrin arrays both exhibit only one oxidation at 0.71 V that corresponds to four electrons per oxidation event, established coulometrically. Relevant data for all the porphyrin complexes are summarized in Table 3.3. These oxidations are similar to those observed for other $[\text{Re}_6(\mu_3\text{-Se})_8]^{2+}$ core-containing derivatives reported in the literature.

Table 3.3. Cluster-based Electrochemical Data of 19-22.

Complex	E_{ox} vs. Fc ⁺ /Fc (v)	Electrode Volume (μL)	Q/C ($\mu\text{C}/\text{mM}$)	n
19	0.72	0.373	134	3.7
20	0.70	0.373	137	3.8
21	0.71	0.394	142	3.7
22	0.71	0.466	184	4.1

The voltammogram of **19** is shown in Figure 3.7. In addition to the cluster-based oxidation at 0.72 V, a second peak at 0.86 V was also observed. This signal was found to be a two-electron oxidation ascribed to the Ni²⁺ ion. Similar observations have been previously reported by other groups studying different nickel porphyrin complexes. The

copper metalloporphyrin cluster array voltammogram (Figure 3.8) has three oxidations occurring at 0.70, 0.90, and 1.10 V, respectively. The first oxidation again corresponds to the simultaneous oxidation of four clusters. The other two oxidations were determined to originate from the Cu^{2+} ion, and each corresponds to a one-electron oxidation event. These observations are consistent with what have been reported for other copper porphyrin complexes.

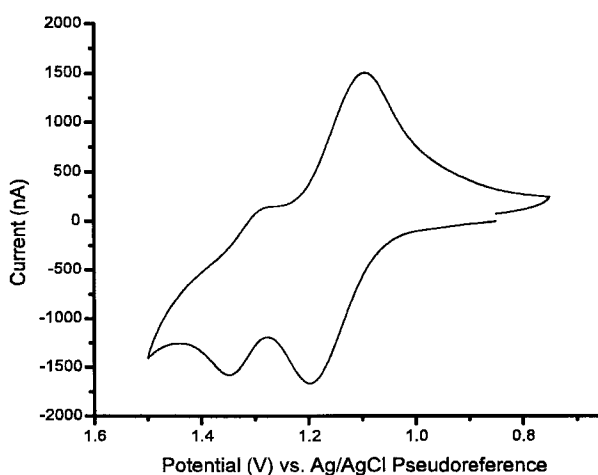


Figure 3.7. Cyclic voltammogram of 19.

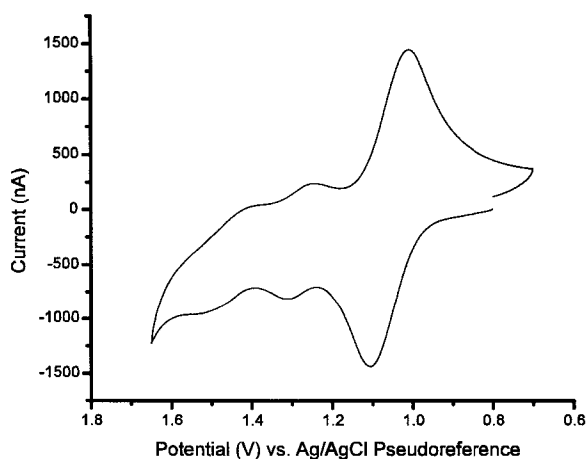


Figure 3.8. Cyclic voltammogram of 20.

3.6. Summary and Perspectives

It has been shown that metal ions can be incorporated into the tetracluster array centered on the tetrapyrrolyl porphyrin platform. Specifically, the synthesis and characterization of Co^{2+} , Ni^{2+} , Cu^{2+} , and Zn^{2+} complexes of **14** were demonstrated. The electrochemistry of these novel metalloporphyrins revealed a combination of the metalloporphyrin and metal cluster oxidations with little, if any, interactions between the two moieties. Furthermore, insights were gained into the photophysics of these assemblies with the examination of the effects of different solvents upon the electronic spectra of the Zn^{2+} tetracluster metalloporphyrin. Future work will include the study of possible catalytic properties, supramolecular construction of extended one-dimensional stacks of metalloporphyrins linked via axial coordination of the central metal ion, as well as two-dimensional arrays via secondary interactions involving the peripheral clusters. Electronic properties of these novel cluster arrays will be probed, as will their self-organization on the nanoscale.

CHAPTER 4

Metallo-dendrimers Supported by $[\text{Re}_6(\mu_3\text{-Se})_8]^{2+}$ Core-Containing Clusters

Abstract

Ligand substitution of **8** with three pyridyl-based ditopic ligands, namely 1,2-bis(4-pyridyl)ethane (**25**), (*E*)-1,2-bis(4-pyridyl)ethene (**26**), and 4,4'-trimethylenedipyridine (**27**), produced three new cluster complexes (**28**, **29**, and **30**) wherein the pyridyl-based ligand coordinates the originally nitrile capped Re(III) site via one of the two N atoms; the other 4-pyridyl group is readily available for further metal complexation. All three complexes were characterized by microanalysis (CHN) and NMR (^1H , ^{31}P , ^{77}Se). The molecular structure of complex **28** has also been established crystallographically. Reactions of these cluster-based ligands with **5**, a cluster derivative fully solvated with acetonitrile, yielded the first *bona fide* metal cluster dendrimers (**31** - **33**), featuring the cluster building blocks at the core, within the branches, and on the periphery of a dendritic architecture. These dendritic cluster arrays were characterized by microanalysis (CHN) and NMR (^1H , ^{31}P , ^{77}Se). The formation of the heptacluster dendrimers was confirmed by comparative ^{77}Se NMR studies of the nitrile solvate **5**, the cluster ligands (**28** - **30**), and the cluster dendrimers (**31**- **33**). Electrochemical studies of **32** have shown two well-defined redox events, one corresponding to a six-electron oxidation and the other, to a one-electron oxidation. These observations are in agreement with the molecular structure of the dendrimers featuring a central cluster unit and six

peripheral ones. It provides an interesting example of electrochemically interactive multicluster system. The unusual electrochemical behavior of **32** is discussed in terms of charge build-up as well as through-bond coupling.

4.1. Introduction

Dendrimers are a class of highly branched, monodisperse, synthetic polymers emanating from a central core. Figure 4.1 depicts the structure of a generic dendrimer with the highlight of three distinct structural regions: the core, the branching units, and the surface functional groups

With such a unique architecture, it is possible to position functional groups in a controlled manner to a specific region of dendrimers, and the potential of creating useful new materials is enormous.¹⁵⁰⁻¹⁵³

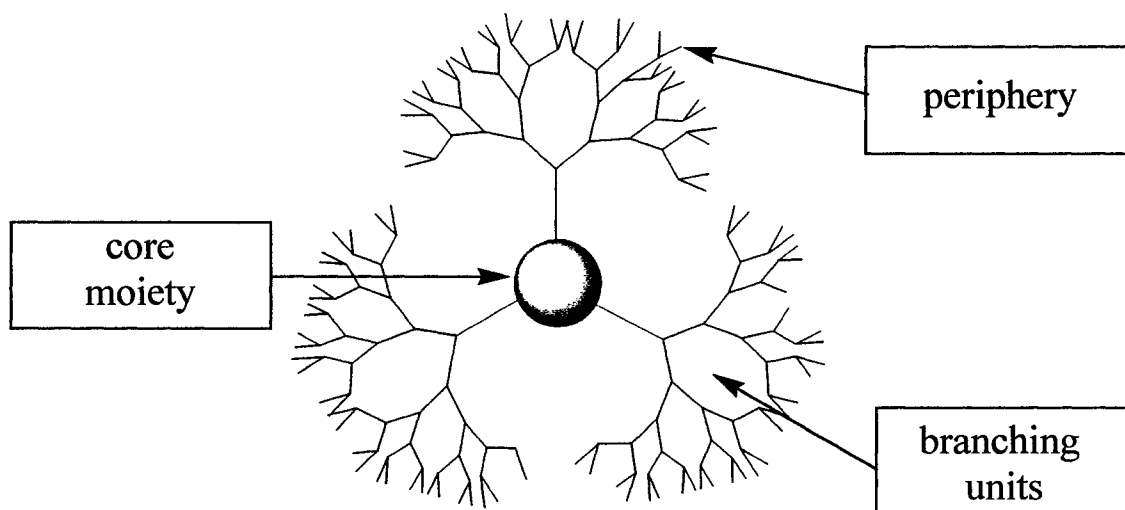


Figure 4.1. A generic dendrimer structure highlighting specific structural regions.

The integration of well-established inorganic and organometallic chemistry with the newly developed dendrimer chemistry is one strategy by which functionality can be introduced into dendritic framework. Within this context, new composite materials referred to as metallodendrimers are created (Figure 4.2).¹⁵⁴⁻¹⁵⁹ The impetus is to combine the unique electronic, magnetic, or catalytic properties of metals with the organic properties and nanoscopic dimensions of dendrimers, thus affording materials that have potential uses in drug delivery,^{160,161} catalysis,¹⁶² and biomedical imaging.¹⁶³ Well-defined metal clusters can in principle replace single metal centers, but offer two advantages over the mononuclear complex-based design. The accessible multiple metal sites of a cluster allow for structurally unique positioning of the ligands and therefore, the realization of structurally unique functional materials. More importantly, the inherent metal-metal and/or metal-ligand interactions provide opportunities for realizing interesting and possibly useful physical and chemical properties, potentially giving rise to new functional composite materials. Though it is expected that the study of metal cluster-based dendrimers will produce many compelling research opportunities with important consequences, only a handful of metal cluster dendrimers have been reported to date.

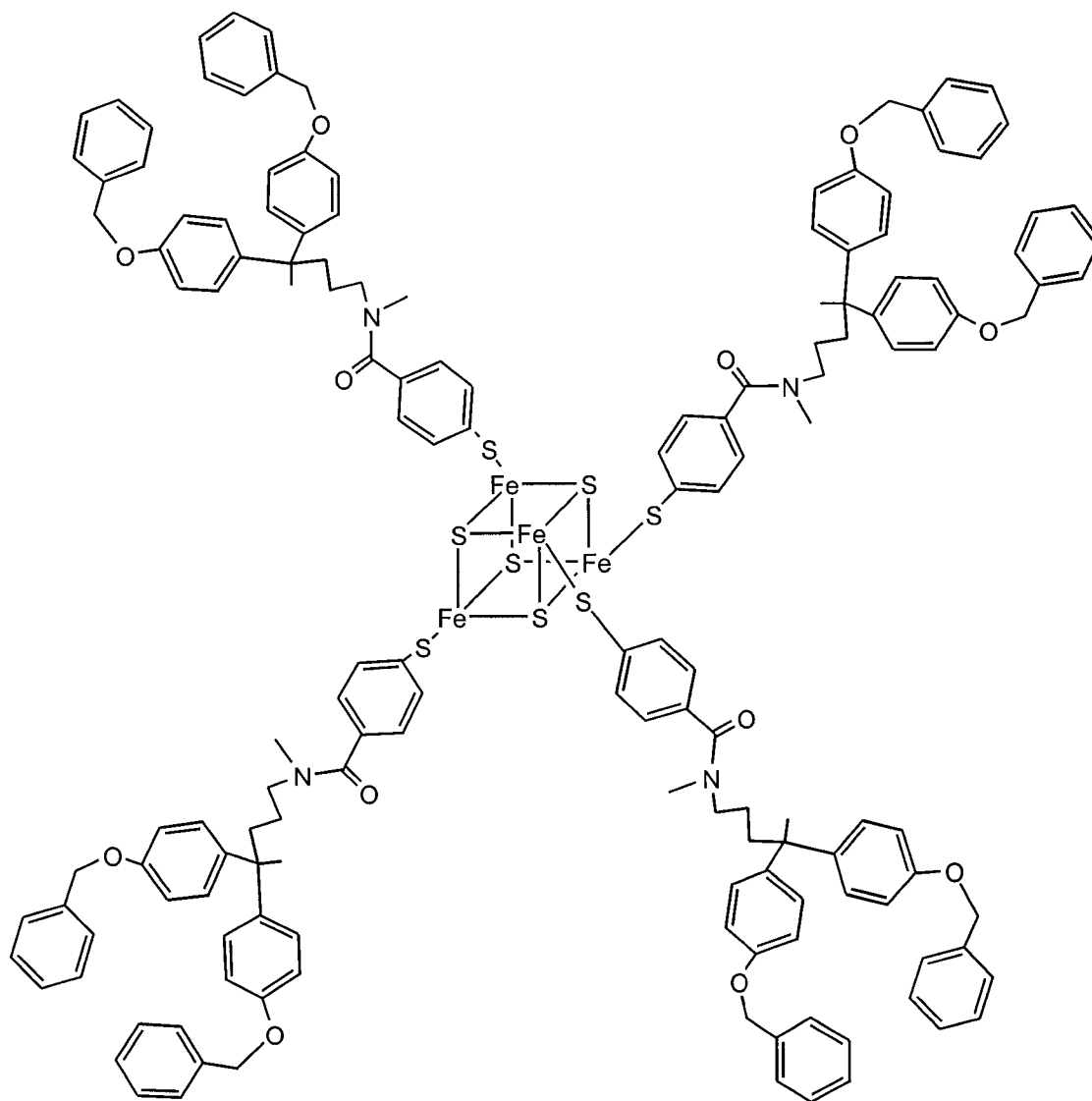


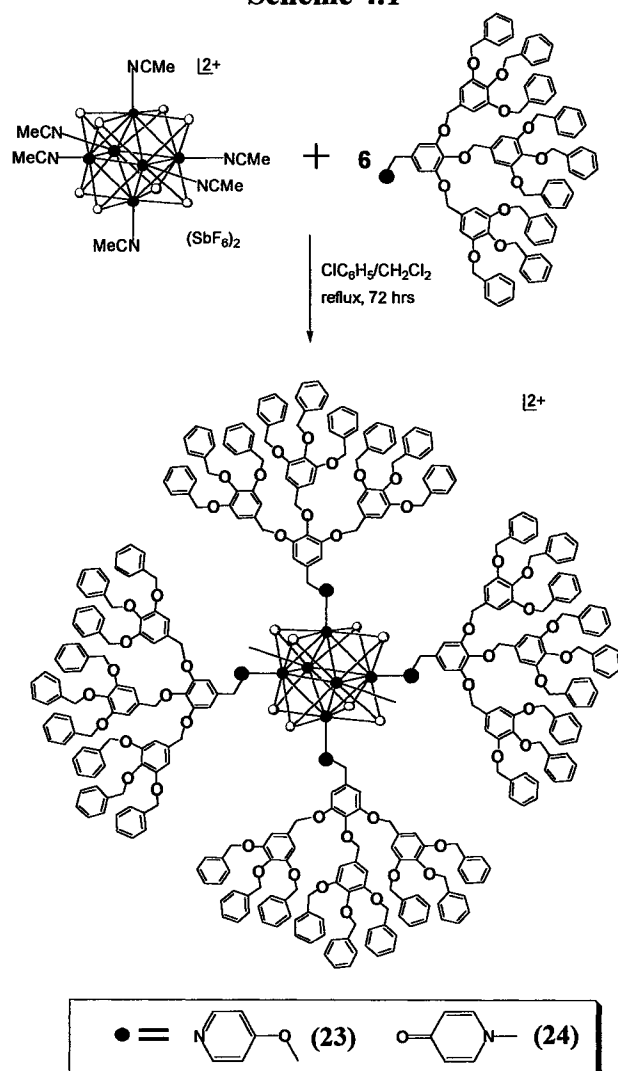
Figure 4.2. Structural depiction of Gorman's first-generation dendrimer featuring a Fe_4S_4 cluster at the core.

The first metal cluster supported metallodendrimers were reported by Gorman and coworkers. They prepared metallodendrimers centered on a $[\text{Fe}_4\text{S}_4]^{2+}$ cluster.¹⁶⁴ They were able to demonstrate that the organic dendritic ligands (dendrons) regulated both the kinetics and potential of the cluster-based redox processes. They also speculated that these compounds could have applications for information storage based upon the electrochemical behavior. Luck and coworkers prepared dendrimers containing dimolybdenum centers and reported that the larger the dendrimer, the more positive the oxidation potential.¹⁶⁵ Wang and Zheng reported the initial efforts using the $[\text{Re}_6(\mu_3\text{-Se})_8]^{2+}$ cluster as a core motif (Scheme 4.1).⁵⁵ These novel compounds exhibit intriguing photophysical properties. Dramatic color changes with slightly structurally different dendrons (Figure 4.3) have been observed. Gorman and coworkers subsequently reported dendrimers supported by an analogous $[\text{Mo}_6(\mu_3\text{-Cl})_8]^{4+}$ core, but no property investigation was reported.¹⁶⁶

Several other groups have introduced metal clusters onto the periphery of dendrimers (Figure 4.4). For example, Rossell and coworkers have coordinated four different types of gold containing clusters to the exterior of dendrimers, including AuMo_2 , AuMn_2 , $[\text{AuFe}_3(\text{CO})_{11}]$, and $[\text{AuFe}_2(\text{CO})_7(\text{PPh}_2)]$.¹⁶⁷⁻¹⁷⁰ Their work has culminated in a metallodendrimer that contains 192 Fe_2Au clusters. Shephard and coworkers, in an attempt to prepare monodisperse nanoparticles with well-defined molecular structures and surface functional groups, constructed clusters of clusters containing $[\text{Ru}_5(\text{CO})_{12}]$ and $[\text{Au}_2\text{Ru}_6(\text{CO})_{16}]$.¹⁷¹ Chérioux and coworkers prepared dendrimers based on dinuclear ruthenium or rhodium units and explored the catalytic potential of these novel materials.¹⁷² They found that a ruthenium-containing dendritic cation increases the catalytic activity of

$[\text{Rh}(\text{CO})_2\text{Cl}_2]$ for the carbonylation of methanol. Astruc and Alonso also synthesized and studied ruthenium cluster metallodendrimers and observed interesting and potentially useful electronic and photophysical properties.¹⁷³ Newkome and coworkers attached polyoxometalates to the surface of hydroxylated dendrimers and determined that there was considerable catalytic activity as well.¹⁷⁴

Scheme 4.1



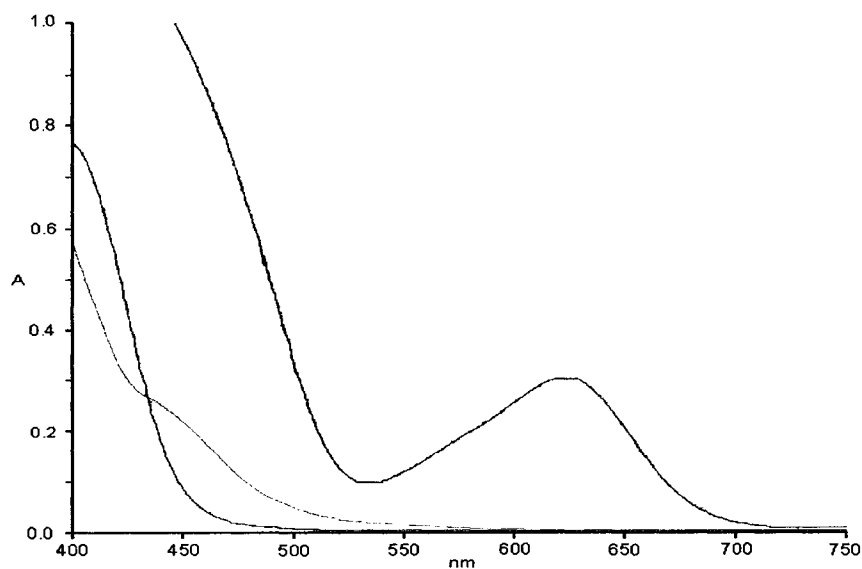


Figure 4.3. Electronic spectra of **5** (—), **23** (---), and **24** (···).

None of the above mentioned reports have exploited more than one region of a dendrimer's architecture until Constable and coworkers incorporated $[\text{C}_2\text{Co}(\text{CO})_6]$ clusters both on the periphery and in the branches (Figure 4.5).¹⁷⁵ This was the first report of more than one region being modified by clusters in a single dendritic system. However, no one has successfully synthesized a *bona fide* cluster metallodendrimer characterized by the presence of cluster motif at the core, within the dendrons, and on the surface. The creation of such a molecule is of significance for a couple of reasons: (1) to demonstrate the feasibility of constructing this new class of dendrimers, and (2) to create novel materials by selectively modifying the structure of a dendrimer and introducing functionalities at specific positions.

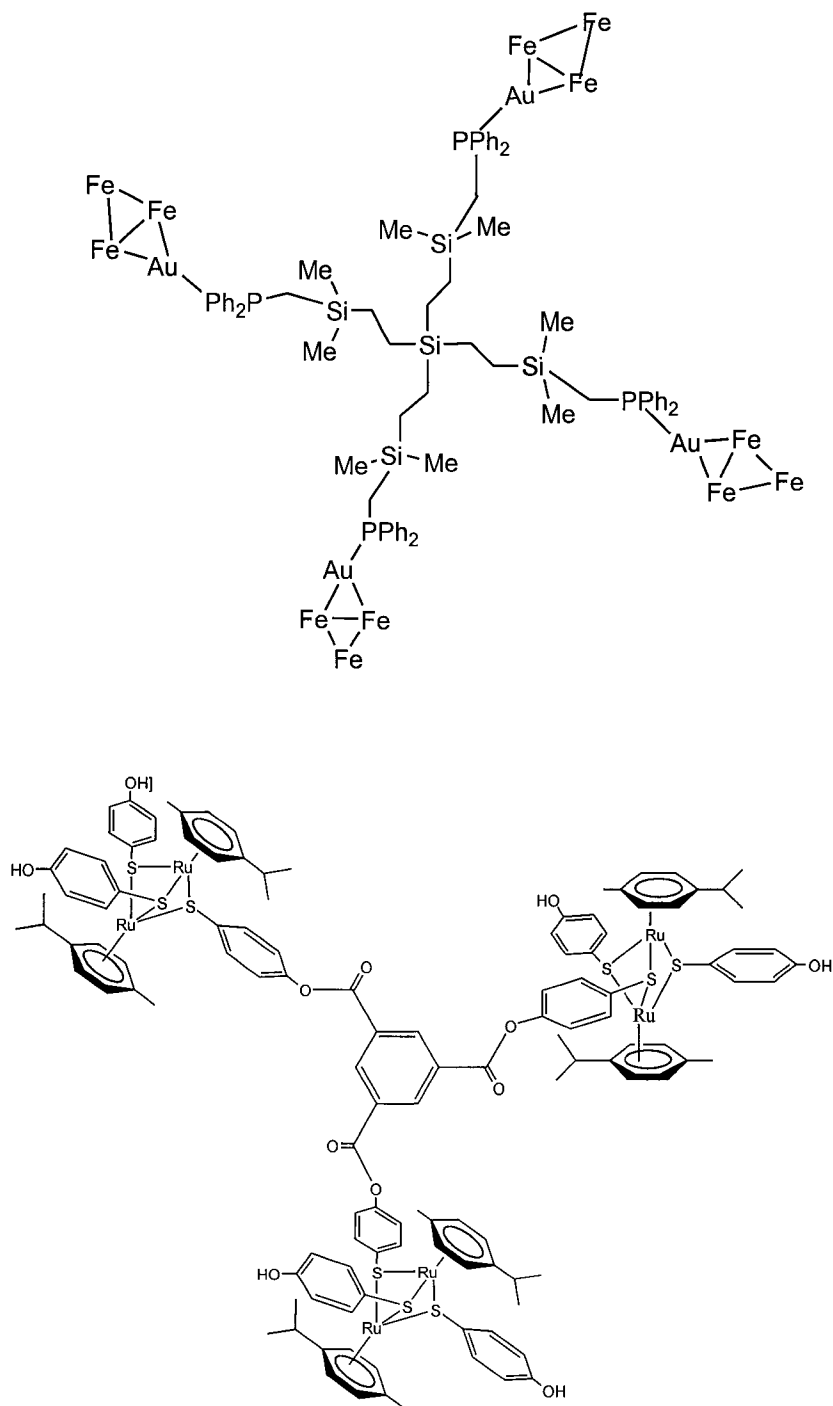


Figure 4.4. Representative dendrimers featuring surface-bound metal clusters.

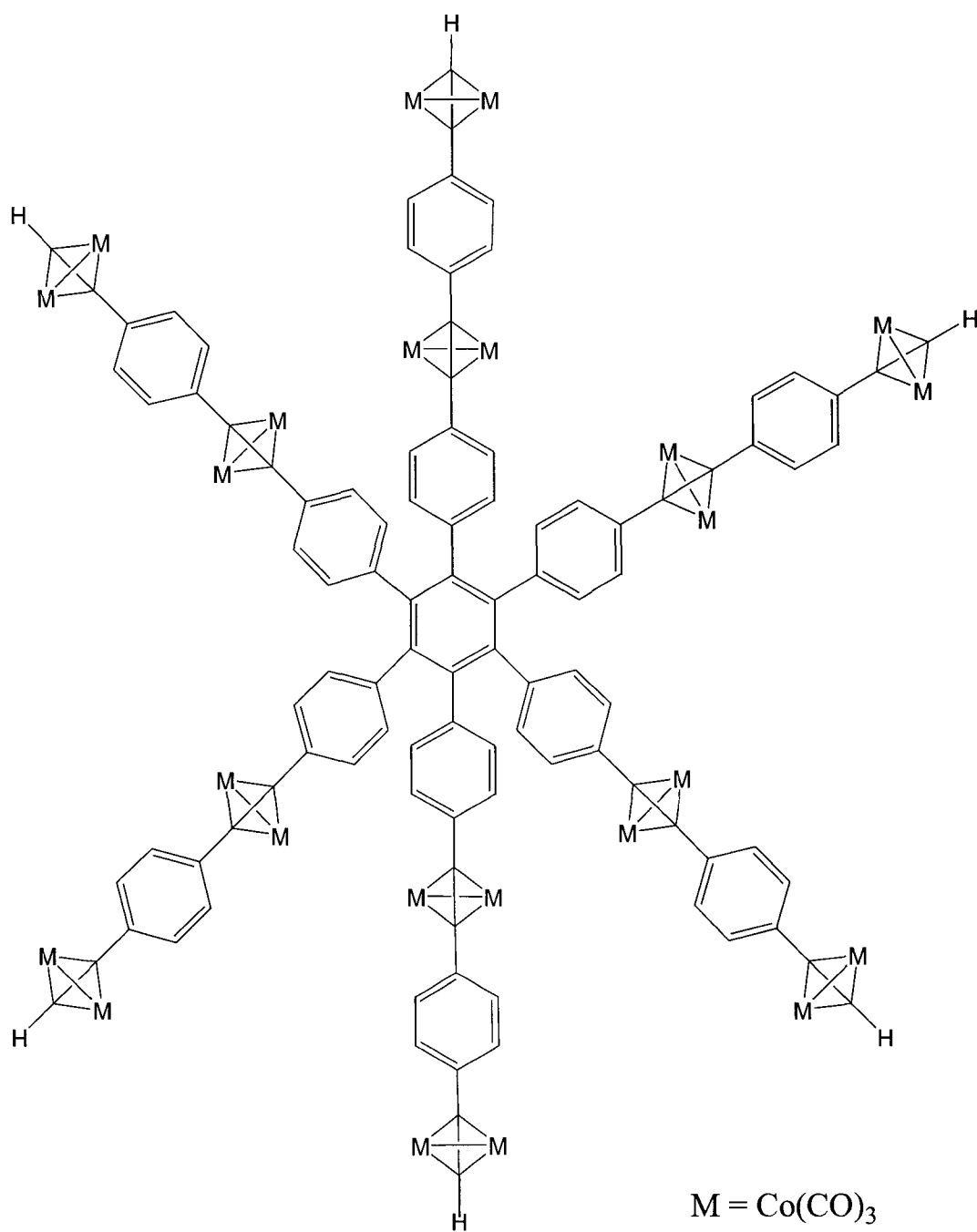


Figure 4.5. Molecular structure of a dendrimer supported by a cobalt carbonyl cluster.

This chapter details our efforts in making the very first, albeit the first generation, *bona fide* metal cluster dendrimers that are characterized by the presence of clusters at the core, within the branches, and on the periphery of a dendritic architecture.⁵⁶ Herein, the design and synthesis of three heptacluster dendrimers featuring one central and six peripheral cluster units bridged by dipyridyl-based ligands are elaborated. The targeted dendrimers were characterized by NMR (¹H, ³¹P, ⁷⁷Se) and elemental analysis. Their electrochemical and photophysical properties were also studied.

4.2. Experimental

General Considerations.

1,2-bis(4-pyridyl)ethane (**25**), 1,2-bis(4-pyridyl)ethene (**26**), 4,4'-trimethylenedipyridine(**27**), (*n*-Bu₄N)PF₆, and AgSbF₆ were obtained from Aldrich and used as received. Complexes **5** and **8** were prepared according to published procedures.³¹⁻³³ The silica gel (mesh size 200-400) used for flash column chromatography was purchased from Natland International Corporation, Research Triangle Park, North Carolina. ¹H and ³¹P NMR spectra were recorded on a Varian AM-300 spectrometer in CD₂Cl₂. Chemical shifts of ³¹P spectra were referenced to 85% H₃PO₄ ($\delta = 0$ ppm, with negative values meaning upfield). ⁷⁷Se NMR spectra were recorded on a Bruker 500 spectrometer in CD₃CN. Chemical shifts of ⁷⁷Se spectra were referenced to diphenyldiselenide [460 ppm relative to a 6% solution (v/v) of dimethylselenide in CD₃CN (0 ppm)]. Elemental analyses (CHN) were performed by Desert Analytics Laboratory, Tucson, Arizona.

Complex 28. A mixture of **8** (362 mg, 0.127 mmol) and **25** (860 mg, 4.67 mmol) in 50 mL of a chlorobenzene/nitromethane mixture (v/v 10:1) was stirred under reflux for 24 hours. The orange-red residue obtained upon removal of the solvent was washed with toluene (4 x 50 mL) to remove unreacted **25**. The resulting orange-red powder was subjected to flash column chromatography using silica gel and an eluting solvent mixture of dichloromethane and acetonitrile (5:1 v/v; R_f = 0.50). Yield: 0.320 g (85.3%). ¹H NMR: δ

1.00-1.40 (m), 2.00-2.40 (m), 3.10 (s), 7.10 (d), 7.42 (bs), 8.55 (bs), 9.10 (d). ^{31}P NMR: δ -21.67 (s), -24.97 (s). ^{77}Se NMR: δ -307 (s), -361 (s). Anal. Calcd for $\text{C}_{42}\text{H}_{87}\text{N}_2\text{P}_5\text{Re}_6\text{Se}_8\text{Sb}_2\text{F}_{12}$: C, 17.17; H, 3.18; N, 0.93. Found: C, 16.81; H, 2.96; N, 1.00.

Complex 29 was obtained as an orange-red powder in a manner similar to **28** except that **26** was used in place of **25**. Yield: 0.309 g (82.7%). ^1H NMR: δ 1.00-1.60 (m), 2.00-2.30 (m), 7.35-7.53 (m), 8.62 (d), 9.20 (d). ^{31}P NMR: δ -24.95 (s), -28.29 (s). ^{77}Se NMR: δ -305 (s), -360 (s). Anal. Calcd for $\text{C}_{42}\text{H}_{85}\text{N}_2\text{P}_5\text{Re}_6\text{Se}_8\text{Sb}_2\text{F}_{12}$: C, 17.17; H, 3.18; N, 0.93. Found: C, 16.81; H, 2.96; N, 1.00.

Complex 30 was obtained as an orange powder in a manner similar to **28** except that **27** was used in place of **25**. Yield: 0.143 g (52.4%). ^1H NMR: δ 0.99-1.16 (m), 2.05-2.30 (m), 2.67-2.85(m), 7.12 (d), 7.21 (d), 8.45 (d), 9.12 (d). ^{31}P NMR: δ -22.56 (s), -25.82 (s). ^{77}Se NMR: δ -306 (s), -361 (s). Anal. Calcd for $\text{C}_{43}\text{H}_{89}\text{N}_2\text{P}_5\text{Re}_6\text{Se}_8\text{Sb}_2\text{F}_{12}$: C, 17.17; H, 3.18; N, 0.93. Found: C, 16.81; H, 2.96; N, 1.00.

$\{\text{Re}_6(\mu_3\text{-Se})_8[(\text{Re}_6(\mu_3\text{-Se})_8(\text{PEt}_3)_5(4,4'\text{-py}_2\text{C}_2\text{H}_4)]_6)\}(\text{SbF}_6)_{14}$ (31). A mixture of **5** (14.0 mg, 0.0056 mmol) and **25** (100 mg, 0.0333 mmol) in 75 mL of chlorobenzene was stirred under reflux for 2 hours. The light brown residue obtained upon removal of the solvent was subjected to Soxhlet extraction with chlorobenzene for 48 hours. Yield: 0.080 g (68%). ^1H NMR: δ 1.05-1.40 (m), 2.10-2.40 (m), 3.10 (s), 7.20-7.40 (md), 9.15 (d), 9.55 (d). ^{31}P NMR: δ -24.89 (s), -28.56 (s). ^{77}Se NMR: δ -249 (s), -307 (s), -361 (s). Anal. Calcd for $\text{C}_{252}\text{H}_{522}\text{N}_{12}\text{P}_{30}\text{Re}_{42}\text{Se}_{56}\text{Sb}_{14}\text{F}_{84}$: C, 14.99; H, 2.61; N, 0.83. Found: C, 15.19; H, 2.66; N, 0.94.

$\{\text{Re}_6(\mu_3\text{-Se})_8[(\text{Re}_6(\mu_3\text{-Se})_8(\text{PEt}_3)_5(4,4'\text{-py}_2\text{C}_2\text{H}_2))_6](\text{SbF}_6)_{14}\}$ (**32**) was obtained as a light brown powder in a manner similar to **31** except that **26** was used in place of **25**. Yield: 0.080 g (50%). ^1H NMR: δ 1.05-1.20 (m), 2.10-2.30 (m), 7.40-7.60 (md), 9.20 (d), 9.65 (d). ^{31}P NMR: δ -24.93 (s), -28.43 (s). ^{77}Se NMR: δ -240 (s), -305 (s), -360 (s). Anal. Calcd for $\text{C}_{252}\text{H}_{510}\text{N}_{12}\text{P}_{30}\text{Re}_{42}\text{Se}_{56}\text{Sb}_{14}\text{F}_{84}$: C, 15.00; H, 2.55; N, 0.83. Found: C, 15.33; H, 2.67; N, 1.02.

$\{\text{Re}_6(\mu_3\text{-Se})_8[(\text{Re}_6(\mu_3\text{-Se})_8(\text{PEt}_3)_5(4,4'\text{-py}_2\text{C}_3\text{H}_6))_6](\text{SbF}_6)_{14}\}$ (**33**) was obtained as a light brown powder in a manner similar to **31** except that **27** was used instead of **25**. Yield: 0.070 g (50%). ^1H NMR: δ 1.05-1.30 (m), 2.15-2.35 (m), 7.10-7.35 (m), 9.15 (d), 9.55 (d). ^{31}P NMR: δ -19.10 (s), -22.42 (s). ^{77}Se NMR: δ -248 (s), -307 (s), -360 (s). Anal. Calcd for $\text{C}_{258}\text{H}_{534}\text{N}_{12}\text{P}_{30}\text{Re}_{42}\text{Se}_{56}\text{Sb}_{14}\text{F}_{84}$: C, 15.27; H, 2.63; N, 0.83. Found: C, 15.30; H, 2.76; N, 0.82.

Other Physical Measurements.

Electronic absorption spectra in dichloromethane solutions were recorded on a Perkin Elmer Lambda 10 spectrophotometer. Electrochemical studies were carried out using a thin layer electrode whose design has been described in Chapter 2.

X-ray Structure Determinations.

An orange block of **28** having approximate dimensions of 0.09 x 0.10 x 0.27 mm was mounted on a glass fiber in a random orientation. Data were collected on the SMART1000 system using graphite monochromated Mo $K\alpha$ radiation ($\lambda = 0.71073\text{\AA}$).

Cell constants and an initial orientation matrix were determined from reflections obtained in three orthogonal 5° wedges of reciprocal space. A total of 4898 frames at a

detector setting covering $0^\circ < 2\theta < 60^\circ$ were collected, having an omega scan width of 0.15° and an exposure time of 10 seconds. A total of 80327 reflections were integrated and retained, of which 16388 were unique. Of the unique reflections, 12908 (78.8%) were observed $I > 2\sigma(I)$. Empirical absorption and decay corrections were applied using the program SADABS.

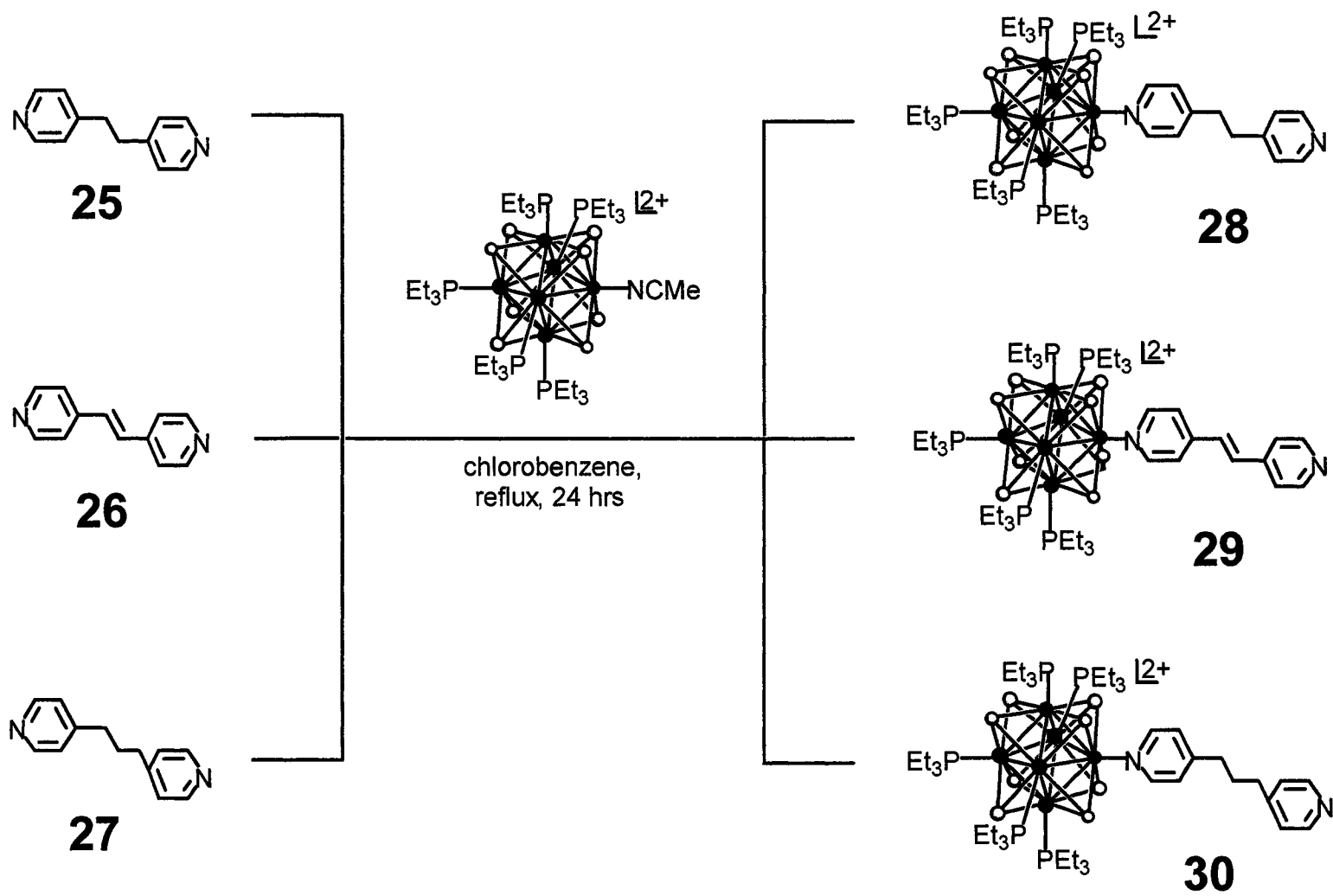
The structure was solved using SHELXS in the Bruker SHELXTL (Version 5.0) software package. Refinements were performed using SHELXL and illustrations were made using XP. Solution was achieved utilizing direct methods followed by Fourier synthesis. Hydrogen atoms were added at idealized positions, constrained to ride on the atom to which they are bonded and given thermal parameters equal to 1.2 or 1.5 times U_{iso} of that bonded atom. The final anisotropic full-matrix least squares refinement based on F^2 of all reflections converged (maximum shift/esd = 0.005) at $R1 = 0.0417$, $wR2 = 0.0790$ and goodness-of-fit = 1.057. "Conventional" refinement indices using the 12908 reflections with $F > 4 \sigma(F)$ are $R1 = 0.0299$, $wR2 = 0.0753$. The model consisted of 662 variable parameters, X constraints, and 13 restraints. There were 18 correlation coefficients between 0.694 and 0.5. All correlation coefficients were between the thermal parameters of the multiple fluorines with unresolved disorder. The highest and lowest peaks on the final difference map were 2.190 and $-2.170 e/\text{\AA}^3$, respectively. Scattering Factors and anomalous dispersion were taken from International Tables Vol. C, Tables 4.2.6.8 and 6.1.1.4.

4.3. Synthesis and Characterization

4.3.1. Synthesis of Cluster Dendrons

Synthesis and characterization of metal cluster dendrons is the first step in synthesizing the targeted dendrimers. The reaction of the acetonitrile solvate **8** with an excess of **25**, **26**, or **27** in a mixture of chlorobenzene/nitromethane (v/v 5:1) under reflux (Scheme 4.2) produced the desired dendrons. As an example, reacting **8** with an excess of **25** afforded **28** in good yields after column chromatography using a mixture of dichloromethane/acetonitrile (v/v 5:1). Several spectroscopic studies support the proposed structure and stereochemistry of **28**. Upon the formation of **28**, the proton resonance of the coordinated nitrile of **8** disappears, indicating the displacement of the bonded solvent molecule. This is corroborated by the emergence of a signal at 9.10 ppm (a, Figure 4.6), attributable to the α -H of the coordinated pyridyl moiety; this is significantly shifted from the corresponding resonance of the uncoordinated pyridyl moiety at 8.55 ppm. Also clear from Figure 4.6 is the noticeable but less dramatic shift of the β -H signal. The ^{31}P NMR spectrum of **28** (a, Figure 4.6) is straightforward, showing two ^{31}P resonances at -21.67 and -24.97 ppm in a relative ratio of 4:1, which is characteristic of a pentaphosphine-substituted isomer. The corresponding signals of the starting cluster solvate appear at -19.10 and -23.3 ppm, respectively. The ^{77}Se NMR is also unsophisticated, showing two resonances of equal intensities at -307 and -361 ppm, in agreement with the two distinct environments for the eight Se atoms.

Scheme 4.2



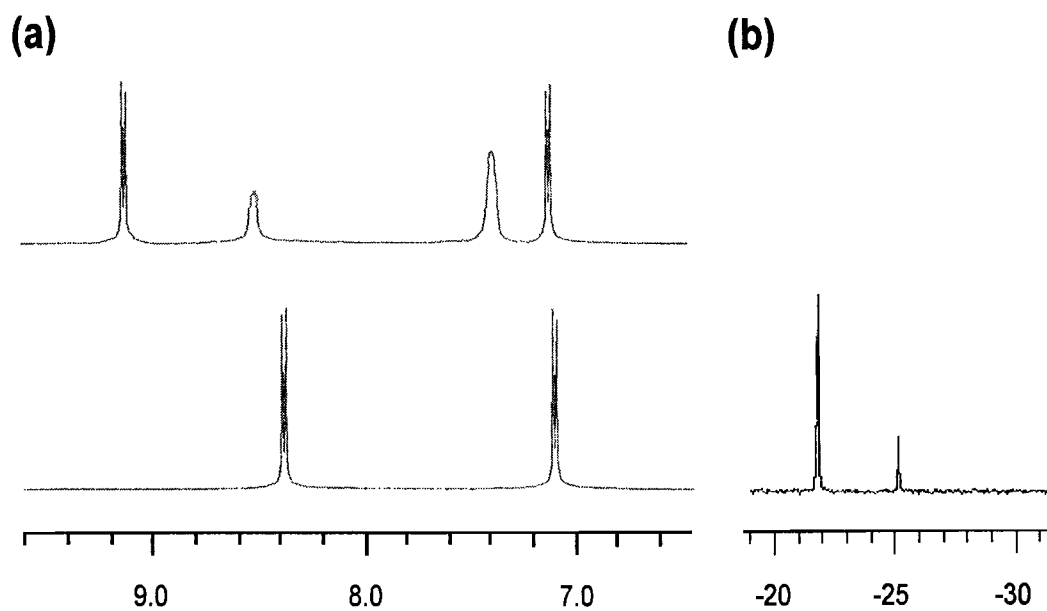


Figure 4.6. (a) ^1H NMR spectra of **25** (bottom) and **28** (top). Only the aromatic resonances are shown. (b) ^{31}P NMR spectrum of **28**.

The syntheses of **29** and **30** were accomplished in the same manner as **28**. As in the case of **28**, formation of **29** and **30** is marked by the displacement of acetonitrile with **26** or **27**, as confirmed by ^1H NMR spectroscopy. The coordinated α -H and β -H resonances are centered at 9.10 and 7.42 ppm for **29** and 9.12 and 7.21 ppm for **30**. Two signals with a 4:1 relative intensity in the ^{31}P spectrum confirm two different phosphine environments characteristic of the pentaphosphine-substituted isomer. The ^{77}Se NMR has two resonances of equal intensity.

4.3.2. X-ray Crystallography of Complex 28

The structure of **28** was determined and the crystal data and refinement parameters are reported in Table 4.1. Parameters describing the cluster core and its terminal bonding are summarized in Table 4.2 and are unremarkably similar to the corresponding values reported for similar compounds. The dipyriddy organic ligands are well-known to be excellent spacers for supramolecular design. As a consequence of the freedom of rotation exhibited by the ethylene group, **25** can adopt two different conformations, *anti* or *gauche*. Due to steric hindrance the majority of the structures featuring this ligand are oriented in the *anti* conformation. However, there are examples in the literature where **25** assumes the *gauche* conformation. These structures are usually stabilized by metal coordination¹⁷⁶⁻¹⁷⁸ or hydrogen-bonding.¹⁷⁹⁻¹⁸⁰ The ligand having a torsion angle of 56.4(9)° similar to the values reported for analogous structures, and is clearly in the *gauche* conformation (Figure 4.7). This conformation is stabilized in the present structure by hydrogen bonding interaction of the uncoordinated pyridyl nitrogen and triethylphosphine ligands of a neighboring [Re₆(μ₃-Se)₈]²⁺ cluster.

Table 4.1. Crystallographic Data and Structural Refinement of **28**.

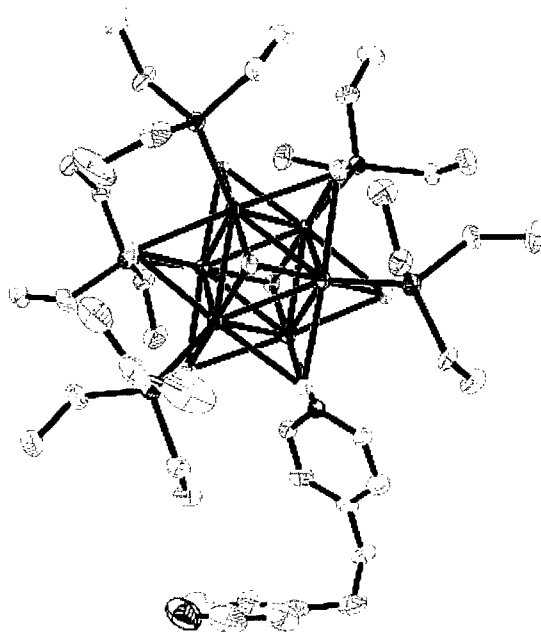
Empirical formula	$C_{42}H_{87}F_{12}N_2P_5Re_6Sb_2Se_8$
Formula weight	2995.37
Crystal size	0.27 x 0.10 x 0.09 mm
Crystal system	Monoclinic
Space group	$P2_1/n$
Unit cell dimensions	$a = 16.960(10) \text{ \AA}$ $\beta = 96.263(2)^\circ$ $b = 20.695(9) \text{ \AA}$ $c = 20.184(10) \text{ \AA}$
Volume, Z	$7044.3(6) \text{ \AA}^3, 4$
Density, calcd Mg/m^3	2.824
Abs. coeff., mm^{-1}	15.330
$F(000)$	5440
Theta range for data collection	1.41 to 28.34°
Limiting indices	$-22 \leq h \leq 22, -27 \leq k \leq 27, -26 \leq l \leq 25$
Reflections utilized	80327
Independent reflections	16388 [R(int) = 0.0472]
Data/restraint/parameter	16388/13/662
GOF on F^2	1.057
R indices [$I > 2\sigma(I)$]	R1 = 0.0229, wR2 = 0.753
R indices (all data) ^a	R1 = 0.0417, wR2 = 0.0790

$$^a R1 = \sum ||F_o| - |F_c|| / \sum |F_o|, wR2 = \{ \sum [w(F_o^2 - F_c^2)^2] / \sum [w(F_o^2)^2] \}^{1/2}.$$

Table 4.2. Selected bond lengths (Å) and angles (°) of **28**.

Bond lengths	
Re-Re	2.6287(3)-2.6463(3); mean 2.636
Re-Se	2.505(6)-2.533(6); mean 2.517
Re-P	2.466(15)-2.479(14); mean 2.476
Re-N	2.203(4)

Bond angles	
Re-N-C	121.5(4) and 121.8(4)
C(3)-C(6)-C(7)-C(11)	56.4(9)

**Figure 4.7.** An ORTEP view (50% probability) showing cationic core of **28**. Color schemes: C (gray), N (blue), P (purple), Re (green), Se (brown)

4.3.3. Synthesis of Cluster-Based Metallodendrimers

These metal cluster dendritic arrays feature a $[\text{Re}_6(\mu_3\text{-Se})_8]^{2+}$ central core bridged by pyridyl-based ditopic ligands to six peripheral $[\text{Re}_6(\mu_3\text{-Se})_8(\text{PEt}_3)_5]^{2+}$ cluster units. The synthesis is based upon the divergent methodology for dendrimer construction as described in the literature. Unfortunately, the initial attempted synthesis utilizing 4,4'-dipyridyl, the simplest pyridyl-based ditopic ligand, failed to produce the desired dendrimer. One possible explanation is that the charge build up is too great for such a compact structure, but the reason remains to be determined.

The next attempt used the more complex derivative **28**. As a representative, **5** and 6 equivalents of **28** in chlorobenzene were stirred under reflux for 2 hours (Scheme 4.3). The solution contained primarily the desired product **31**, in addition to a small amount of unidentified impurities. Initially, the purification of the cluster dendrimer appeared to be the road block. Both flash column chromatography and recrystallization failed to produce pure cluster dendrimer **31**. However, since the precipitate formed appears to be the major product **31**, it seemed reasonable to believe that extraction with chlorobenzene could separate the desired product from the more soluble impurities. Soxhlet extraction was thus employed using chlorobenzene as the extraction solvent. Indeed, pure **31** was obtained as a light brown solid after extraction for 72 hours.

Upon formation of **31**, the proton resonances of the coordinated nitriles of $[\text{Re}_6(\mu_3\text{-Se})_8(\text{MeCN})_6](\text{SbF}_6)_2$ disappear, indicating that all the bonded solvent molecules are displaced. Also supporting this are the disappearance of the α -H resonance at 8.55 ppm of

the uncoordinated pyridyl of **28** and the accompanying appearance of a signal at 9.55 ppm (a, Figure 4.8), due to coordination to the cationic cluster. Less drastic is the downfield shift from 9.10 to 9.15 ppm of the α -H of the coordinated pyridyl moiety and the convergence of the pyridyl β -H between 7.20 and 7.40 ppm. The observation of two pyridyl-based resonances shifted well downfield with respect to any signals of **25** clearly indicates that both pyridyl nitrogen atoms are now coordinated to clusters, but in different chemical environments. Also, the convergence of the β -H is consistent with a more symmetrical chemical environment experienced by these protons. The simplicity of the ^1H NMR is due to the symmetric structure of **31**, where all the bridging ligands are equivalent. The ^{31}P NMR spectrum of **31** is unsophisticated, showing two ^{31}P resonances in a relative ratio of 4:1 shifted downfield from -24.89 and -28.56 ppm to -21.67 and -24.97 ppm, (b, Figure 4.8).

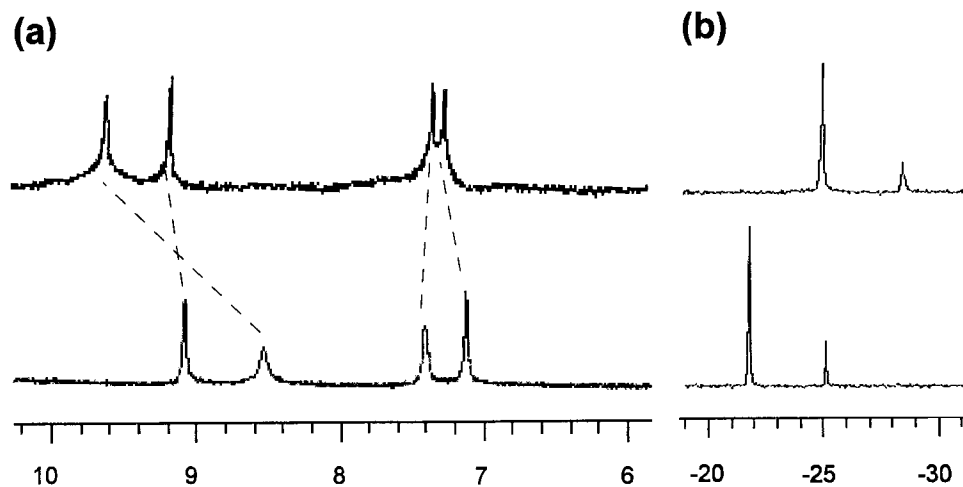


Figure 4.8. (a) ^1H NMR spectra of **28** (bottom) and **31** (top). Only the aromatic resonances are shown. (b) ^{31}P NMR spectra of **28** (bottom) and **31** (top).

The most convincing evidence supporting the formation of the desired heptacluster dendrimers is provided by the comparative ^{77}Se NMR studies of **8**, **28**, and **31**. Complex **5** is completely symmetrical and gives rise to one ^{77}Se resonance peak at -284 ppm (bottom, Figure 4.9). As mentioned previously, **28** has two distinct ^{77}Se resonances with a 1:1 ratio (middle, Figure 4.9). The selenium atoms of **31** are present in three different chemical environments (top, Figure 4.9). The relative signal intensity indicates a ratio of 3:3:1 for the different types of selenium; such a ratio is mandated by, and thus in agreement with, the formulation of the heptacluster dendrimer. More significant is the signal at -249 ppm, which is a new feature when the spectrum is compared with that of **28**, and is assigned to the selenium atoms associated with the central cluster. This resonance is shifted downfield by 35 ppm from its equivalent at -284 ppm for **8**. The ^{77}Se resonances of the peripheral clusters remain essentially unchanged, likely because the local structural alteration upon dendrimers

formation is minimal. The use of ^{77}Se NMR has been instrumental for the characterization of many selenium-containing compounds and is especially valuable when the product cannot be unambiguously established by other characterizations techniques, such as mass spectrometry. Microanalysis (CHN) is also in agreement with the expected stoichiometry.

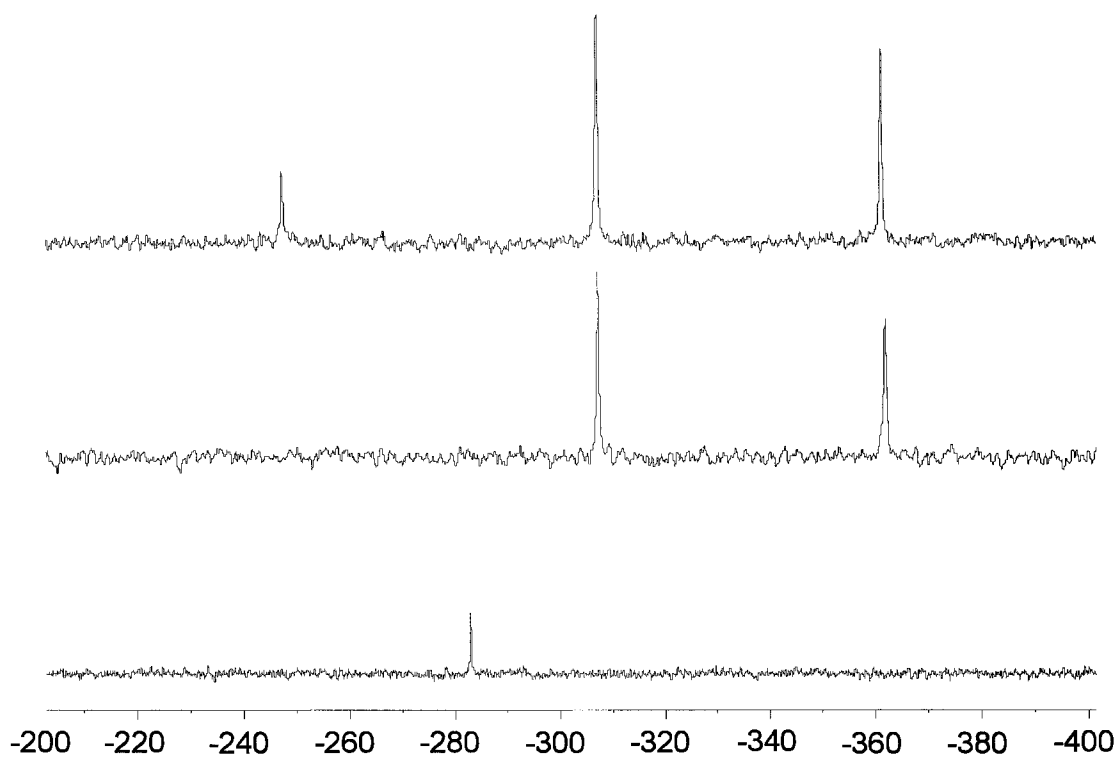


Figure 4.9. ^{77}Se NMR spectra of **5** (bottom), **28** (middle), and **31** (top).

Encouraged by the successful synthesis and purification of **31**, two additional cluster metallodendrimers, **32** and **33**, were prepared analogously. Similar to **31**, the formation of **32** and **33** are accompanied by the loss of the upfield ^1H NMR signal, corresponding to the displacement of all the bonded nitriles of the central cluster. Corroborating is the appearance of downfield signals, attributable to the α -H atoms of the coordinated pyridyl moiety. The ^{31}P NMR spectra are not complicated, as is expected, showing two resonance peaks with a relative ratio of 4:1. The ^{77}Se NMR spectra have three different chemical shifts in a 3:3:1 intensity ratio, which is in agreement with the formation of the heptacluster dendrimers. The signal at -240 ppm confirms that the bonded solvent molecules were replaced by six dendrons, creating a different chemical environment around the central cluster core.

4.4. Electronic Spectroscopic Studies

Shown in Figure 4.10 are the absorption spectra of the three dendrons in dichloromethane solutions. The broad, mostly featureless absorption in the region 210-500 nm is due to ill-resolved ligand-to-metal cluster charge transfer transitions. Though it has been demonstrated that dramatic color changes can occur when structurally different ligands are allowed to react with the cluster core, this was not the case with these dipyriddy-based ligands. The spectra of **28-30** are almost identical, as are their respective molar absorptivity. Figure 4.11 shows the electronic spectra of the corresponding metallodendrimers. Complexes **31** and **33** have very similar absorption spectra to those of the dendrons, but **32** has two ill-defined peaks in the region of 270-400 nm, not observed in any other spectra. This is thought to be due to changes in chemical and electronic structures caused by delocalization through the conjugated ligand system.

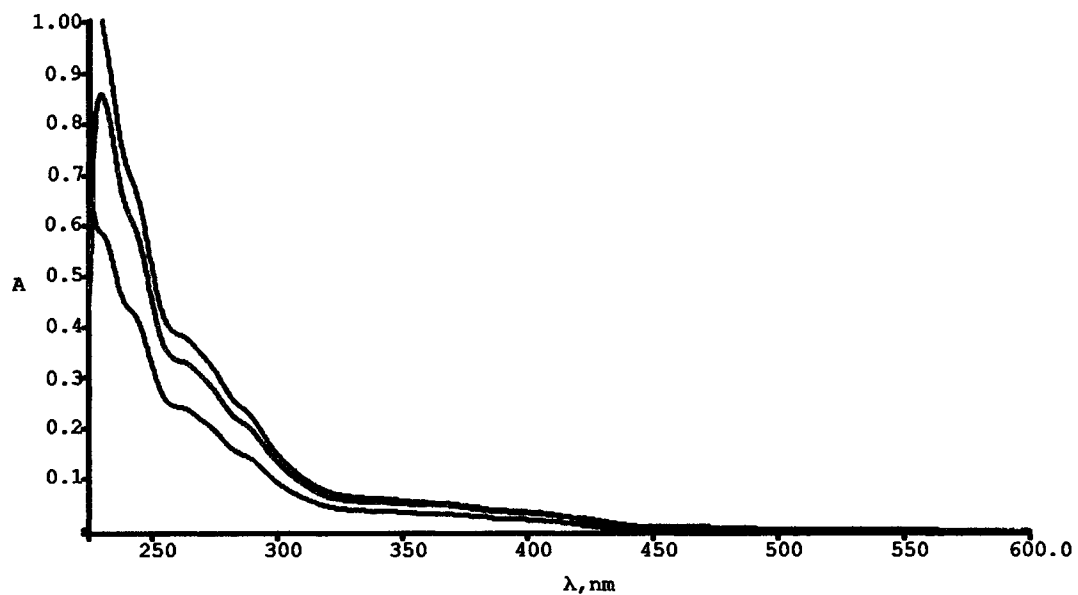


Figure 4.10. Electron spectra of 28 (—), 29 (—), and 30 (—).

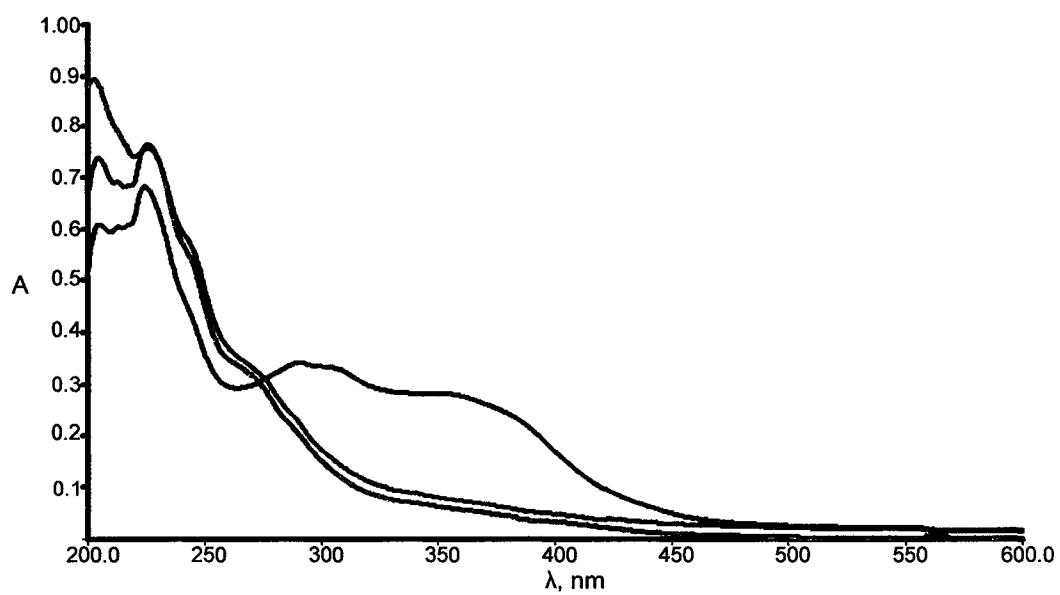


Figure 4.11. Electron spectra of 31 (—), 32 (—), and 33 (—).

4.5. Electrochemical Studies

Cyclic voltammetry was performed to determine the oxidation potentials of the dendrons and dendrimers. Relevant data are listed in Table 4.3. All three dendrons **28-30** have similar oxidations at 0.70, 0.72, and 0.68 V, respectively. Coulometry was not performed on the dendrons because there are literature precedents which suggest that only one electron oxidation will occur.

Table 4.3. Electrochemical Data for **28-33**.

Complex	E_{ox} vs. Fc^+/Fc (V)	Electrode Volume (μL)	Q/C ($\mu\text{C}/\text{mM}$)	n
28	0.70	----	----	----
29	0.72	----	----	----
30	0.68	----	----	----
31	0.71	0.373	237	6.6
32	0.73, 0.88	0.373	207, 39	5.8, 1.1
33	0.69	0.373	255	7.1

Electrochemistry of the dendrimers is of great interest because of possible electronic communication between the cluster units. It is demonstrated by ^{77}Se NMR that the peripheral clusters are chemically different from the central cluster. Therefore, there is the possibility of electronic interaction between the clusters on the periphery and the cluster at the core of the dendrimer. Dendrimer **33** has a similar voltammogram to that of the dendrons. The dendrimer gives rise to one oxidation occurring at 0.69 V (top, Figure 4.12) Coulometric studies reveal that this dendrimer has no observable electronic interaction between clusters

and that all seven clusters oxidize simultaneously. This suggests that each cluster acts like a single cluster species. Dendrimer **31** also exhibits one oxidation event corresponding to seven electrons. Unlike **33**, however, the cyclic voltammogram of **31** is not as straightforward (middle, Figure 4.12). Since the only change to the structure is the length of the linker molecule, it seems that the effect is due to build up of charge around the complex. This would have the effect of slowing down the process of removing all seven of the electrons from a specific complex. A competition would be set up between those complexes that have had multiple electrons removed and those who are just getting their first electron removed. Due to this process the oxidation wave is complicated. The remaining dendrimer **32**, however, gives rise to two oxidations occurring at 0.73 and 0.88 V in a 6:1 ratio (bottom, Figure 4.12). The difference in the results cannot be rationalized with a charge build-up argument because the change in the length of the linker ligand is minimal when compared to **31**. This suggests the ability to delocalize the charge build-up through the conjugated ligand **29**, which would make removal of electrons from the core cluster more difficult and its oxidation would thus occur at a higher potential than the peripheral clusters, which is indeed what has been observed. This is the first known example of electronic coupling between clusters bridged by dipyriddy ligands.

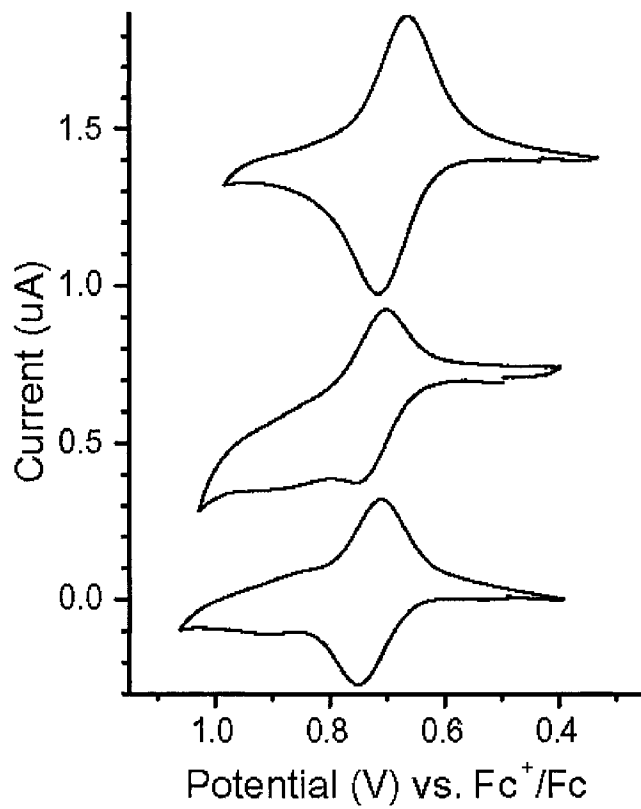


Figure 4.12. Cyclic voltammograms of 32 (bottom), 31 (middle), and 33 (top).

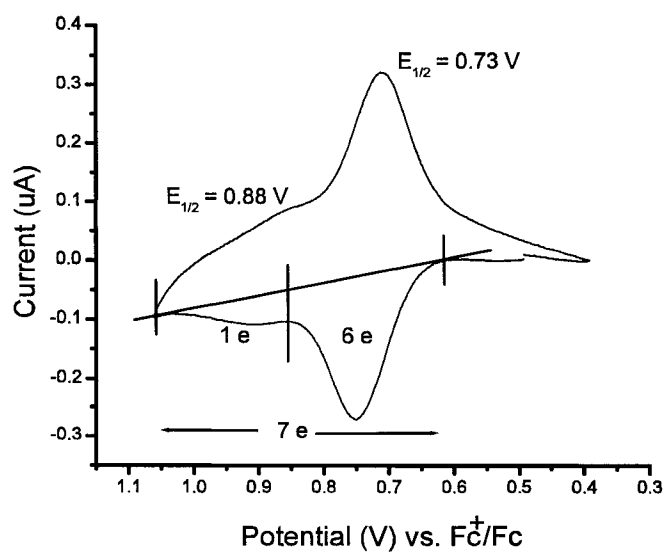


Figure 4.13. Cyclic voltammogram of 32.

4.6. Summary and Perspectives

It has been shown that structurally well-defined metal cluster complexes can be incorporated into dendritic architectures. Specifically, we have achieved the goals of synthesizing and characterizing the first *bona fide* dendrimers of metal clusters based upon the $[\text{Re}_6(\mu_3\text{-Se})_8]^{2+}$ building blocks that are situated at the core, within the branches, and on the periphery of the dendrimers. The identity and stereochemistry of the metallodendrimers have been established, with the most convincing evidence supplied by a unique comparative ^{77}Se NMR study. One metallocluster dendrimer showed electronic interaction between the cluster at the core and the clusters on the periphery of the dendrimer, while the other two showed no interactions. Areas that still need to be explored include: (1) higher-generation dendrimers, (2) different linker moieties that can incorporate other functions or properties, and (3) mixed linker units that will allow incorporation of more than one type of functions.

CHAPTER 5

Isosteric $[\text{Re}_6(\mu_3\text{-Se})_8]^{2+}$ Clusters as Precursors to Cluster-Polymer Hybrid Materials

Abstract

Cluster complexes of the general formula $[\text{Re}_6(\mu_3\text{-Se})_8(\text{PEt}_3)_n(4\text{-vinylpyridine})_6]_n(\text{SbF}_6)_2$ [**34** ($n = 5$); **35** ($n = 4$, *trans*-); **36** ($n = 4$, *cis*-)], site-differentiated with inert triethylphosphine and polymerizable 4-vinylpyridine ligands, were prepared by de-iodination of corresponding $[\text{Re}_6(\mu_3\text{-Se})_8(\text{PEt}_3)_n\text{I}_{6-n}]\text{I}_{n-4}$ (**2-4**, $n = 4, 5$) with AgSbF_6 in the presence of 4-vinylpyridine. These new cluster derivatives were characterized by elemental analysis (CHN) and NMR (^1H and ^{31}P) spectroscopy. In addition, the molecular structures of **34** and **35** have also been established by single crystal X-ray diffraction. Free radical copolymerization of cluster **34** with styrene afforded high molecular weight cluster-polystyrene hybrid **37** with a relatively low polydispersity index. Cluster incorporation into the polymeric framework is indicated by the orange color characteristic of the metal cluster and further confirmed by NMR spectroscopy. The NMR studies also established the structural integrity of the cluster building blocks upon hybrid formation. Cyclic voltammetry of the cluster-containing hybrid revealed a reversible, cluster-based oxidation event. Copolymerization of clusters **35** and **36** also resulted in cluster-polystyrene hybrids, but the materials were less well-defined, possibly an indication of cross-linking due to the presence of two polymerizable ligands on each cluster monomer.

5.1. Introduction

The creation of novel materials with improved property and performance is a continually expanding frontier at the interface of chemistry and materials science. A significant advance in this pursuit has been the development of hybrid materials that are characterized by spatially identifiable domains of organic and inorganic components organized into a single molecular framework. This unique class of materials offer exceptional opportunities not only to combine the desirable properties from both worlds, but also to create truly unique properties not exhibited by either component. For example, it has been found that inorganic-polymer hybrids can enhance conductivity, mechanical toughness, optical activity, and catalytic activity. More recently, hybrid materials have been used to fabricate membranes that exhibit enhanced permeability and selectivity for molecular separation of large organic molecules over small gases.

The novel properties unique to composite materials originate from the synergism between the inorganic and organic components, which in turn, is dictated by the subtle interfacial interactions between these dissimilar and commonly incompatible phases. It is the nature and degree of such interfacial interactions that play a pivotal role in the characteristics of resulting composites, such as solubility, optical and electrical properties, and mechanical strength. Recognizing the critical importance of such interactions in engineering novel properties, Sanchez and Ribot¹⁸¹ classify hybrid materials into two general categories, distinguishing "class I materials", in which the inorganic and organic components interact only weakly and noncovalently, from "class II materials", in which the constituents are more strongly linked through ionic or covalent bonding. It is therefore critically

important to be able to clearly define the interfacial interactions, whether they are covalent or noncovalent. Even more important is the ability to systematically tune the interfacial interactions so that the properties of the composite materials can be modulated and their performance be optimized.

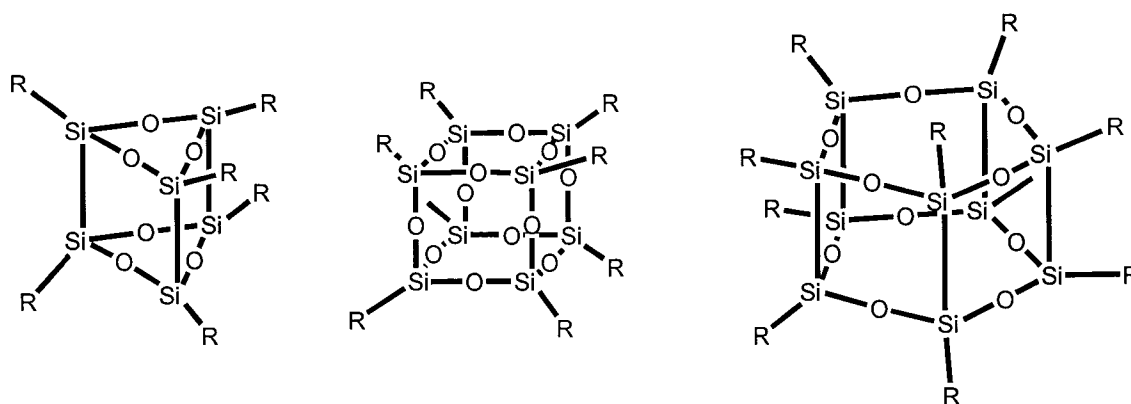


Figure 5.1. Representatives of polyhedral oligomeric silsesquioxanes.

However, hybrid materials sprang originally from sol-gel chemistry, and the interfacial interactions of sol-gel materials are typically poorly defined. A solution to this problem is to interconnect preformed and *structurally well-defined* organic and/or inorganic building blocks. Particularly successful has been the use of polyhedral oligomeric silsesquioxanes (POSS, Figure 5.1) as constituents for synthesizing inorganic-organic composite materials.^{182,183} The POSS precursors can be homo-polymerized or co-polymerized with suitable organic monomers to produce a wide variety of high-performance plastics. Physical properties of these materials, such as porosity, thermal stability, refractive index, optical clarity, chemical resistance, hydrophobicity, and dielectric constant can be controlled at the molecular level by employing judiciously designed POSS precursors

combined with the use of appropriate polymerization techniques. These materials are being evaluated in diverse applications ranging from "super absorbents" for waste water remediation to materials for fabrication of non-linear optical devices.

The successful application of POSS in making useful hybrid materials with more or less well-defined interfacial interactions has broadened our view on what is conceivable with other inorganic building blocks. Along this direction is a new area utilizing structurally well-defined metal clusters as building blocks for the synthesis of inorganic-organic composites. Such materials, combining the advantages of both metal clusters and organic polymers, are expected to find applications in a variety of upcoming advanced technologies, including biomedical imaging and organic light-emitting devices.

Encouraging results have been generated using two distinct types of metal clusters. The first is represented by the work of Schubert,¹⁸⁴ Sanchez,¹⁸⁵ and their respective coworkers in making hybrid cluster-polymer hybrids using metal oxide/alkoxide (Figure 5.2) clusters as the inorganic components. Hybrids featuring such clusters have been prepared via either homo-polymerization of the cluster-bound polymerizable group(s) or co-polymerization of such cluster-based monomers with suitable organic monomers. The structural integrity and the physical and chemical properties of the clusters are retained in most cases upon their incorporation into the polymers. It has been shown that cluster-supported composites exhibit enhanced thermal and chemical stability and mechanical strength. Moreover, in marked contrast to their pure organic counterparts, cluster-reinforced polymers swell instead of dissolving in common organic solvents, suggesting cross-linking due to the inorganic building blocks. Diffraction studies have revealed that the distribution of the clusters in the

polymeric matrices is largely homogeneous and without cluster aggregation or phase separation over extended storage periods. The size and shape of the clusters and the number of polymerizable surface groups per cluster has been found to play a small but significant role in modifying the properties of the nanocomposites. The independent research by Nocera, Shriver, and DiSalvo constitutes the second direction of creating cluster-polymer hybrid materials, wherein hexanuclear transition metal halide or chalcogenide clusters are utilized (Figure 5.3). The Nocera¹⁸⁶ and Shriver^{187,188} groups almost concurrently reported the incorporation of hexanuclear metal chalcogenide clusters into a polymeric matrix by reacting poly(4-vinylpyridine) (PVP) with cluster precursors, including $\text{Mo}_6\text{Cl}_{12}$, $[\text{Mo}_6\text{Cl}_8\text{Cl}_4(\text{EtOH})_2]$, and $[\text{Mo}_6\text{Cl}_8(\text{SO}_3\text{CF}_3)_6]^{2-}$. It has been found that the materials obtained from $\text{Mo}_6\text{Cl}_{12}$ and $[\text{Mo}_6\text{Cl}_8\text{Cl}_4(\text{EtOH})_2]$ retain the photophysics and oxygen reactivity of the parent cluster, but the polymer-bound triflate derivative lacks the characteristic luminescence profile. The observations were rationalized in terms of the different extent to which the different cluster precursors interact with the polymeric matrix; the presumably more extensive coupling between the polymer and the triflate precursor may establish additional non-radiative decay pathways, not present in the starting cluster, which compete effectively with luminescent decay. However, the exact reasons for these disparities in photophysical properties remains unclear, inviting comparative studies using a series of closely related but systematically altered clusters.

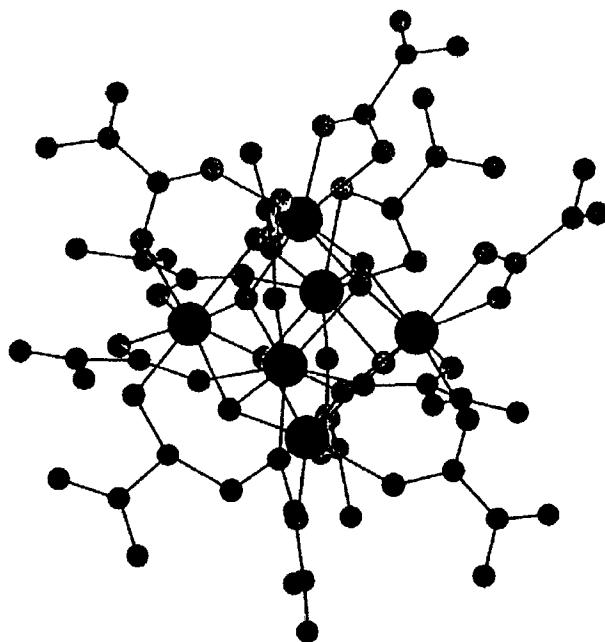


Figure 5.2. The molecular structure of $Zr_6(OH)_4O_4(\text{methacrylate})_{12}$.

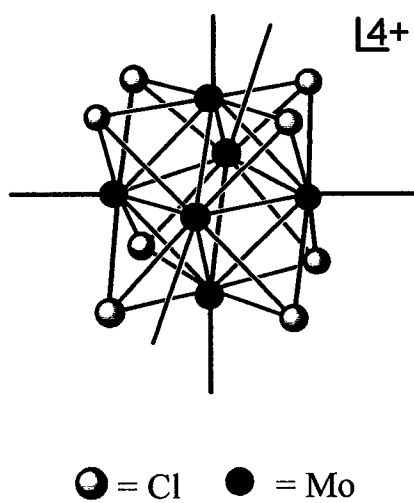
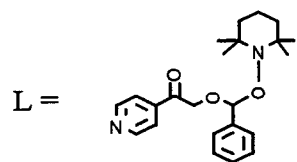
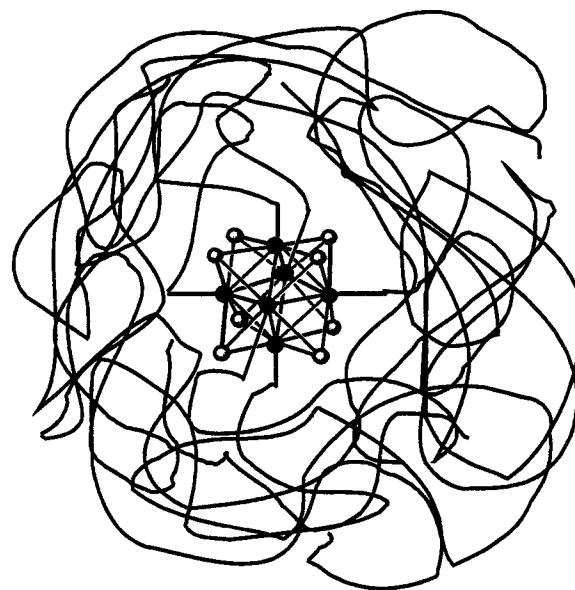
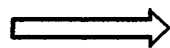
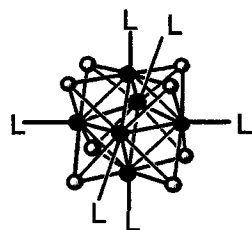


Figure 5.3. Structural representation of the Mo_6Cl_8 cluster core.

One obvious drawback of the above synthesis is the anticipated masking of coordinating pyridyl groups by the steric bulk of the polymer; the coordinating functionality may not be easily accessible. As such, the density of cluster incorporation may be low, and the homogeneity of the cluster distribution may be a serious concern in terms of possible aggregation and phase separation.

The collaborative work by DiSalvo and Fréchet¹⁸⁹ offered a potential solution to the phase separation/cluster aggregation problem. By co-polymerizing *n*-vinylimidazole (NVI) with $[\text{Mo}_6\text{Cl}_8(\text{NVI})_6]^{4+}$, a monomer featuring the organic monomer as ligand, these researchers successfully prepared composites of polyvinylimidazole cross-linked by the cluster units. It is still not possible, however, to modulate the properties of such materials by systematically altering the structure and composition of the cluster building blocks. More recently, DiSalvo and Sogah¹⁹⁰ reported the synthesis of a star-shaped polystyrene by growing divergently the polymer chains using W_6S_8 cluster complexes equipped with polymerization-initiating nitroxyl ligands (Scheme 5.1). Unimolecularly dispersed metal clusters in a well-defined soluble polymer matrix - a true polymer-cluster hybrid - is produced. Fine distribution of the clusters has also been illustrated by electron microscopic experiments. Unfortunately, detailed characterization and property investigation of these materials are unavailable.

Scheme 5.1



● = Cl ● = Mo, W

The progress made with the use of metal oxide/alkoxide and hexanuclear halide/chalcogenide clusters suggest high potentials for future developments. However, a number of issues associated with these previous efforts are obvious. First of all, alkoxide groups are known to be unstable toward water or other types of nucleophiles. As a result, radical polymerization reactions, typically employed for the synthesis of cluster-polymer hybrid materials, must be performed in a nonprotic solvent such as toluene, benzene, or tetrahydrofuran. Second, many of the metal clusters studied have a rather small core structure. Due to the bulk of the accompanying alkoxide groups, access to the polymerizable functionalities may be sterically hindered. As a result, the polymerization reaction may be sluggish or even impossible. Third, the cluster-based monomers have been shown to be amenable only to free radical polymerization, with or without organic monomers. Clusters with functional groups that would allow the application of other polymerization techniques, such as epoxide or controlled radical polymerization or polyaddition reactions, are clearly desirable, but presently unavailable. Fourth, it is yet to establish in a systematic manner, how the structure (stereochemistry and the number of polymerizable functional groups) of a cluster building block affects the properties of the final hybrids. However, almost all the clusters studied so far are substituted with multiple polymerizable groups, leading to highly cross-linked polymers, and only the influence of the reaction mixture composition (cluster loading) on certain physical properties of the hybrids has been studied. Lastly, other than the property enhancements similar to those observed for POSS-reinforced polymers, the potentially exciting and important value-adding properties anticipated of cluster-containing nanocomposites remain largely unrealized.

By making use of the recently intensively investigated hexarhenium chalcogenide clusters, the work discussed in this chapter is aimed at establishing a novel chemical system or platform to address some, if not all, of the problems, elaborated above. Specifically, the existence of multiple metal sites and the well-behaved synthetic chemistry allow for the construction of a complete kit of systematically altered building blocks that are different only in the number and steric arrangement of the polymerizable ligand(s). The degree of polymerization, the composition and structure, and ultimately, the property of these composites may thus be controlled and optimized, and the structure-property relation may be established. Functionally, these clusters are luminescent, and the luminescence has been found to be dependent on the rhenium coordination environment, suggesting that one might be able to tune the optical properties of the final materials containing these clusters. The inherent properties of the cluster species can now be expressed in a confined, controllable, and systematically modifiable environment.

To this end, we designed and synthesized a set of complexes containing the $[\text{Re}_6(\mu_3\text{-Se})_8]^{2+}$ cluster core. These new cluster derivatives, featuring at least one polymerizable 4-vinylpyridine ligand, in addition to inter and site-protecting triethylphosphine ligands, are then applied to co-polymerization with styrene to produce the desired cluster-polymer hybrids.

5.2. Experimental

General Considerations.

4-vinylpyridine, styrene, 2,2'-azo-bis-isobutyronitrile (AIBN), (*n*-Bu₄N)PF₆, and AgSbF₆ were obtained from Aldrich and used as received. Styrene was purified according to published procedures. Cluster complexes **2-4** were prepared according to published procedures.³¹⁻³³ The silica gel (mesh size 200-400) used for flash column chromatography was purchased from Natland International Corporation, Research Triangle Park, North Carolina. ¹H and ³¹P NMR spectra were recorded on a Varian AM-300 spectrometer in CD₃CN. Chemical shifts of ³¹P spectra were referenced to 85% H₃PO₄ (δ = 0 ppm, with negative values meaning upfield). Elemental analyses (CHN) were performed by Desert Analytics Laboratory, Tucson, Arizona.

[Re₆(μ₃-Se)₈(PEt₃)₅(4-vinylpyridine)](SbF₆)₂ (34). To a mixture of **4** (100 mg, 0.0386 mmol) and 4-vinylpyridine (200mg, 1.90 mmol) in 50 mL of tetrahydrofuran was added AgSbF₆ (100 mg, 0.292 mmol). The mixture was stirred in the absence of light at room temperature for 24 hours, exposed to light for 2 hours, and then filtered to afford a light orange solution. The orange-red residue obtained upon removal of the solvent was treated with 20 mL of dichloromethane. The resulting mixture was filtered through a plug of cotton, and the filtrate was collected. After removal of the solvent, the orange-red residue was subjected to flash column chromatography using silica gel and an eluting solvent mixture of dichloromethane and acetonitrile (v/v 20:1; *R_f* = 0.70). Yield: 70.2 mg (62.1%). ¹H NMR

(300 MHz, CD₂Cl₂): 1.02-1.20(m), 2.05-2.29(m), 5.72(d), 6.16(d), 6.73(dd), 7.25(d), 9.12(d).

³¹P NMR: -20.49, -23.82. Anal. Calcd for C_{38.5}H_{85.5}N_{1.5}F₁₂OP₅Re₆Se₈Sb₂ (**34**·0.5DMF): C, 15.66; H, 2.92; N, 0.71. Found: C, 15.61; H, 3.09; N, 0.64.

Trans-[Re₆(μ₃-Se)₈(PEt₃)₄(4-vinylpyridine)₂](SbF₆)₂ (35**)** was obtained as an orange powder in a manner similar to **34** except that **2** was used in place of **4** (Yield: 43%). ¹H NMR (300 MHz, CD₃CN): 1.10-1.21(m), 2.28-2.39(m), 5.72(d), 6.12(d), 6.78(dd), 7.28(d), 9.08(d). ³¹P NMR: -22.28. Anal. Calcd for C₃₈H₇₄N₂F₁₂P₄Re₆Se₈Sb₂: C, 15.72; H, 2.55; N, 0.96. Found: C, 15.96; H, 2.62; N, 1.18.

Cis-[Re₆(μ₃-Se)₈(PEt₃)₄(4-vinylpyridine)₂](SbF₆)₂ (36**)** was obtained as an orange powder in a manner similar to **34** except that **3** was used in place of **4** (Yield: 47%). ¹H NMR (300 MHz, CD₃CN): 1.05-1.20(m), 2.14-2.35(m), 5.74(d), 6.23(d), 6.82(dd), 7.35(d), 9.33(d). ³¹P NMR: -21.87, -24.65. Anal. Calcd for C₃₈H₇₄N₂F₁₂P₄Re₆Se₈Sb₂: C, 15.72; H, 2.55; N, 0.96. Found: C, 15.79; H, 2.66; N, 0.95.

Complex 34-Polystyrene Hybrid (37). A mixture of **34** (20.0 mg, 6.90 μmol), AIBN (3.0 mg, 0.018 mmol), and styrene (180.0 mg, 1.7 mmol) in 1.0 mL of acetonitrile was de-oxygenated by the freeze-pump-thaw method and then stirred at 78°C under dry nitrogen for 12 hours. Dropwise addition of the cooled reaction mixture to a mixture of diethyl ether/petroleum ether (v/v1:1) generated an orange-yellow precipitate. The precipitate was collected, washed with diethyl ether/petroleum ether (v/v 1:1; 3 x 5 mL), and re-dissolved in a minimum amount of dichloromethane to give an orange-red solution. Trituration of this solution with diethyl ether/petroleum ether afforded a sticky orange-red solid as the product

(40 mg). Its molecular weight was determined by gel-permeation chromatography using polystyrene as the standard to be $M_n = 344,388$ Da with a polydispersity index of 1.33. ^1H NMR (300 MHz, CD_2Cl_2): 1.15(b), 1.49(b), 1.83(b), 2.24(b), 6.61(b), 7.09(b). ^{31}P NMR: -19.88, -23.09.

Complex 2-Polystyrene Hybrid (38) in a manner similar to **37** except that **35** was used in place of **34**. ^1H NMR (300 MHz, CD_2Cl_2): 1.15(b), 1.48(b), 1.83(b), 2.32(b), 6.61(b), 7.09(b). ^{31}P NMR: -21.11.

Complex 3-Polystyrene Hybrid (39) in a manner similar to **37** except that **36** was used in place of **34**. ^1H NMR (300 MHz, CD_2Cl_2): 1.16(b), 1.54(b), 1.84(b), 2.19(b), 6.61(b), 7.10(b). ^{31}P NMR: -22.16, -23.53.

Other Physical Measurements.

Cyclic voltammograms were acquired with an EG&G Instruments 283 potentiostat, using 500 μm diameter Pt working electrode, a Pt counter electrode, and an Ag/AgCl pseudoreference electrode freshly prepared by plating a thin layer of AgCl onto a Ag wire from a saturated KCl solution. ($n\text{-Bu}_4\text{N}$)PF₆ (0.1 M acetonitrile solution) was used as supporting electrolyte. The working electrode was cleaned between each experiment by polishing with 0.3- μm alumina paste for 1 minute, followed by copious solvent rinses. After each voltammetric experiment, ferrocene was added (ca. 1 nM). An additional voltammogram was then recorded, and the potential axis was calibrated against the formal potential for the ferrocenium/ferrocene (Fc^+/Fc) redox couple.

Gel Permeation Chromatography.

The polymer samples were dissolved at 5 mg/ml in dichloromethane and run by a Waters 2695 Separations Module at 1 ml/min using dichloromethane as the mobile phase. Jordi DVB columns (500, 1000, and 10000 Å) were used at ambient temperature. A Waters 2996 Photodiode Array was used as the detector.

X-ray Structure Determinations.

Complex 34.

An orange triangular plate of **34** having approximate dimensions of 0.02 x 0.12 x 0.15 mm was mounted on a glass fiber in a random orientation. Data were collected on a Bruker SMART 1000 CCD detector X-ray diffractometer at 173(2) K using graphite monochromated Mo K α radiation ($\lambda = 0.71073$ Å).

Cell constants and an orientation matrix for integration were determined from reflections obtained in three orthogonal 5° wedges of reciprocal space. A total of 3686 frames at 1 detector setting covering $0^\circ < 2\theta < 60^\circ$ were collected, having an omega scan width of 0.2° and an exposure time of 20 seconds. The frames were integrated using the Bruker SAINT software package's narrow frame algorithm. A total of 39156 reflections were integrated and retained, of which 13919 were unique. Of the unique reflections, 9280 (66.7%) were observed $I > 2\sigma(I)$. Empirical absorption and decay corrections were applied using the program SADABS.

The structure was solved using SHELXS in the Bruker SHELXTL (Version 5.0) software package. Refinements were performed using the freely available SHELXL and

illustrations were made using XP. Solution was achieved utilizing direct methods followed by Fourier synthesis. Hydrogen atoms were added at idealized positions, constrained to ride on the atom to which they are bonded and given thermal parameters equal to 1.2 or 1.5 times U_{iso} of that bonded atom. The final anisotropic full-matrix least squares refinement based on F^2 of all reflections converged (maximum shift/esd = 0.002) at $R1 = 0.1005$, $wR2 = 0.0880$ and goodness-of-fit = 0.970. "Conventional" refinement indices using the 9280 reflections with $F > 4\sigma(F)$ are $R1 = 0.0531$, $wR2 = 0.0774$. The model consisted of 685 variable parameters, 1 constraint, and 434 restraints. There were 24 correlation coefficients between 0.8 and 0.67, all involving thermal parameters of the anion F atoms. The highest and lowest peaks on the final difference map were 1.617 and $-1.056 \text{ e}/\text{\AA}^3$, respectively. Scattering Factors and anomalous dispersion were taken from International Tables Vol C Tables 4.2.6.8 and 6.1.1.4.

Complex 35.

A red block of approximate dimensions of 0.15 x 0.20 x 0.40 mm was mounted on a glass fiber in a random orientation. Data were collected on the SMART1000 system using graphite monochromated Mo K radiation ($\lambda = 0.71073 \text{\AA}$).

Initial cell constants and an orientation matrix for integration were determined from reflections obtained in three orthogonal 5° wedges of reciprocal space. A total of 909 frames at 1 detector setting covering $0^\circ < 2\theta < 60^\circ$ were collected, having an omega scan width of 0.3 and an exposure time of 10 seconds, excluding the fourth run in which only 562 frames were collected. The frames were integrated using the Bruker SAINT software package's narrow frame algorithm. A total of 35919 reflections were integrated and retained

of which 14590 were unique. Of the unique reflections, 9761 (67%) were observed $I > 2\sigma(I)$. Empirical absorption corrections were applied using the program Sadabs, Shelx197, Sheldrick, G.M. (1997).

The structure was solved using SHELXS in the Bruker SHELXTL (Version 5.0) software package. Refinements were performed using SHELXL and illustrations were made using XP. Solution was achieved utilizing Patterson methods followed by Fourier synthesis. Hydrogen atoms were added at idealized positions, constrained to ride on the atom to which they are bonded and given thermal parameters equal to 1.2 or 1.5 times U_{iso} of that bonded atom. The final anisotropic full-matrix least squares refinement based on F^2 of all reflections converged (maximum shift/esd = 0.001) at $R1 = 0.0870$, $wR2 = 0.1195$ and goodness-of-fit = 0.968. "Conventional" refinement indices using the 9761 reflections with $F > 4 \sigma(F)$ are $R1 = 0.0516$, $wR2 = 0.1073$. The model consisted of 649 variable parameters and 0 restraints. The highest and lowest peaks on the final difference map were $2.407 \text{ e}/\text{\AA}^3$ and $-3.165 \text{ e}/\text{\AA}^3$. Scattering Factors and anomalous dispersion were taken from International Tables Vol C Tables 4.2.6.8 and 6.1.1.4.

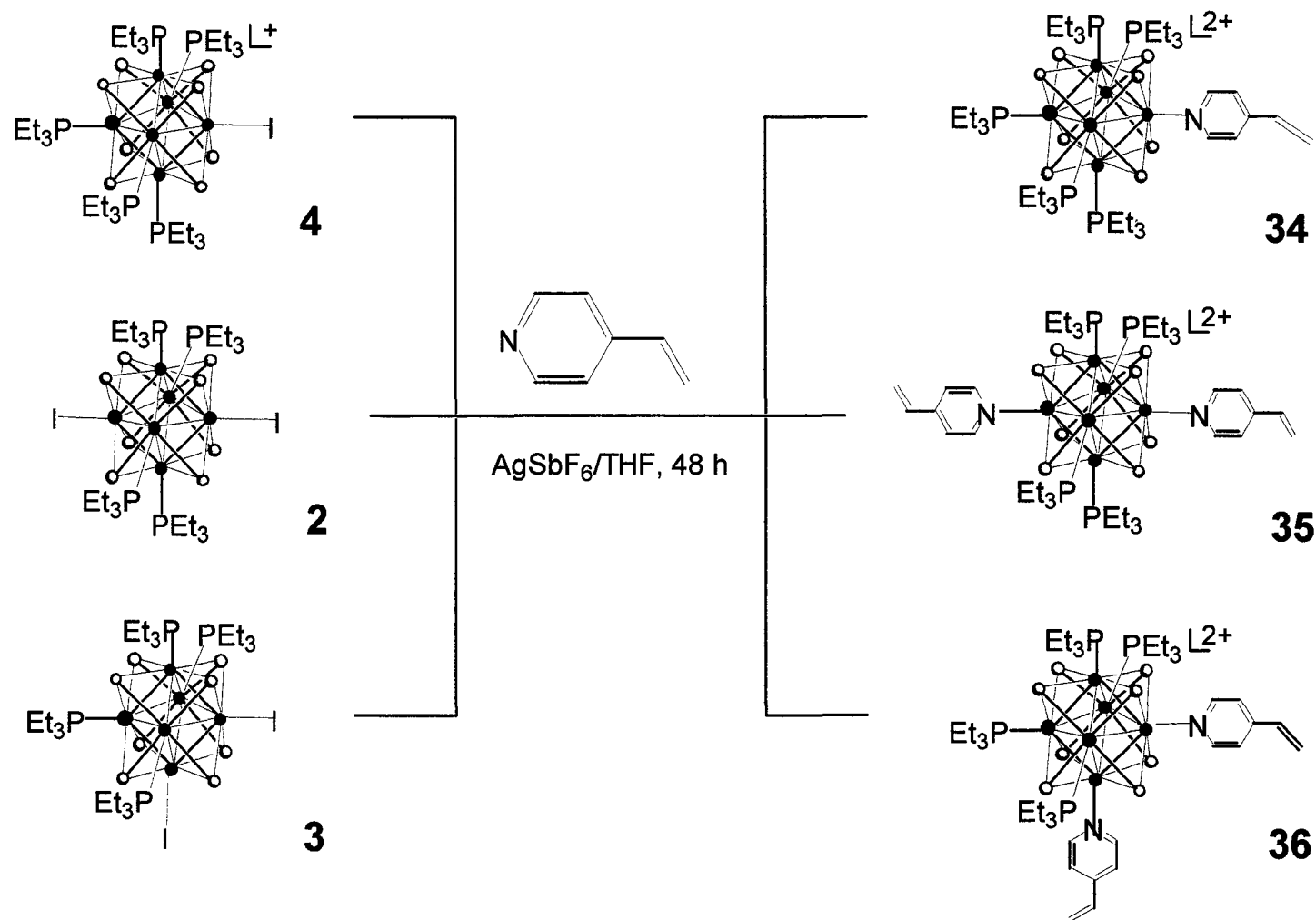
5.3. Synthesis and Characterization

5.3.1. Synthesis of Polymerizable Cluster Complexes

The synthesis of the targeted cluster complexes is set out in Scheme 5.2. Addition of AgSbF_6 to a solution of the starting cluster and an excess of 4-vinylpyridine in tetrahydrofuran caused an immediate yellow precipitation, presumably that of AgI . Removal of iodide was followed by the binding of 4-vinylpyridine to afford the desired products in good yields. The complexes are readily soluble in dichloromethane, acetonitrile, and other common polar organic solvents to yield orange-red solutions. The compounds were identified spectroscopically. Complexes **34** and **35** were also confirmed by X-ray diffraction analysis. Among the most interesting spectroscopic observations are the ^1H resonances of 4-vinylpyridine upon binding to the cluster. The well-defined doublet at 9.12 ppm corresponds to the α -H of the coordinated pyridyl moiety, which is shifted significantly downfield with respect to the free ligand. The signal at 7.25 ppm is associated with the β -H of the coordinated pyridyl moiety and is shifted slightly from 7.05 ppm of the uncoordinated ligand. Further, the other three sets of resonances associated with the vinyl protons are downfield from that of free 4-vinylpyridine (Figure 5.4). Similar downfield shifts of comparable magnitude have also been observed for *trans*- and *cis*-tetratriethylphosphine substituted clusters. Clusters **34-36** are readily differentiated by their ^{31}P NMR spectra, whose resonances occur in the interval -20 to -25 ppm in acetonitrile solution (Figure 5.5). In each case, unsophisticated patterns of ^{31}P resonances are observed. For complex **34**, two signals in a relative integration of 4:1 are shown at -24.80 and -28.00 ppm, respectively,

consistent with the pentaphosphine-substituted structure. For complex **35**, a single signal at -22.28 is observed, while resonances of equal intensity are observed for **36** at -21.87 and -24.65 ppm, respectively. Alternative syntheses of complexes **34-36** were also attempted. However, the reaction between the corresponding acetonitrile solvates with an excess of 4-vinylpyridine in chlorobenzene under reflux only produced mixtures that were hard to purify despite the fact that such ligand substitution reactions have been very successful for the preparation of a variety of other cluster derivatives. This may have been due to some unwanted reactions (polymerization of 4-vinylpyridine, for example) as a result of the rather forcing conditions.

Scheme 5.2



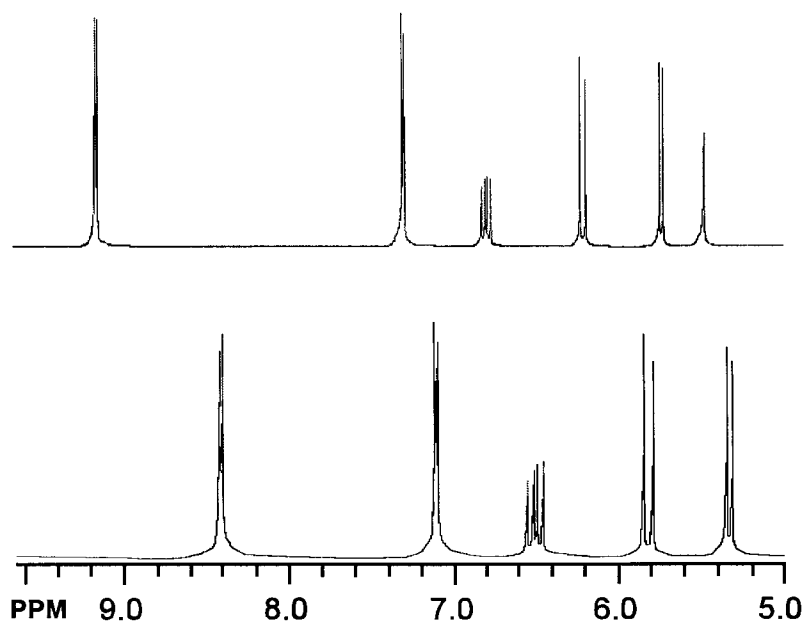


Figure 5.4. Partial showing of the ^1H NMR spectra of 4-vinylpyridine (bottom) and 34 (top).

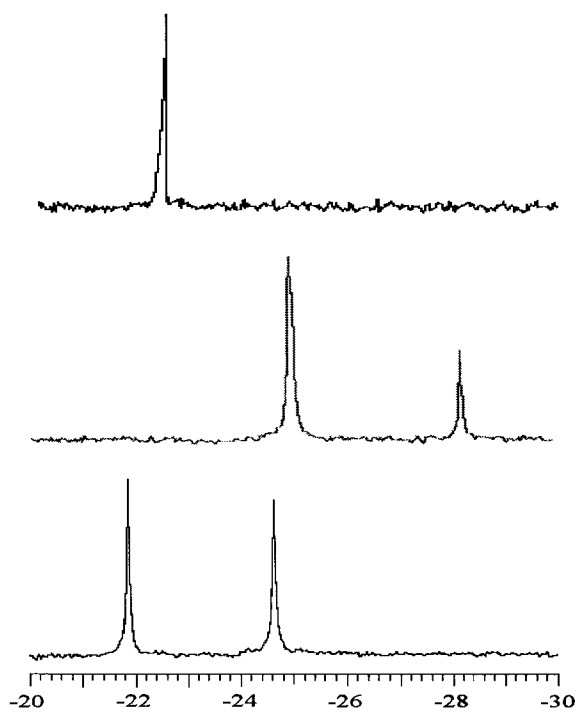


Figure 5.5. ^{31}P NMR spectra of 35 (top), 34 (middle), and 36 (bottom).

5.3.2. X-ray Structural Determinations of 34 and 35

The molecular structures of cluster **34** and **35** were established by single-crystal X-ray diffraction. Crystal data and structure refinement parameters are reported in Tables 5.1 and 5.2. Dimensional data describing the cluster core of both structures are collected in Table 5.3 and 5.4. The values are unremarkably close to those reported for similar compounds. The molecular structures are depicted in Figure 5.6. The cluster core in both structures, as expected, contains a Re_6 octahedron concentric with a Se_8 cube whose atoms cap the triangular octahedral faces. The correct stereochemical phosphine substitution is readily apparent. The 4-vinylpyridine ligand is bound to the non-phosphine protected rhenium site via the pyridyl nitrogen, while its vinyl group is disposed, as expected, away from the molecular bulk, establishing a site readily accessible for further transformations.

Table 5.1. Crystallographic Data and Structural Refinement of **34**.

Empirical formula	$C_{40}H_{89}F_{12}N_2OP_5Re_6Sb_2Se_8$
Formula weight	2989.36
Crystal size	0.02 x 0.12 x 0.15 mm
Crystal system	Monoclinic
Space group	$P2_1$
Unit cell dimensions	$a = 11.748(1) \text{ \AA}$ $\beta = 94.411(3)^\circ$ $b = 15.122(2) \text{ \AA}$ $c = 19.941(2) \text{ \AA}$
Volume, Z	$3531.8(7) \text{ \AA}^3, 2$
Density, calcd. Mg/m^3	2.810
Abs. coeff., mm^{-1}	15.288
$F(000)$	2714
Theta range for data collection	1.02 to 26.04°
Limiting indices	$-14 \leq h \leq 14, -18 \leq k \leq 18, -24 \leq l \leq 24$
Reflections utilized	39156
Independent reflections	13919 [R(int) = 0.0896]
Data/restraint/parameter	13919/434/685
GOF on F^2	0.970
R indices [$I > 2\sigma(I)$]	R1 = 0.0531, wR2 = 0.0774
R indices (all data) ^a	R1 = 0.1005, wR2 = 0.0880

$$^a R1 = \sum \|F_o\| - \|F_c\| / \sum \|F_o\|, wR2 = \{\sum [w(F_o^2 - F_c^2)^2] / \sum [w(F_o^2)^2]\}^{1/2}.$$

Table 5.2. Crystallographic Data and Structural Refinement of **35**.

Empirical formula	$C_{38}H_{71}F_{12}N_2P_4Re_6Sb_2Se_8$	
Formula weight	2900.23	
Crystal size	0.40 x 0.20 x 0.15 mm	
Crystal system	Triclinic	
Space group	<i>P</i> -1	
Unit cell dimensions	$a = 12.0859(16) \text{ \AA}$	$\alpha = 87.429(3)^\circ$
	$b = 15.157(2) \text{ \AA}$	$\beta = 88.613(3)^\circ$
	$c = 19.853(2) \text{ \AA}$	$\gamma = 67.517(3)^\circ$
Volume, <i>Z</i>	$3356.8(8) \text{ \AA}^3, 2$	
Density, calcd. Mg/m ³	2.869	
Abs. coeff., mm ⁻¹	16.057	
<i>F</i> (000)	2610	
Theta range for data collection	1.03 to 27.06°	
Limiting indices	$-15 \leq h \leq 15, -19 \leq k \leq 19, -25 \leq l \leq 25$	
Reflections utilized	35727	
Independent reflections	14584 [R(int) = 0.0718]	
Data/restraint/parameter	14584/0/649	
<i>GOF</i> on <i>F</i> ²	0.968	
R indices [<i>I</i> > 2σ(<i>I</i>)]	R1 = 0.0516, wR2 = 0.1073	
R indices (all data) ^a	R1 = 0.0870, wR2 = 0.1195	

$$^a R1 = \sum ||F_o| - |F_c|| / \sum |F_o|, wR2 = \{ \sum [w(F_o^2 - F_c^2)^2] / \sum [w(F_o^2)^2] \}^{1/2}.$$

Table 5.3. Selected bond lengths (Å) of **34** and **35**.

Complex 34	
Re-Re	2.6272(1)-2.6454(1); mean 2.6369
Re-Se	2.505(2)-2.520(2); mean 2.513
Re-P	2.463(5)-2.485(5); mean 2.474
Re-N	2.220(13)
C=C (vinyl)	1.265(10)
Complex 35	
Re-Re	2.6298(1)-2.6436(6); mean 2.6363
Re-Se	2.5050(12)-2.5240(13); mean 2.5211
Re-P	2.474(5)-2.489(5); mean 2.481
Re-N	2.196(9) and 2.208(9)
C=C (vinyl)	1.265(10)

Table 5.4. Selected bond angles (°) of **34** and **35**.

Complex 34	
Re-N-C	121.3(12) and 122.0(11)
C-C=C(vinyl)	117(3)
Complex 35	
Re-N-C	121.4(7)-122.6(8); mean 122.0
C-C=C(vinyl)	117(12) and 118(12)

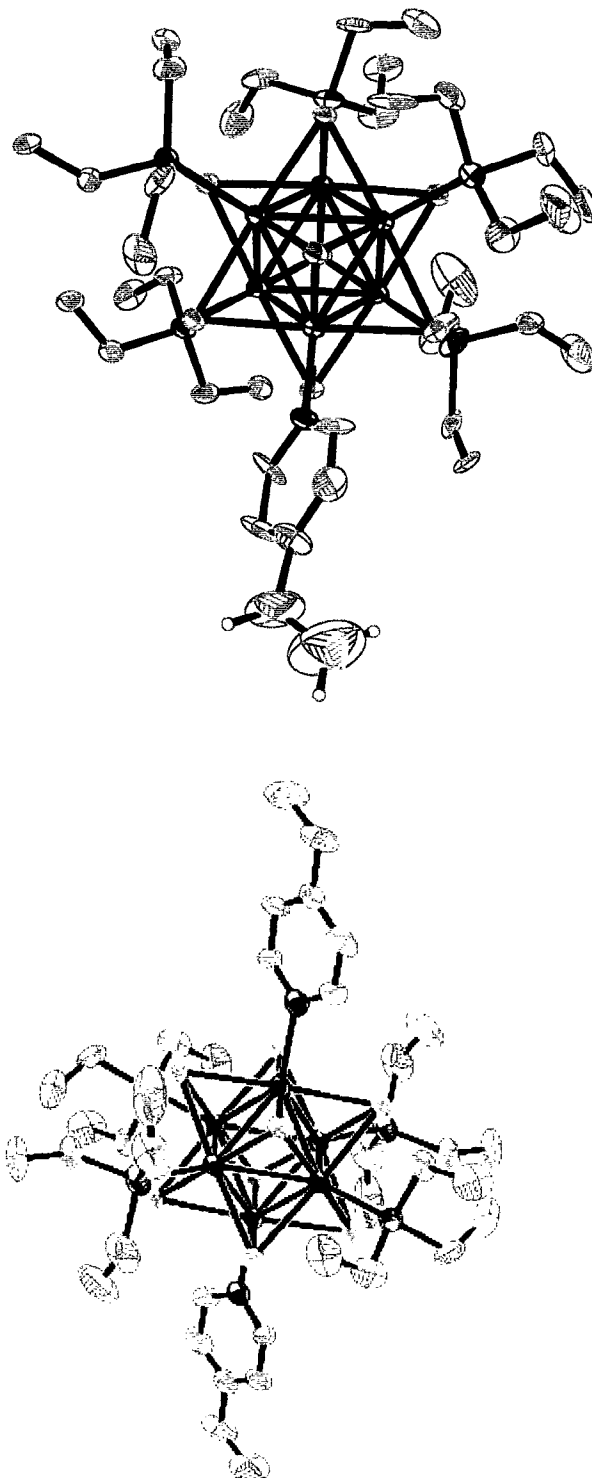
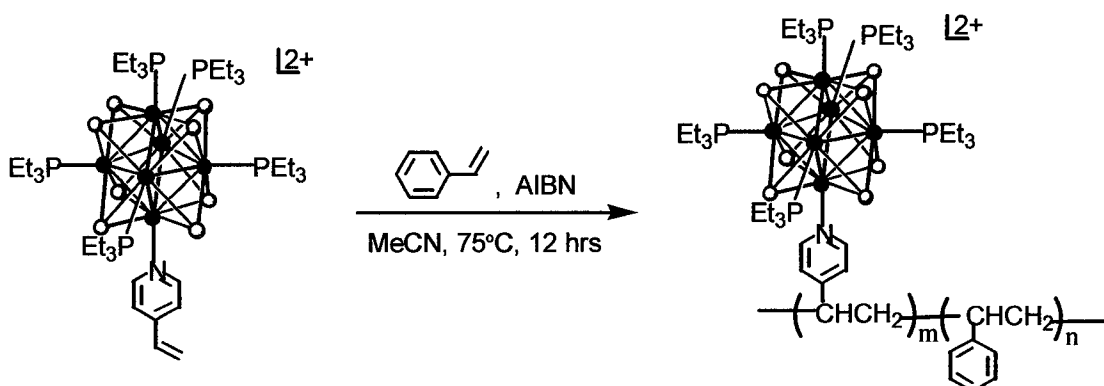


Figure 5.6. An ORTEP view (50% probability) showing the cationic cluster core of **34** (top) and **35** (bottom). Color schemes: C (gray), N (blue), P (purple), Re (green), Se (brown).

Scheme 5.3



5.3.3. Syntheses of Cluster-Polystyrene Hybrids

With the desired polymerizable clusters in hand, reactions leading to cluster-containing polymeric materials in desired local substitution patterns or stereochemistry were undertaken. The reaction employed, set out in Scheme 5.3, proceeds by co-polymerizing complexes **34-36** with an excess of styrene in acetonitrile. The purified products exhibit an orange color, characteristic of the parent cluster, and hence, a qualitative support of its incorporation into the polymeric support. Additional supporting evidence comes from comparative NMR (^1H and ^{31}P) studies of the **37** and **34**. The ^1H NMR spectrum of the **37** (a, top, Figure 5.7) is considerably broadened as compared with that of **34** (a, bottom, Figure 5.7). Also of notice is the upfield shift of the pyridyl α -H resonance from 9.12 to ca. 8.66 ppm (inset, Figure 5.7) upon polymerization. The remaining resonances in the aromatic region are significantly broadened compared to **34**, but the shape and chemical shift are typical of polystyrene. Saturation of the vinylpyridine double bond is confirmed by the disappearance of the proton signals at 5.72 and 6.16 ppm (bottom, Figure 5.7) attributed to

the terminal CH₂ of the vinyl group of **34**; the new resonances are inadvertently obscured by the triethylphosphine signals. As indicated by the ³¹P NMR of the hybrid (b, top, Figure 7), not only the cluster core remains intact, the cluster stereochemistry is also preserved, as two considerably broadened peaks with a relative integration of 4:1 are observed. The unsophisticated ³¹P NMR spectrum also points to the purity of the product as well as a chemically homogeneous environment for the dispersed cluster units. Nevertheless, direct evidence for a fine dispersion of the cluster in the polymeric matrix remains to be obtained by electron microscopy. The cluster:styrene ratio was estimated to be 1:26 on the basis of ¹H NMR integration of the hybrid, corresponding to a cluster loading of 51.8 wt% or 3.7 mol%. Its molecular weight was determined by gel-permeation chromatography using polystyrene as the standard to be *M_n* = 344,388 Da with a polydispersity index of 1.33 (Figure 5.8), corresponding to an average of 70 repeating units, each composed of 1 cluster and 26 styrene.

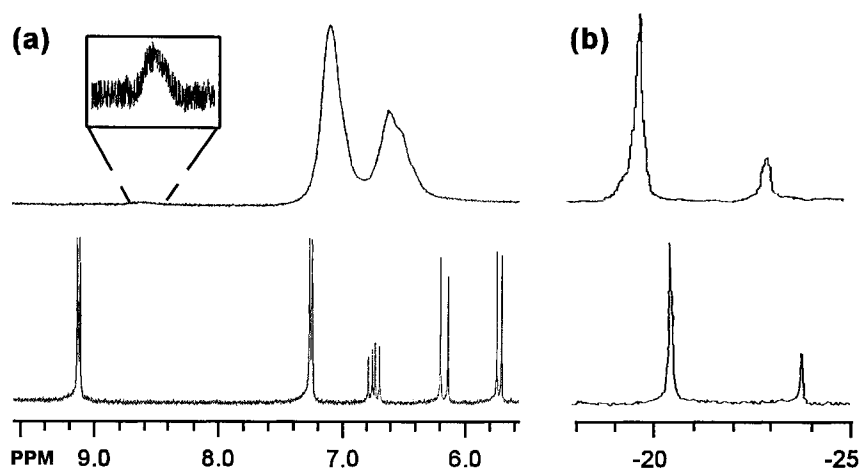


Figure 5.7. (a) Partial showing of the ¹H NMR spectra of **34** (bottom) and **37** hybrid (top). (b) ³¹P NMR spectra of **34** (bottom) and **37** hybrid (top).

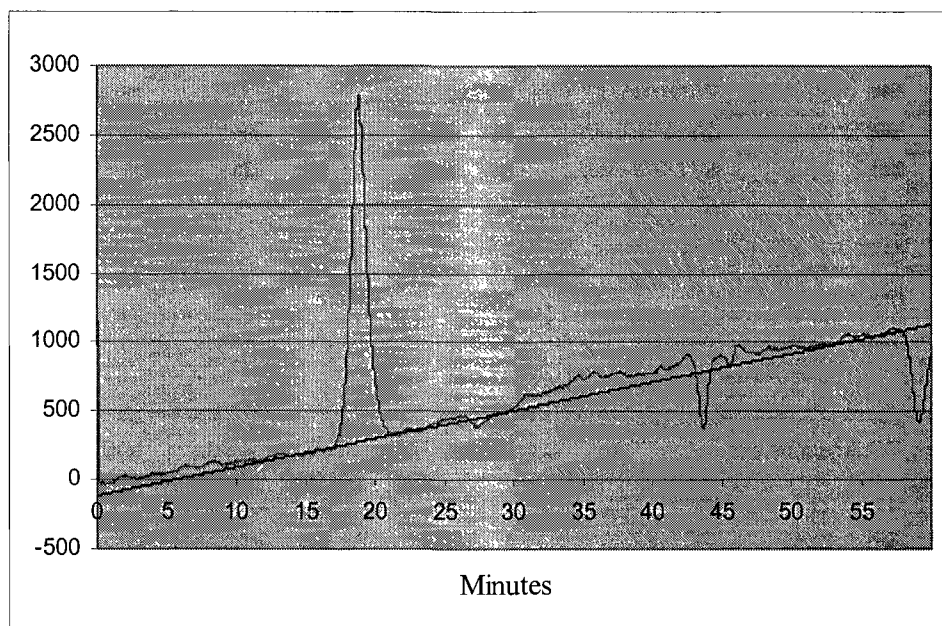


Figure 5.8. GPC trace of **37**.

Encouraged by the successful synthesis of the polymeric hybrid containing the pentaphosphine-substituted cluster unit, we sought the preparation of cluster-polymer hybrids by employing the other two cluster monomers **35** and **36**. These two cluster precursors are expected to produce more complicated hybrids as cross-linking is expected due to the presence of two polymerizable ligands. Furthermore, the *trans*- and *cis*- stereochemistry is expected to create some disparity in polymer properties. Indeed, analogous copolymerization reactions employing **35** and **36** proceed smoothly, and sticky orange-red materials were obtained in both cases. For **35**, upon copolymerization with styrene, the vinyl double bond is completely saturated, as indicated by the absence of the peaks at 6.20 and 5.72 ppm. As in case of hybrid **34**, the resulting saturated resonances are obscured by the triethylphosphine signals. The aromatic proton resonances are considerably broadened

compared to that of the monomer, and are typical of polystyrene. Also noticeable is the upfield shift of the pyridyl protons from 9.12 to 8.55 ppm. The ^{31}P NMR is unsophisticated with a slightly broadened resonance at -21.11 ppm. This is consistent with the equivalent chemical environments that would occur if the cluster core were incorporated into the polymer matrix, and is also typical of a *trans*-tetratphosphine-substituted isomer. The cluster loading could not be determined due to poor resolution of the α -H of the coordinated pyridine. Due to the potential cross-linking that may occur with two possible polymerizable groups the molecular weight of the polymers formed spanned a very large range.

Complex **36** has the potential to create the most complex polymeric system because the polymerizable groups are positioned at a right angle, thus creating some stereochemical constraints during polymerization reaction. The ^1H NMR is similar to the previous polymers. Saturation is confirmed by the disappearance of the double bond protons at 6.22 and 5.75 ppm. The resonances corresponding to the saturated proton are not visible due to the overlap with the triethylphosphine signals. The aromatic proton resonances are broad, but typical of polystyrene. Also, the pyridyl peak has shifted upfield from 9.33 to 8.98 ppm. Unlike the spectra of the other two hybrids, the ^{31}P NMR of **39** is complex. Although two sets of significantly broadened resonances centered at -22.16 and -23.52 ppm, respectively, were observed, each set contains many poorly resolved signals, possibly an indication of the complexity of polymerization due to the *cis*- arrangement of the vinyl groups. As with copolymer of **35**, the molecular weight of the polymers formed spanned a very large range.

5.4. Electrochemical Studies.

Electrochemical studies have been carried out to determine if the polymeric matrix has any effects on the redox potential of the clusters. Cyclic voltammetry revealed only one chemically reversible oxidation step at $E_{1/2} = 0.77$ V ($\Delta E_p = 100$ mV) vs. the Fc^+/Fc redox couple (Fc = ferrocene; $E^\circ = 0.46$ V vs. SCE; 0.70 V vs. NHE) for **37**, comparable to that ($E_{1/2} = 0.76$ V) observed for the starting cluster **34** (Figure 5.9). The observation of a single oxidation event at the same potential as the free cluster suggests that the clusters are unperturbed by the polymerization, are noninteracting, and are effectively in the same environment, in agreement with the conclusion reached by the comparative NMR studies detailed above. However, the smaller peak current for the hybrid, when compared to that of a solution of free clusters with an equivalent cluster concentration, is indicative of the slower diffusion when incorporated into the high molecular weight polymer. Additionally, any masking of buried cluster units would contribute to this decrease.

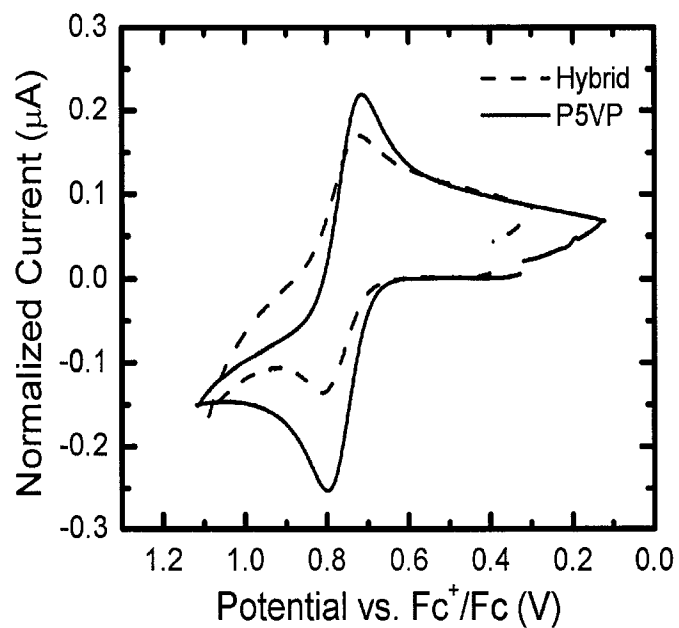


Figure 5.9. Cyclic voltammograms of **34** and the hybrid **37** in CH_3CN solutions. The current scale for polystyrene sybrid has been normalized such that the voltammograms can be compared at the same effective molar concentration of clusters.

5.5. Summary and Perspectives

The goals of this work were to create a new series of polymerizable cluster complexes and to explore their applications as precursors to novel cluster-containing inorganic-polymer hybrids. To this end, three cluster complexes of the general formula $[\text{Re}_6(\mu_3\text{-Se})_8(\text{PEt}_3)_n(4\text{-vinylpyridine})_{6-n}](\text{SbF}_6)_2$ [**34** ($n = 5$); **35** ($n = 4$, *trans*-); **36** ($n = 4$, *cis*-)], site-differentiated with inert triethylphosphine and polymerizable 4-vinylpyridine ligands were prepared. Polymerization reactions of these novel derivatives with styrene were investigated. It has been found that each of these cluster-based monomers is capable of co-polymerization with styrene to afford cluster-polystyrene hybrids. In the case of cluster **34**, polymeric hybrid of high molecular weight and low polydispersity index was obtained. Both the integrity of the cluster and its stereochemistry are maintained upon polymerization, as can be concluded from comparative ^1H and ^{31}P NMR studies of the monomer and copolymers. Electrochemical studies revealed no electronic communication between clusters within a single cluster-polymer hybrid. By utilizing these isosteric building blocks, it is possible to control the loading of clusters and to tune the properties of the resulting hybrid materials. Future work will include the optimization of reaction conditions in the hope that more well-defined hybrids using **35** and **36** can be obtained. In addition, the potentially interesting electrochemical and photophysical properties of these novel materials will be investigated, with an eye on their applications as organic light-emitting and redox-active coating materials.

Overall Summary and Outlook

The body of this dissertation is concerned with the chemistry of the hexarhenium selenide cluster and its use as a synthetic building block. Two themes underlay the research presented here: (1) to create of novel supramolecular arrays and (2) to provide possible solutions to problems associated with the synthesis of inorganic-organic hybrid materials.

Chapter 2 discussed the use of star-shaped scaffolding to develop a molecular Tinkertoy kit containing pieces which incorporate a variety of angles. Further functionalization of a molecular Tinkertoy based upon TPyP by incorporation of metal ions was discussed in chapter 3 along with the new electrochemical and photophysical properties observed. A new metallodendrimer motif containing clusters at the core, within the branches, and on the periphery was developed and discussed in chapter 4. Also examined is the hitherto unseen electrochemical communication between $[\text{Re}_6(\mu_3\text{-Se})_8]^{2+}$ clusters bridged by an organic moiety. Chapter 5 provides possible solutions to problems involved with the synthesis of inorganic-organic hybrid materials. A demonstration-of-feasibility synthesis was provided demonstrating the successful copolymerization of $[\text{Re}_6(\mu_3\text{-Se})_8]^{2+}$ vinylpyridine derivative with styrene.

This dissertation has laid the ground-work for continued research in this area. Examples of future work includes exploration of different types of molecular Tinkertoys, synthesis of more complex extended arrays based upon these cluster-based Tinkertoys. Higher-generation dendrimers, as well as dendrimers containing different organic bridges need to be looked into. Finally, just the surface of hybrid inorganic-organic hybrid materials

has been touched. By changing the monomer and the initiator, more interesting polymers maybe formed with greater control over the resulting structure and properties.

References.

- (1) Lehn, J.-M. *Supramolecular Chemistry: Concepts and Perspectives*; New York: VCH: **1995**.
- (2) Evans, O. W.; Lin, W. Crystal Engineering of NLO Materials Based on Metal-Organic Coordination Networks. *Acc. Chem. Res.* **2002**, *35*, 511-522.
- (3) Moulton, B.; Zaworotko, M. J. From Molecules to Crystal Engineering: Supramolecular Isomerism and Polymorphism in Network Solids. *Chem. Rev.* **2001**, *101*, 1629-1658.
- (4) Prins, L. J.; Reinhoudt, D. N.; Timmerman, P. Noncovalent Synthesis Using Hydrogen Bonding. *Angew. Chem., Int. Ed.* **2001**, *40*, 2382-2426.
- (5) Leininger, S.; Olenyuk, B.; Stang, P. J. Self-Assembly of Discrete Cyclic Nanostructures Mediated by Transition Metals. *Chem. Rev.* **2000**, *100*, 853-908.
- (6) Caulder, D. N.; Raymond, K. N. The Rational Design of High Symmetry Coordination Clusters. *J. Chem. Soc., Dalton Trans.* **1999**, 1185-1200.
- (7) Yaghi, O. M.; Li, H.; Davis, C.; Richardson, D.; Groy, T. L. Synthetic Strategies, Structure Patterns, and Emerging Properties in the Chemistry of Modular Porous Solids. *Acc. Chem. Res.* **1998**, *31*, 474-484.
- (8) Fujita, M. Metal-Directed Self-Assembly of Two- and Three-Dimensional Synthetic Receptors. *Chem. Soc. Rev.* **1998**, *27*, 417-426.
- (9) Batten, S. R.; Robson, R. Interpenetrating Nets: Ordered, Periodic Entanglement. *Angew. Chem., Int. Ed.* **1998**, *37*, 1460-1494.
- (10) Fyfe, M. C. T.; Stoddart, J. F. Synthetic Supramolecular Chemistry. *Acc. Chem. Res.* **1997**, *30*, 393-401.
- (11) Mascal, M. Noncovalent Design Principles and the New Synthesis. *Contemp. Org. Synth.* **1994**, *1*, 31-46.
- (12) Cotton, F. A. Transition-Metal Compounds Containing Clusters of Metal Atoms. *Quarterly Reviews, Chem. Soc.*, **1966**, *20*, 389-401.
- (13) Eddaoudi, M.; Moler, D.; Li, H.; Reineke, T. M.; O'Keeffe, M.; Yaghi, O. M. Modular Chemistry: Secondary Building Units as a Basis for the Design of Highly Porous and Robust Metal-Organic Carboxylate Frameworks. *Acc. Chem. Res.* **2001**, *34*, 319-330.

- (14) *Metal Clusters in Chemistry*, Braunstein, P., Oro, L. A., Raithby, P. R. Eds.; New York: Wiley-VCH, **1999**.
- (15) Eddaoudi, M.; Kim, J.; Rosi, N.; Vodak, D. T.; Wachter, J.; O'Keeffe, M.; Yaghi, O. M. Systematic Design of Pore Size and Functionality in Isoreticular Metal-Organic Frameworks and their Application in Methane Storage. *Science* **2002**, *295*, 469-472.
- (16) Rosi, N. L.; Eckert, J.; Eddaoudi, M.; Vodak, D. T.; Kim, J.; O'Keeffe, M.; Yaghi, O. M. Hydrogen Storage in Microporous Metal-Organic Frameworks. *Science* **2003**, *300*, 1127-1129.
- (17) Seo, J. S.; Whang, D.; Lee, H.; Jun, S. I.; Oh, J.; Jeon, Y. J.; Kim, K. A Homochiral Metal-Organic Porous Material for Enantioselective Separation and Catalysis. *Nature* **2000**, *404*, 982-986.
- (18) Cotton, F. A.; Lin, C.; Murillo, C. A. Supramolecular Arrays Based on Dimetal Building Units. *Acc. Chem. Res.* **2001**, *34*, 759-771.
- (19) Bain, R. L.; Shriver, D. F.; Ellis, D. E. Extended Materials Based on the $[\text{Mo}_6\text{Cl}_8]^{4+}$ Building Block Bridged by 4,4'-Bipyridine. *Inorg. Chim. Acta* **2001**, *325*, 171-174.
- (20) Prokopuk, N.; Weinert, C. S.; Siska, D. P.; Stern, C. L.; Shriver, D. F. Hydrogen-Bonded Hexamolybdenum Clusters: Formation of Inorganic-Organic Networks. *Angew. Chem., Int. Ed.* **2000**, *39*, 3312-3315.
- (21) Jin, S.; DiSalvo, F. J. 3-D Coordination Network Structures Constructed from $[\text{W}_6\text{S}_8(\text{CN})_6]^{6-}$ Anions. *Chem. Mater.* **2002**, *14*, 3448-3457.
- (22) Disalvo, F. J. Some Remarkable Properties of Transition Metal Chalcogenide Compounds. *Annales de Chimie* **1982**, *7*, 109-118.
- (23) Gabriel, J. C. P.; Boubekour, K.; Uriel, S.; Batail, P. Chemistry of Hexanuclear Rhenium Chalcohalide Clusters. *Chem. Rev.* **2001**, *101*, 2037-2066.
- (24) Saito, T. Rhenium Sulfide Cluster Chemistry. *J. Chem. Soc., Dalton Trans.* **1999**, 97-106.
- (25) Fischer, O.; Odermatt, R.; Bongi, G.; Jones, H.; Chevrel, R.; Sergent, M. Superconductivity in the Ternary Molybdenum Sulfides. *Phys. Lett. A* **1973**, *45*, 87-88.
- (26) Tulsky, E. G.; Long, J. R. Dimensional Reduction: A Practical Formalism for Manipulating Solid Structures. *Chem. Mater.* **2001**, *13*, 1149-1166.

- (27) Long, J. R.; McCarty, L. S.; Holm, R. H. A Solid State Route to Molecular Clusters: Access to the Solution Chemistry of $[\text{Re}_6\text{Q}_8]^{2+}$ (Q = S, Se) Core-Containing Clusters via Dimensional Reduction. *J. Am. Chem. Soc.* **1996**, *118*, 4603-4616.
- (28) Long, J. R.; Williamson, A. S.; Holm, R. H. Dimensional Reduction of $\text{Re}_6\text{Se}_8\text{Cl}_2$: Sheets, Chains and Discrete Clusters Composed of Chloride-Terminated $[\text{Re}_6\text{Q}_8]^{2+}$ (Q = S, Se) Cores. *Angew. Chem., Int. Ed. Engl.* **1995**, *34*, 226-229.
- (29) Prokopuk, N.; Shriver, D. F. The Octahedral M_6Y_8 and M_6Y_{12} Clusters of Group 5 and 6 Transition Metals. *Adv. Inorg. Chem.* **1998**, *46*, 1-49.
- (30) *Early Transition Metal Clusters with π -Donor Ligands*, Chisholm, M. H. Ed.; New York: VCH, **1995**.
- (31) Zheng, Z.; Long, J. R.; Holm, R. H. A Basis Set of Re_6Se_8 Cluster Building Blocks and Demonstration of Their Linking Capability: Directed Synthesis of an $\text{Re}_{12}\text{Se}_{16}$ Dicluster. *J. Am. Chem. Soc.* **1997**, *119*, 2163-2171.
- (32) Zheng, Z.; Holm, R. H. Cluster Condensation by Thermolysis: Synthesis of a Rhomb-Linked $\text{Re}_{12}\text{Se}_{16}$ Dicluster and Factors Relevant to the Formation of the $\text{Re}_{24}\text{Se}_{32}$ Tetracluster. *Inorg. Chem.* **1997**, *36*, 5173-5178.
- (33) Zheng, Z.; Gray, T.; Holm, R. H. Synthesis and Structures of Solvated Monoclusters and Bridged Di- and Triclusters Based on the Cubic Building Block $[\text{Re}_6(\mu_3\text{-Se})_8]^{2+}$. *Inorg. Chem.* **1999**, *38*, 4888-4895.
- (34) Willer, M. W.; Long, J. R.; McLauchlan, C. C.; Holm, R. H. Ligand Substitution Reactions of $[\text{Re}_6\text{S}_8\text{Br}_6]^{4+}$: A Basis Set of Re_6S_8 Clusters for Building Multicluster Assemblies. *Inorg. Chem.* **1998**, *37*, 328-333.
- (35) Gray, T. G.; Holm, R. H. Site-Differentiated Hexanuclear Rhenium(III) Cyanide Clusters $[\text{Re}_6\text{Se}_8(\text{PEt}_3)_n(\text{CN})_{6-n}]^{n-4}$ ($n = 4, 5$) and Kinetics of Solvate Ligand Exchange on the Cubic $[\text{Re}_6\text{Se}_8]^{2+}$ Core. *Inorg. Chem.* **2002**, *41*, 4211-4216.
- (36) Chen, Z.-N.; Yoshimura, T.; Abe, M.; Sasaki, Y.; Ishizaka, S.; Kim, H.-B.; Kitamura, N. Chelate Formation around a Hexarhenium Cluster Core by the Diphosphane Ligand $\text{Ph}_2\text{P}(\text{CH}_2)_6\text{PPh}_2$. *Angew. Chem., Int. Ed.* **2001**, *40*, 239-242.
- (37) Gray, T. G.; Rudzinski, C. M.; Meyer, E. E.; Holm, R. H.; Nocera, D. G. Spectroscopic and Photophysical Properties of Hexanuclear Rhenium(III) Chalcogenide Clusters. *J. Am. Chem. Soc.* **2003**, *125*, 4755-4770.
- (38) Gray, T. G.; Rudzinski, C. M.; Nocera, D. G.; Holm, R. H. Highly Emissive Hexanuclear Rhenium(III) Clusters Containing the Cubic Cores $[\text{Re}_6\text{S}_8]^{2+}$ and $[\text{Re}_6\text{Se}_8]^{2+}$. *Inorg. Chem.* **1999**, *38*, 5932-5933.

- (39) Arratia-Pérez, R.; Hernández-Acevedo, L. The $\text{Re}_6\text{Se}_8\text{Cl}_6^{4-}$ and $\text{Re}_6\text{Se}_8\text{I}_6^{4-}$ Cluster Ions: Another Example of Luminescent Clusters? *J. Chem. Phys.* **1999**, *111*, 168-172.
- (40) Arratia-Pérez, R.; Hernández-Acevedo, L. Calculated Paramagnetic Resonance Parameters (g , A_{hfi}) of the $\text{Re}_6\text{S}_8\text{Br}_6^{3-}$, $\text{Re}_6\text{S}_8\text{I}_6^{3-}$, and $\text{Re}_6\text{Se}_8\text{I}_6^{3-}$ Cluster Ions. *J. Chem. Phys.* **2003**, *118*, 7425-7430.
- (41) Monk, P. M. S.; Mortimer, R. J.; Rosseinsky, D. R. *Electrochromism*, New York: VCH, **1995**.
- (42) Köhler, A.; Wilson, J. S.; Friend, R. H. Fluorescence and Phosphorescence in Organic Materials. *Adv. Mater.* **2002**, *14*, 701-707.
- (43) Bennett, M. V.; Beauvais, L. G.; Shores, M. P.; Long, J. R. Expanded Prussian Blue Analogues Incorporating $[\text{Re}_6\text{Se}_8(\text{CN})_6]^{3-/4-}$ Clusters: Adjusting Porosity via Charge Balance. *J. Am. Chem. Soc.* **2001**, *123*, 8022-8032.
- (44) Bennett, M. V.; Shores, M. P.; Beauvais, L. G.; Long, J. R. Expansion of the Porous Solid $\text{Na}_2\text{Zn}_3[\text{Fe}(\text{CN})_6]_2 \cdot 9\text{H}_2\text{O}$: Enhanced Ion-Exchange Capacity in $\text{Na}_2\text{Zn}_3[\text{Re}_6\text{Se}_8(\text{CN})_6]_2 \cdot 24\text{H}_2\text{O}$. *J. Am. Chem. Soc.* **2000**, *122*, 6664-6668.
- (45) Beauvais, L. G.; Shores, M. P.; Long, J. R. Cyano-Bridged Re_6Q_8 (Q = S, Se) Cluster-Cobalt(II) Framework Materials: Versatile Solid Chemical Sensors. *J. Am. Chem. Soc.* **2000**, *122*, 2763-2772.
- (46) Naumov, N. G.; Virovets, A. V.; Sokolov, N. S.; Artemkina, S. B.; Fedorov, V. E. A Novel Framework Type for Inorganic Clusters with Cyanide Ligands: Crystal Structures of $\text{Cs}_2\text{Mn}_3[\text{Re}_6\text{Se}_8(\text{CN})_6]_2 \cdot 15\text{H}_2\text{O}$ and $\text{Co}_3[\text{Re}_6\text{Se}_8(\text{CN})_6]_2 \cdot 14.5\text{H}_2\text{O}$. *Angew. Chem., Int. Ed.* **1998**, *37*, 1943-1945.
- (47) Itasaka, A.; Abe, M.; Yoshimura, T.; Tsuge, K.; Suzuki, M.; Imamura, T.; Sasaki, Y. Octahedral Arrangement of Porphyrin Moieties Around Hexarhenium(III) Cluster Cores: Structure of (μ_3 -Selenido) Hexa-(5-(4-pyridyl)-10,15,20-tritolyiporphyrin)-Hexarhenium(III). *Angew. Chem., Int. Ed.* **2002**, *41*, 463-466.
- (48) Kim, Y.; Park, S. M.; Nam, W.; Kim, S. J. Crystal Structure of the Two-Dimensional Framework $[\text{Mn}(\text{salen})_4[\text{Re}_6\text{Te}_8(\text{CN})_6][\text{salen} = \text{N}, \text{N}'\text{-Ethylenebis(salicylideneaminato)}]$. *Chem. Commun.* **2001**, 1470-1471.
- (49) Kim, Y.; Park, S. M.; Kim, S. J. Three-Dimensional Framework Containing $\text{Mn}(\text{salen})^+$ and $\text{Re}_6\text{Se}_8(\text{CN})_6^{4-}$ Cluster. *Inorg. Chem. Commun.* **2002**, *5*, 592-595.
- (50) Kim, Y.; Choi, S. K.; Park, S. M.; Nam, W.; Kim, S. J. Synthesis and Reactivity of Rhenium Cluster-Supported Manganese Porphyrin complexes, *Inorg. Chem. Commun.* **2002**, *5*, 612-615

- (51) Site-differentiated, phosphine-ligated $W_6(\mu_3-S)_8$ clusters have also been reported recently. See: Jin, S.; Venkataraman, D.; DiSalvo, F. J. Ligand Substitution Reactions of $W_6S_8L_6$ with Tricyclohexylphosphine (L = 4-tert-Butylpyridine or *n*-Butylamine): ^{31}P NMR and Structural Studies of $W_6S_8(PCy_3)_n(4\text{-tert-butylpyridine})_{6-n}$ ($0 < n \leq 6$) Complexes. *Inorg. Chem.* **2000**, *39*, 2747-2757.
- (52) Schweiger, M.; Seidel, S. R.; Arif, A. M.; Stang, P. J. The Self-Assembly of an Unexpected, Unique Supramolecular Triangle Composed of Rigid Subunits. *Angew. Chem., Int. Ed.* **2001**, *40*, 3467-3469.
- (53) Selby, H. D.; Zheng, Z.; Gray, T. G.; Holm, R. H. Bridged Multiclusters Derived from the Face-Capped Octahedral $[Re_6Se_8]^{2+}$ Cluster Core. *Inorg. Chim. Acta* **2001**, *312*, 205-208.
- (54) Roland, B. K.; Selby, H. D.; Carducci, M. D.; Zheng, Z. Built to Order: Molecular Tinkertoys from The $[Re_6(\mu_3-Se)_8]^{2+}$ Clusters. *J. Am. Chem. Soc.* **2002**, *124*, 3222-3223.
- (55) Wang, R.; Zheng, Z. Dendrimers Supported by the $[Re_6Se_8]^{2+}$ Metal Cluster Core. *J. Am. Chem. Soc.* **1999**, *121*, 3549-3550.
- (56) Roland, B. K.; Carter, C.; Zheng, Z. Routes to Metallodendrimers of the $[Re_6(\mu_3-Se)_8]^{2+}$ Core-Containing Clusters. *J. Am. Chem. Soc.* **2002**, *124*, 6234-6235.
- (57) Selby, H. D.; Roland, B. K.; Carducci, M. D.; Zheng, Z. Hydrogen-Bonded Extended Arrays of the $[Re_6(\mu_3-Se)_8]^{2+}$ Core-Containing Clusters. *Inorg. Chem.*, **2003**, *42*, 1656-1662.
- (58) Selby, H. D.; Orto, P.; Carducci, M. D.; Zheng, Z. Novel Concentration Driven Structural Interconversion in Shape-Specific Solids Supported by the Octahedral $[Re_6(\mu_3-Se)_8]^{2+}$ Cluster Core. *Inorg. Chem.* **2002**, *41*, 6175-6177.
- (59) Selby, H. D.; Orto, P.; Zheng, Z. A Modular Crystal Engineering Approach to Coordination Polymers Supported by the Face-Capped $[Re_6(\mu_3-Se)_8]^{2+}$ Clusters. *Polyhedron* **2003**, in press.
- (60) Roland, B. K.; Selby, H. D.; Cole, J. R.; Zheng, Z. *J. Chem. Soc., Dalton Trans.* **2003**, submitted.
- (61) Mironov, Y. V.; Cody, J. A.; Albrecht-Schmitt, T. E.; Ibers, J. A. Cocrystallized Mixtures and Multiple Geometries: Syntheses, Structures, and NMR Spectroscopy of the Re_6 Clusters $[NMe_4]_4[Re_6(Te_{8-n}Se_n)(CN)_6]$ ($n = 0-8$). *J. Am. Chem. Soc.* **1997**, *119*, 493-498.

- (62) Roland, B. K.; Flora, W. H.; Carducci, M. D.; Armstrong, N. R.; Zheng, Z. *J. Cluster Sci.* **2003**, submitted.
- (63) Atwood, J. L.; Lehn, J.-M. *Comprehensive Supramolecular Chemistry*. 1st Ed. Oxford, UK ; New York : Pergamon, **1996**.
- (64) Merkle, R. C. Molecular Building Blocks and Development Strategies for Molecular Nanotechnology. *Nanotechnology*, **2000**, *11*, 89-99.
- (65) Kaszynski, P.; Michl, J. [n]Staffanes: A Molecular Size "Tinkeroxy" Construction Set for Nanotechnology. Preparation of End-Functionalized Telomers and a Polymer of [1.1.1]Propellane. *J. Am. Chem. Soc.* **1998**, *110*, 5225-5226.
- (66) Tykwinski, R. R.; Stang, P. J. Preparation of Rigid-Rod, Di- and Trimetallic α -Acetylide Complexes of Iridium(III) and Rhodium(III) via Alkynyl(phenyl)iodonium Chemistry. *Organometallics* **1994**, *13*, 3203-3208.
- (67) Muller, J.; Base, K.; Magnera, T. F.; Michl, J. Rigid-Rod Oligo-*p*-Carboranes for Molecular Tinkertoys. An Inorganic Langmuir-Blodgett Film with a Functionalized Outer Surface. *J. Am. Chem. Soc.* **1992**, *114*, 9721-9722.
- (68) Hassenruck, K.; Murthy, G. S.; Lynch, V. M.; Michl, J. "Mixed Staffanes" as Intermediate-Length Staffs for Molecular Tinkertoys. Parent Hydrocarbons and Terminal Diiodides Combining Bicyclo[1.1.1]pentane with Cubane or Bicyclo[2.2.2]octane Units. *J. Org. Chem.* **1990**, *55*, 1013-1016.
- (69) Kobayashi, K.; Shirasaka, T.; Sato, A.; Horn, E.; Furukawa, N. Self-Assembly of a Radially Functionalized Hexagonal Molecule: Hexakis(4-hydroxyphenyl)benzene. *Angew. Chem. Int. Ed.* **1999**, *38*, 3483-3486.
- (70) Long, N. J.; Martin, A. J.; Fabra de Biani, F.; Zanello, P. Synthetic and Electrochemical Studies of some Metal Complexes of 1,2,5-triethynylbenzene. *J. Chem. Soc., Dalton Trans.* **1998**, 2017-2021.
- (71) Fink, H.; Long, N. J.; Martin, A. J.; Opromolla, G.; White, A. J.; Williams, D. J.; Zanello, P. Ethynylferrocene Compounds of 1,3,5-Tribromobenzene *Organometallics* **1997**, *16*, 2646-2650.
- (72) Uno, M.; Dixneuff, P. H. Organometallic Trikel: Novel Tris(vinylideneruthenium(II)), Tri(alkynylruthenium(II)), and Triruthenium-Triferrocenyl Complexes. *Angew. Chem. Int. Ed.* **1998**, *37*, 1714-1717.
- (73) Leininger, S.; Stang, P. J. Synthesis and Characterization of Organoplatinum Dendrimers with 1,2,5-Triethynylbenzene Building Blocks. *Organometallics* **1998**, *17*, 3981-3987.

- (74) Werner, H.; Bachmann, P.; Laubender, M.; Gevert, O. Di- Tri- Alkyne- and Vinylidenerhodium(I) Complexes Including the X-ray Crystal Structure of a Dendrimer- Like Rh₃ Compound. *Eur. J. Inorg. Chem.* **1998**, 1217-1224.
- (75) Seidel, S. R.; Stang, P. J. High-Symmetry Coordination Cages via Self-Assembly. *Acc. Chem. Res.* **2002**, *35*, 972-983.
- (76) Michl, J.; Magnera, T. F. Two-Dimensional Supramolecular Chemistry with Molecular Tinkertoy. *Proc. Natl. Acad. Sci.* **2002**, *99*, 4788-4792.
- (77) Magnera, T. F.; Peshlherbe, L. M.; Korblova, E.; Michl, J. The Organometallic "Molecular Tinkertoy" Approach to Planar Grid Polymers. *J. Organomet. Chem.* **1997**, *548*, 83-89.
- (78) Manimaran, B.; Rajendran, T.; Lu, Y-L.; Lee, G.-H.; Peng, S.-M.; Lu, K.-L. Self-Assembly of Fourteen Components into a Soluble, Neutral, Metalloprismatic Cage. *Eur. J. Inorg. Chem.* **2001**, 633-636.
- (79) Garcia-Frutos, E. M.; Fernandez-Lazaro, F.; Maya, E. M.; Vazquez, P.; Torres, T. Copper-Mediated Synthesis of Phthalocyanino-Fused Dehydro[12]- and[18] annulenes. *J. Org. Chem.* **2000**, *65*, 6841-6846.
- (80) Davila, J.; Harriman, A.; Milgrom, L. R. A Light-Harvesting Array of Synthetic Porphyrins. *Chem. Phys. Lett.* **1987**, *136*, 427-430.
- (81) Wennerstrom, O.; Ericsson, H.; Ratson, I.; Svensson, S.; Pimlott, W. *Meso-Tetra(meso-Tetraphenporphyrinyl)Porphyrin*, A Macrocyclic with Five Covalently Linked Porphyrin Units. *Tetrahedron Lett.* **1989**, *30*, 1129-1132.
- (82) Rucareanu, S.; Mongin, O.; Schuwey, A.; Hoyler, N.; Gossauer, A. Supramolecular Assemblies between Macrocyclic Porphyrin Hexamers and Star-Shaped Porphyrin Arrays. *J. Org. Chem.* **2001**, *66*, 4973-4988.
- (83) Mogin, O.; Gossauer, A. Tripodaphyrins, a New Class of Porphine Derivatives Designed for Nanofabrication. *Tetrahedron Lett.* **1996**, *37*, 3825-3828.
- (84) Mogin, O.; Gossauer, A. Synthesis of Nanometer-sized Homo- and Heteroorganometallic Tripodaphyrins. *Tetrahedron Lett.* **1997**, *53*, 6835-6846.
- (85) Hsiao, J.-S.; Krueger, B. P.; Wagner, R. W.; Johnson, T. E.; Delaney, J. K.; Mauzerall, D. C.; Fleming, G. R.; Lindsey, J. S.; Bocian, D. F.; Donohoe, R. J. Soluble Synthetic Multiporphyrin Arrays. 2. Photodynamics of Energy-Transfer Processes. *J. Am. Chem. Soc.* **1996**, *118*, 11181-11193.

- (86) Wagner, R. W.; Johnson, T. E.; Li, F.; Lindsey, J. S. Synthesis of Ethyne-Linked or Butadiyne-Linked Porphyrin Arrays Using Mild, Copper-Free, Pd-mediated Coupling Reactions. *J. Org. Chem.* **1995**, *60*, 5266-5273.
- (87) Wagner, R. W.; Johnson, T. E.; Li, F.; Lindsey, J. S. Soluble Synthetic Multiporphyrin Arrays. 1. Modular Design and Synthesis. *J. Am. Chem. Soc.* **1996**, *118*, 11166-11180.
- (88) Li, J.; Lindsey, J. S. Efficient Synthesis of Light-Harvesting Arrays Composed of Eight Porphyrins and One Phthalocyanine. *J. Org. Chem.* **1999**, *64*, 9101-9108.
- (89) Li, J.; Diers, J. R.; Seth, J.; Yang S.-I.; Bocian, D. F.; Holten, D.; Lindsey, J. S. Synthesis and Properties of Star-Shaped Multiporphyrin-Phthalocyanine Light-Harvesting Arrays. *J. Org. Chem.* **1999**, *64*, 9090-9100.
- (90) Li, F.; Gentemann, S.; Kalsbeck, W. A.; Seth, J.; Lindsey, J. S.; Holten, D.; Bocian, D. F. Effects of Central Metal Ion (Mg, Zn) and Solvent on Singlet Excited-State Energy Flow in Porphyrin-Based Nanostructures. *J. Mater. Chem.* **1997**, *7*, 1245-1262.
- (91) Seth, J.; Palaniappan, V.; Johnson, T. E.; Prathapan, S.; Lindsey, J. S.; Bocian, D. E. Investigation of Electronic Communication in Multi-Porphyrin Light-Harvesting Arrays. *J. Am. Chem. Soc.* **1994**, *116*, 10578-10592.
- (92) Prathapan, S.; Johnson, T. E.; Lindsey, J. S. Building-Blocks Synthesis of Porphyrin Light-Harvesting Arrays. *J. Am. Chem. Soc.* **1993**, *115*, 7519-7520.
- (93) Sugiura, K.-I.; Tanaka, H.; Matsumoto, T.; Kawai, T.; Sakata, Y. A Mandala-patterned Bandanna-shaped porphyrin oligomer, C₁₂₄₄H₁₃₅₀N₈₄Ni₂₀O₈₈, having a unique size and geometry. *Chem. Lett.* **1999**, 1193-1194.
- (94) Kimura, M.; Hamakawa, T.; Hanabusa, K.; Shirai, H.; Kobayashi, N. Synthesis of Multicomponent Systems Composed of One Phthalocyanine and Four Terpyridine Ligands. *Inorg. Chem.* **2001**, *40*, 4775-4779.
- (95) Kimura, M.; Hamakawa, T.; Muto, T.; Hanabusa, K.; Shirai, H.; Kobayashi, N. Five-Nuclear Complexes of Zinc (II) Phthalocyanine with Directly Linked Terpyridine Ligands. *Tetrahedron Lett.* **1998**, *39*, 8471-8474.
- (96) Rea, N.; Loock, B.; Lexa, D. Porphyrins Bound to Ru(bpy)₂ Clusters: Electrocatalysis of Sulfite. *Inorg. Chim. Acta* **2001**, *312*, 53-66.

- (97) Shi, C.; Anson, F. C. Cobalt *meso*-tetrakis(*N*-methyl-4-pyridiniumyl)porphyrin Becomes a Catalyst for the Electroreduction of O₂ by Four Electrons when [(NH₃)₅Os]ⁿ⁺ (*n* = 2, 3) Groups Are Coordinated to the Porphyrin Ring. *Inorg. Chem.* **1996**, *35*, 7928-7931.
- (98) Jin, Z.; Nolan, K.; McArthur, C. R.; Lever, A. B. P.; Leznoff, C. C. Synthesis, Electrochemical and Spectroelectrochemical Studies of Metal-Press 2,9,16,23-tetraferrocenylphthalocyanine. *J. Organomet. Chem.* **1994**, *468*, 205-212.
- (99) Gonzalez, A.; Vazquez, P.; Torres, T. Synthesis and Characterization of Homo-Dimetallic Ferrocendynyl-Bridged bi(ethenylphthalocyaninato) Complexes. *Tetrahedron Lett.* **1999**, *40*, 3263-3266.
- (100) Poon, K.-W.; Yan, Y.; Li, X.-Y.; Ng, D. K. Synthesis and Electrochemistry of Ferrocenylphthalocyanines. *Organometallics* **1999**, *18*, 3528-3533.
- (101) Wollmann, R. G.; Hendrickson, D. N. Synthesis and Physical Properties of *meso*-Tetraferrocenylporphyrin, the Copper Complex, and the Corresponding Mixed-Valence Oxidation Products. *Inorg. Chem.* **1977**, *16*, 3079-3089.
- (102) Dovidauskas, S.; Toma, H. E.; Araki, K.; Sacco, H. C.; Iamamoto, Y. (5,10,15,20-Tetra(4-pyridyl)porphinato)manganese(III) acetate Modified by Four μ₃-oxo-triruthenium Acetate Clusters: Synthesis, Characterization, Electrochemical Behavior and Catalytic Activity. *Inorg. Chim. Acta* **2000**, *305*, 206-213.
- (103) Araki, K.; Dovidauskas, S.; Winnischofer, H.; Alexiou, A.D. P.; Toma, H. E. A New Highly Efficient Tetra-Electronic Catalyst Based on a Cobalt Porphyrin Bound to Four μ₃-oxo-triruthenium Acetate Clusters. *J. Electroanal. Chem.* **2001**, *498*, 152-160.
- (104) Dovidauskas, S.; Araki, K.; Toma, H. E. Electrochemical and Binding Properties of a *meso*-(4-pyridyl)porphyrinatozinc Supramolecule Containing Four μ₃-oxo-triruthenium Acetate Clusters. *J. Porph. Phthal.* **2000**, *4*, 727-735.
- (105) Toma, H. E.; Araki, K.; Supramolecular Assemblies of Ruthenium Complexes and Porphyrins. *Coord. Chem. Rev.* **2000**, *196*, 307-329.
- (106) Toma, H. E.; Araki, K.; Alexiou, A.D. P.; Nikolaou, S.; Dovidauskas, S. Monomeric and Extended oxo-Centered Triruthenium Clusters. *Coord. Chem. Rev.* **2001**, *219-221*, 187-234.
- (107) Gouterman, M.; Wagniere, G.; Snyder, L. C. Spectra of Porphyrins. II. Four-Orbital Model. *J. Mol. Spectry.* **1963**, *11*, 108-127.

- (108) Sawyer, D. T. *Electrochemistry for Chemists*, 2nd ed.; Wiley: New York, **1995**; pp 203-204.
- (109) Zyss, J.; Ledoux, I. *Nonlinear Optics in Multipolar Media: Theory and Experiments*. *Chem. Rev.* **1994**, *94*, 77-105.
- (110) Wantanabe, Y.; Aida, T.; Inoue, S. Visible-Light-Mediated Living and Immortal Polymerizations of Epoxides Initiated with Zinc Complexes of N-Substituted Porphyrins. *Macromolecules* **1990**, *23*, 2612-1617.
- (111) Hosokawa, Y.; Kuroki, M.; Aida, T.; Inoue S. Controlled Synthesis of Poly(acrylic esters) by Aluminum Porphyrin Initiators. *Macromolecules* **1991**, *24*, 824-829.
- (112) Aida, T.; Kawaguchi, K.; Inoue S. Zinc N-Substituted Porphyrins as Novel Initiators for the Living and Immortal Polymerizations of Episulfide. *Macromolecules* **1990**, *23*, 3887-3892.
- (113) Hovestadt, H.; Keul, H.; Höcker, H. Tetraphenylporphyrin-Aluminium Compounds as Initiators for the Ring-Opening Polymerization of 2,2-Dimethyltrimethylene Carbonate: Synthesis of Homopolymers and Copolymers with ϵ -Caprolactone, Ethylene Oxide and Propylene Oxide. *Polymer* **1992**, *33*, 1941-1945.
- (114) Yoshinaga, K.; Iida, Y. Living Ring-Opening Oligomerization of Cyclosiloxanes with an Aluminum-Tetraphenylporphyrin Complete Initiator. *Chem. Lett.* **1991**, 1057-1058.
- (115) Amass, A. J.; Perry, M.; Riat, D. S.; Tighe, B. J.; Colclough, E.; Steward, M. J. Studies in Ring-Opening Polymerization—XII. The Ring-Opening Polymerization of Oxetane to Living Polymers Using A Porphinato-Aluminium Catalyst. *Eur. Polym. J.* **1994**, *30*, 641-646.
- (116) Takeuchi, D.; Watanabe, Y.; Aida, T.; Inoue S. Lewis Acid-Promoted Anionic Polymerization of a Monomer with High Cationic Polymerizability. Synthesis of Narrow Molecular Weight Distribution Polyoxetane and Polyoxetane-Poly(methylmethacrylate) Block Copolymer with Aluminum Porphyrin Initiators. *Macromolecules* **1995**, *28*, 651-652.
- (117) Komatsu, M.; Aida, T.; Inoue S. Novel Visible-Light-Driven Catalytic Carbon Dioxide Fixation. Synthesis of Malonic Acid Derivatives from CO₂, an α , β -Unsaturated Ester or Nitrile, and Diethylzinc Catalyzed by Aluminum Porphyrins. *J. Am. Chem. Soc.* **1991**, *113*, 8492-8498.
- (118) Sugimoto, H; Aida, T.; Inoue S. Ring-Opening Polymerizations of Lactone and Epoxide Initiated with Aluminum Complexes of Substituted Tetraphenylporphyrins. Molecular Design of Highly Active Initiators. *Macromolecules* **1990**, *23*, 2869-2875.

- (119) Sugimoto, H.; Kuroki, M.; Watanabe, Y.; Kawamura, C.; Aida, T.; Inoue S. High-Speed Living Anionic Polymerization of Methacrylic Esters with Aluminum Porphyrin Initiators. Organoaluminum Compounds as Lewis Acid Accelerators. *Macromolecules* **1993**, *26*, 3403-3410.
- (120) Adachi, A.; Sugimoto, H.; Aida, T.; Inoue S. Controlled Synthesis of High Molecular Weight Poly(Methyl Methacrylate) Based on Lewis Acid-Assisted High-Speed Living Polymerization Initiated with Aluminum Porphyrin. *Macromolecules* **1992**, *25*, 2280-2281.
- (121) Adachi, A.; Sugimoto, H.; Aida, T.; Inoue S. Aluminum Thiolate Complexes of Porphyrin as Excellent Initiators for Lewis Acid-Assisted High-Speed Living Polymerization of Methyl Methacrylate. *Macromolecules* **1993**, *26*, 1238-1243.
- (122) Sugimoto, H.; Kawamura, C.; Kuroki, M.; Aida, T.; Inoue S. Lewis Acid-Assisted Anionic Ring-Opening Polymerization of Epoxide by the Aluminum Complexes of Porphyrin, Phthalocyanine, Tetraazaannulene, and Schiff Base as Initiators. *Macromolecules* **1994**, *27*, 2013-2018.
- (123) Sugimoto, H.; Aida, T.; Inoue S. Lewis Acid-Promoted Living Anionic Polymerization of Alkyl Methacrylates Initiated with Aluminum Porphyrins. Importance of Steric Balance Between a Nucleophile and a Lewis Acid. *Macromolecules* **1994**, *27*, 3672-3674.
- (124) Akatsuka, M.; Aida, T.; Inoue S. Alcohol/Methylaluminum Diphenolate Systems as Novel, Versatile Initiators for Synthesis of Narrow Molecular Weight Distribution Polyester and Polycarbonate. *Macromolecules* **1995**, *28*, 1320-1322.
- (125) Rocha Gonsalves, A. M. d'A. What do We Know About Metalloporphyrin Catalytic Oxidations? *J. Heterocyclic Chem.*, **2002**, *39*, 499-509.
- (126) Porhiel, E.; Bondon, A.; Leroy, J. β -Octafluoro-*meso*-tetraarylporphyrin Iron Complexes as Catalysts for Monooxygenation Reactions. *Tetrahedron Lett.* **1998**, *39*, 4829-4830.
- (127) Anelli, P. L.; Banfi, S.; Legramandi, F.; Montanari, F.; Pozzi, G.; Quici, S. Tailed Mn^{III}-Tetraarylporphyrins Bearing an Axial Ligand and/or a Carboxylic Group: Self-Consistent Catalysts for H₂O or NaOCl Alkene Epoxidation. *J. Chem Soc., Perkin Trans. I*, **1993**, 1345-1357.
- (128) Inoue, S.; Aida, T.; Konishi, K. Selective Synthesis with Metalloporphyrin Catalysts. *J. Molecular Catalysts* **1992**, *74*, 121-129.

- (129) Hoffmann, P.; Labat, G.; Robert, A.; Meunier, B. Highly Selective Bromination of Tetramesitylporphyrin: an Easy Access to Robust Metalloporphyrins, $-\text{Br}_8\text{TMP}$ and $\text{M}-\text{Br}_8\text{TMPS}$. Examples of application in Catalytic Oxygenation and Oxidation Reactions. *Tetrahedron Lett.* **1990**, *30*, 1991-1994.
- (130) Naruta, Y.; Tani, F.; Maruyama, K. Catalytic and Asymmetric Oxidation of Sulphides with Iron Complexes of Chiral 'Twin Coronet' Porphyrins. *J. Chem. Soc., Chem. Commun.* **1990**, 1378-1380.
- (131) O'Malley, S.; Kodadek, T. Synthesis and Characterization of the "Chiral Wall" Porphyrin: A Chemically Robust Ligand for Metal-Catalyzed Asymmetric Epoxidations. *J. Am. Chem. Soc.* **1989**, *111*, 9116-9117.
- (132) Che, C.-M.; Yu, W.-Y. Ruthenium-Oxo and Tosylimido Porphyrin complexes for Epoxidation and Aziridination of Alkenes. *Pure Appl. Chem.* **1999**, *71*, 281-288.
- (133) Toma, H. E.; Araki, K. Synthesis and Electrochemical Behavior of a Tetrametallated Cobalt Porphyrin. *Inorg. Chim. Acta* **1991**, *179*, 293-296.
- (134) Araki, K.; Santos, P. S.; Toma, H. E. Electronic and Resonance Raman Spectra of a Multibridged Iron Polymer. *Spectrosc. Lett.* **1993**, *26*, 1417-1419.
- (135) Shi, C.; Anson, F. C. Multiple Intramolecular Electron Transfer in the Catalysis of the Reduction of Dioxygen by Cobalt *meso*-Tetrakis(4-pyridyl)Porphyrin to Which Four $\text{Ru}(\text{NH}_3)_5$ Groups are Coordinated. *J. Am. Chem. Soc.* **1991**, *113*, 9564-9570.
- (136) Shi, C.; Anson, F. C. Electrocatalysis of the Reduction of O_2 to H_2O by Tetraruthenated Cobalt *meso*-Tetrakis(4-pyridyl)Porphyrin Adsorbed on Graphite Electrodes. *Inorg. Chem.* **1992**, *31*, 5078-5083.
- (137) Shi, C.; Anson, F. C. Electrocatalysis for the Four-Electron Reduction of Dioxygen Based on Adsorbed Cobalt tetrapyridylporphyrin Molecules Linked by Aquaammine Complexes of Ruthenium. *Inorg. Chim. Acta* **1994**, *225*, 215-227.
- (138) Steiger, B.; Shi, C.; Anson, F. C. Electrocatalysis of the Reduction of Dioxygen by Adsorbed Cobalt 5,10,15,20-Tetraarylporphyrins to Which One, Two, or Three $\text{Ru}(\text{NH}_3)_5^{2+}$ Centers are Coordinated. *Inorg. Chem.* **1993**, *32*, 2107-2113.
- (139) Shi, C.; Anson, F. C. Comparison of the Catalytic Reduction of Dioxygen by [5,10,15,20-tetrakis((pentaammineruthenio(II))-4-pyridyl)porphyrinate]cobalt(II) in Solution and on Graphite Electrode Surfaces. *Inorg. Chem.* **1995**, *34*, 4554-4561.

- (140) Steiger, B.; Anson, F. C. New Electrocatalysis for the Four-Electron Reduction of Dioxygen Based on (5,10,15,20-tris(pentaammineruthenio(II)-4-(1-ethylpyridinium-4-yl)porphyrinato)cobalt(II) Immobilized on Graphite Electrodes. *Inorg. Chem.* **1994**, *33*, 5767-5779.
- (141) Steiger, B.; Anson, F. C. Evidence of the Importance of Back-Bonding in Determining the Behavior of Ruthenated Cyanophenyl Cobalt Porphyrins as Electrocatalysts for the Reduction of Dioxygen. *Inorg. Chem.* **1995**, *34*, 3355-3357.
- (142) Steiger, B.; Anson, F. C. [5, 10, 15, 20 - tetrakis(4-((pentaammineruthenio)-cyano)phenyl)porphyrinato]cobalt(II) Immobilized on Graphite Electrodes Catalyzes the Electroreduction of O₂ to H₂O, but the Corresponding 4-Cyano-2, 6- dimethylphenyl Derivative Catalyzes the Reduction Only to H₂O₂. *Inorg. Chem.* **1997**, *36*, 4138-4140.
- (143) Cole, S. J.; Curthoys, G. C.; Magnusson, E. A.; Phillips, J. N. Ligand Binding by Metalloporphyrins. III. Thermodynamic Functions for the Addition of Substituted Pyridines to Nickel(II) and Zinc(II) Porphyrins. *Inorg. Chem.* **1972**, *11*, 1024-1028.
- (144) Nappa, M.; Valentine, J. S. The Influence of Axial Ligands on Metalloporphyrin Visible Absorption Spectra. Complexes of Tetraphenylporphinatozinc. *J. Am. Chem. Soc.* **1978**, *100*, 5075-5080.
- (145) Drago, R. S. The Interpretation of Reactivity in Chemical and Biological Systems with the E and C Model. *Coord. Chem. Rev.* **1980**, *33*, 251-277.
- (146) Gutman, V.; Schmid, R. Empirical Approach to Ligand Effects on the Kinetics of Substitution and Redox Reactions. *Coord. Chem. Rev.* **1974**, *12*, 263-293.
- (147) Kolling, O. W. Soret Red Shift for Zinc Tetraphenylporphine in the Presence of Uncharged Lewis Bases. *Inorg. Chem.* **1979**, *18*, 1175-1176.
- (148) Drago, R. S.; Kroeger, M. K.; Stahlbush, J. R. An E and C Analysis of Donor Number and Soret Band Shifts in Adducts of Zinc Tetraphenylporphine. *Inorg. Chem.* **1981**, *20*, 306-308.
- (149) Bunheleier, E.; Wehner, W.; Vogtle, F. "Cascade" and "Nonskid-chain-like" Syntheses of Molecular Cavity Topologies. *Synthesis* **1978**, 155-158.
- (150) Matthews, O. A.; Shipway, A. N.; Stoddart J. F. Dendrimers – Branching Out from Curiosities Into New Technologies. *Prog. Polym. Sci.* **1998**, *23*, 1-56.
- (151) Bosman, A. W.; Janssen, H. M.; Meijer, E. W. About Dendrimers: Structure, Physical Properties, and Applications. *Chem. Rev.* **1999**, *99*, 1665-1688.

- (152) Fischer, M.; Vogtle, F. Dendrimers: From Design to Application – A Progress Report. *Angew. Chem. Int. Ed.* **1999**, *38*, 884-905.
- (153) Grayson, S. M.; Frechet, J. M. J. Convergent Dendrons and Dendrimers: from Synthesis to Applications. *Chem. Rev.* **2001**, *101*, 3819-3867.
- (154) Balzani, V.; Campagna, S.; Denti, G.; Juris, A.; Serroni, S.; Venturi, M. Designing Dendrimers Based on Transitions-Metal Complexes. Light-Harvesting Properties and Predetermined Redox Patterns. *Acc. Chem. Res.* **1998**, *31*, 26-34.
- (155) Gorman, C. Metallodendrimers: Structural Diversity and Functional Behavior. *Adv. Mater.* **1998**, *10*, 295-309.
- (156) Newkome, G. R.; He, E.; Moorefield, C. N. Suprasuper molecules with Novel Properties: Metallodendrimers. *Chem. Rev.* **1999**, *99*, 1689-1446.
- (157) Stoddart, F. J.; Welton, T. Metal-Containing Dendritic Polymers. *Polyherdron* **1999**, *18*, 3575-3591.
- (158) Hearchaw, M. A.; Moss, J. R. Organometallic and Related Metal-Containing Dendrimers. *Chem. Commun.* **1999**, 1-8.
- (159) Hecht, S.; Frechet, J. M. J. Dendritic Encapsulation of Function: Applying Nature's Site Isolation Principle from Biomimetics to Materials Science. *Angew. Chem. Int. Ed.* **2001**, *40*, 65-91.
- (160) Duncan, R.; Kopecek, J. Soluble Synthetic Polymers as Potential Drug Carriers. *Adv. Polym. Sci.* **1984**, *57*, 51-101.
- (161) Akiyoshi, K. Cascade Polymers as Drug Carriers. *Kagaku (Kyoto)* **1994**, *49*, 442-445.
- (162) Astruc, D.; Chardac, F. Dendritic Catalysts and Dendrimers in Catalysis. *Chem. Rev.* **2001**, *101*, 2991-3023.
- (163) Toth, E.; Pubanz, D.; Vauthey, S.; Helm, L.; Merbach, A. E. The Role of Water Exchange in Attaining Maximum Relaxivities for Dendrimeric MRI Contrast Agents. *Chem. Eur. J.* **1996**, *2*, 1607-1615.
- (164) Gorman, C. B.; Parkhurst, B. L.; Su, W. Y.; Chen, K. Encapsulated Electroactive Molecules Based upon an Inorganic Cluster Surrounded by Dendron Ligands. *J. Am. Chem. Soc.* **1997**, *119*, 1141-1142.

- (165) Liwporncharoenvong, T.; Luck, R. L. Quadruply Bonded Dimolybdenum Atoms Surrounded by Dendrons: Preparation, Characterization and Electrochemistry. *J. Am. Chem. Soc.* **2001**, *123*, 3615-3616.
- (166) Gorman, C. B.; Su, W. Y.; Jiang, H.; Watson, C. M.; Boyle, P. Hybrid Organic-Inorganic, Hexa-Arm Dendrimers Based on an Mo_6Cl_8 Core. *Chem. Commun.* **1999**, 877-878.
- (167) Benito M.; Rossell, O.; Seco, M.; Segales, G. Soluble Iron/Gold Cluster Containing Carbosilane Dendrimers. *Organometallics* **1999**, *18*, 5191-5193.
- (168) Benito M.; Rossell, O.; Seco, M.; Segales, G. Carbosilane Dendrimers Functionalized with AuFe_3 Clusters. *Inorg. Chim. Acta.* **1999**, *291*, 247-251.
- (169) Benito M.; Rossell, O.; Seco, M.; Segales, G. Transition Metal Clusters Containing Dendrimers. *J. Organomet. Chem.* **2001**, *619*, 245-251.
- (170) Benito M.; Rossell, O.; Seco, M.; Segales, G.; Maraval, V.; Laurent, R.; Caminade, A.; Majoral, J. Very Large and Polyanionic Fe/Au Cluster-Containing Dendrimers. *J. Organomet. Chem.* **2001**, *622*, 33-37.
- (171) Feeder, N.; Geng, J.; Goh, P. G.; Johnson, B. F. G.; Martin, C. M.; Shephard, D. S.; Zhou, W. Nanoscale Super Clusters of Clusters Assembled Around a Dendritic Core. *Angew. Chem. Int. Ed.* **2000**, *39*, 1661-1664.
- (172) Chérioux, F.; Thomas, C. M.; Therrien, B.; Süß-Fink, G. Dendritic Systems Based on Dinuclear Ruthenium or Rhodium Units Generating Peripheral Catalytic Sites. *Chem. Eur. J.* **2002**, *8*, 4377-4382.
- (173) Alonso, E.; Astruc, D. Introduction of the Cluster Fragment $\text{Ru}_3(\text{CO})_{11}$ at the Periphery of Phosphine Dendrimers Catalyzed by the Electron-Reservoir Complex $[\text{Fe}^{\text{I}}\text{Cp}(\text{C}_6\text{Me}_6)]$. *J. Am. Chem. Soc.* **2000**, *122*, 3222-3223.
- (174) Zeng, H.; Newkome, G. R.; Hill, C. L. Poly(polyoxometalate) Dendrimers: Molecular Prototypes of New Catalytic Materials. *Angew. Chem., Int. Ed.* **2000**, *39*, 1772-1774.
- (175) Constable, E. C.; Eich, O.; Fenske, D.; Housecroft, C. E.; Johnston, L. A. Metallostars: High-Nuclearity Linearly Developed Nanostructures Containing Multiple Cluster Motifs. *Chem. Eur. J.* **2000**, *6*, 4364-4370.
- (176) Suresh, E.; Bhadbhade, M. M. Metal-Organic Supramolecular Architecture Containing Cationic Cavities: Synthesis and Single Crystal investigation of $\{[\text{Co}(\text{bpe})_2(\text{H}_2\text{O})_2](\text{ClO}_4)(\text{H}_2\text{O})_2\}_n$. *CrystEngComm* **2001**, *13*, 1-3.

- (177) Carranza, J.; Brennan, C.; Sletten, J.; Lloret, F.; Julve, M. Three One-Dimensional Systems with End-To-End Dicyasnamide Bridges Between Copper(II) Centers: Structural and Magnetic Properties. *J. Chem. Soc., Dalton Trans.* **2002**, 3164-3170.
- (178) Hernandez, M. L.; Urtiaga, M. K.; Barandika, M. G.; Cortes, R.; Lezama, L.; Pinta, N. de la; Arriotua, M. I.; Rojo, T. Magnetostructural Characterization of Two M-NCO-bpa Polymers (M = Co, Mn, and bpa = 1,2-bis(4-pyridyl)ethane). *J. Chem. Soc., Dalton Trans.* **2001**, 3010-3014.
- (179) Wang, Q.-M.; Mak, T. C. W. Assembly of Discrete, One-, Two-, and Three Dimensional Silver(I) Supramolecular Complexes Containing Encapsulated Acetylide Dianion with Nitrogen- π -Donor Spacers. *Inorg. Chem.* **2003**, *42*, 1637-1643.
- (180) Ferbinteanu, M.; Marinescu, G.; Roesky, H. W.; Noltemeyer, M.; Schmidt, H.-G.; Andruh, M. $\{Co(\mu\text{-bpe})(\text{bpe})_2(\text{H}_2\text{O})_2\}(0.5\text{bpe})(\text{H}_2\text{O})(\text{ClO}_4)_2\}_n$: A Transition Metal-Organic Network with a Novel Supramolecular Architecture (bpe = 1,2-bis(4-pyridyl)ethane). *Polyhedron* **1998**, 1-7.
- (181) Sanchez, C.; Ribot, F. Design of Hybrid Organic-Inorganic Materials Synthesized via Sol-Gel Chemistry. *New. J. Chem.* **1994**, *18*, 1007-47.
- (182) Shea, K. J.; Loy, D. A. Bridged Polysilsesquioxanes. Molecular-Engineered Hybrid Organic-Inorganic Materials. *Chem. Mater.* **2001**, *13*, 3306-3319.
- (183) Zhang, C.; Bunning, T. J.; Laine, R. M. Synthesis and Characterization of Liquid Crystalline Silsesquioxanes. **2001**, *13*, 3653-3662.
- (184) Schubert, U. Polymers Reinforced by Covalently Bonded Inorganic-Clusters. *Chem. Mater.* **2001**, *13*, 3487-3494.
- (185) Snachez, C.; Soler-Illia, G. J. de A. A.; Ribot, F.; Lalot, T.; Mayer, C. R.; Cabuil V. Designed Hybrid Organic-Inorganic Nanocomposites from Functional Nanobuilding Blocks. *Chem. Mater.* **2001**, *13*, 3061-3083.
- (186) Jackson, J. A.; Newsham, M. D.; Worsham, C.; Nocera, D. G. Efficient Singlet Oxygen Generation from Polymers Derivatized with Hexanuclear Molybdenum Clusters. *Chem. Mater.* **1996**, *8*, 558-564.
- (187) Robinson L. M.; Lu, H.; Hupp, J. T.; Shriver, D. F. Nature of the Interaction and Photophysical Properties of $[Mo_6Cl_8(SO_3CF_3)_6]^{2-}$ and $[Mo_6Cl_8Cl_6]^{2-}$ on Silica Gel. *Chem. Mater.* **1995**, *7*, 43-49.
- (188) Robinson, L. M.; Shriver, D. F. Synthesis and Photophysical Properties of Polymer-Bound Hexanuclear Molybdenum Clusters. *J. Coord. Chem.* **1996**, *37*, 119-129.

- (189) Golden, J. H.; Deng, H. G.; DiSalvo, F. J.; Frechet, J. M.; Thompson, P. M. Monodisperse Metal Clusters 10 Angstroms in Diameter in a Polymeric Host: The "Monomer as Solvent" Approach. *Science* **1995**, *268*, 1463-1466.
- (190) Sogah, D. Y.; Weimer, M. W.; Jin, S.; Disalvo, F. J.; Venkataraman, D. Polystyrene Star Nanostructures with Molybdenum and Tungsten Cluster Core. *Polym. Mater. Sci. Eng.* **2001**, *84*, 845-846.